University of Southampton

FACULTY OF ENGINEERING, SCIENCE AND MATHEMATICS

SCHOOL OF CIVIL ENGINEERING AND THE ENVIRONMENT

Analytic Structures

Kenneth Anthony Lewis

Thesis for the degree of Doctor of Philosophy

September 2007

Abstract

University of Southampton

ABSTRACT

Faculty of Engineering, Science and Mathematics

School of Civil Engineering and the Environment

Doctor of Philosophy

Analytic Structures

by Kenneth Anthony Lewis

This thesis presents the development of an innovative method for describing the behaviour of steel members under load. It uses a direct solution to a set of six differential equations key to the state of a cross-section of a member. Because the method focuses upon cross-sectional response to loading, it incorporates member deflection and is ideal for use in numerical equation solvers which are becoming more prevalent as personal computing power continues to rise. The six equations are described, a novel method for ascertaining their solutions is introduced and the whole system is set to work. Simulated structures include a family of pinned struts of varying slenderness, and single-span steel portal frames. The method may be used at varying levels of detail, having the flexibility to make use of a selection of stress-strain relationships, and families of struts are tested under a number of these conditions. The results of these simulations are compared and the result best comparable to design code crushing strength is that which carries the most data: a full elastic-plastic-strain-hardening stress strain curve used in simulations which consider the impact of bending moments and thrusts through each cross-section, without neglecting the internal stresses of hot-rolled steel sections. The portal frame computer models are an evolution of the strut simulations, providing a rigorous analysis of a sample frame as well as comparisons with existing design methods. Results from both series of structural model are discussed before future developments of the method and its application to enhanced simulations.

Contents

List of Figures

List of Tables

Acknowledgements

This document was prepared and typeset in the excellent and free LaTeX document system using `graphicx`, `lscape`, `natbib`, `supertabular` and `multirow` extensions with *MikTex 2.5*. All image files were prepared for typesetting using OpenOffice.org. It is the author's regret that a completely free-as-in-freedom computer system was not used for all aspect of this project: computer simulations were run in Wolfram Research's *Mathematica*; text and graphics drafted in *Microsoft Office*; both running under Microsoft's *Windows XP* operating system. If there are any missing 'm's in this docuent, it's the b@*#$ keyboard, the sole weak feature of the notebook computer used.

Chapter 1

Introduction

Few fields of human enterprise have been untouched by the impact of computer-based data processing to help provide a better understanding of their mechanisms. Structural steel design has benefited enormously from the availability of stiffness-matrix-based analysis tools and the explosion in available personal computing power in the past 20 years. Such tools sit within the bounds of their mathematical methodology, codified safe design methods and available time to analyze the computer simulation. This project sets out to extend the mathematical methodology, work within present codes and supply analysis tools which provide accurate results in a time-efficient way. In so doing, it sidesteps the conventional terminology of 'first-order' and 'second-order' models, using a differential equation model of the structural member with computer-based numerical equation solvers. The numerical equation solvers provide a high-detail, numerical solution to the differential equation model, collating the impact of every response to loading included in the model, not only the first- or second-level solutions. In contrast to existing stiffness matrix-based methods and their fixed points at which member behaviour is evaluated, Analytic Structures provides a continuous analysis of each member within the framework. Further, solving a model written in terms of differential equations using so-called 'intelligent' differential equation solvers, which are both able to improve their numerical accuracy if the density of the solution requires it and to avoid numerical singularities, provides an unprecedented level of detail in the structural behaviour analysed. This also accommodates the benefits of using a full-detail stress-strain response and the residual stresses (or internal strains) of hot-rolled steel. The model is deployed in two collections of models: first, a buckling strut for which exceptional correlation is shown with the BS5950 (Table 24) Series A Buckling Curve; and second, steel portal frames at a variety of spans. While preparing these simulations, the work records the importance of internal strain data during the strain-hardening phase of buckling and to the behaviour of slender ($\lambda > 130$) struts. The failure methods and ultimate

limit state values for the portal frame simulations are comparable to existing methods. Additionally, the method compares well with a manual Second-Order analysis from SCI P-292, showing that the Analytic Structures model is as good as the present best methods for structural steelwork design.

The present context to the field of research is introduced in Chapter Two, describing the growth of mathematical representations of member behaviour, both as pen-and-paper analysis and digital computation, and in terms of best-design-practice codes.

Subsequently, the core mathematics is introduced in Chapter Three. Starting with the axes, naming and sign conventions, the notion of parameterising a member so that its deformed position can be followed is introduced before the six equations of state which form the core of the method. The type and variety of stress-strain relationships used is next introduced, along with a method to include the internal stresses arising from hot-rolled steel fabrication.

The notion of a tabulated store of loading and associated curvature deflection is next introduced (Chapter Four), following two paths of either moment-only curvature table or a moment-axial-curvature surface. The necessary tools for producing such a table are included also. Finally, the produced relationships are tested against expected values of curvature arising from loading.

Chapter Five contains the method deployed in simulations of a pinned strut. Using a variety of stress-strain curves and moment-curvature relations, a selection of slendernesses, from stocky to extremely slender, were tested, described and analyzed.

Chapter Six applies the model so far developed to portal frame structures. A concerted effort is made to analyze and describe the loading response and failure mechanism of a 30.0m span frame. Additionally, comparisons are made with existing first-order manual design analysis, computer-based analysis and second-order analysis. Finally, the behaviour predicted by the

Analytic Structures method is compared to first- and second-order manual analyses over a range of span-to-height ratios.

Chapter Seven summarises the work presented here and draws conclusions before introducing potential avenues for extending Analytic Structures. Chapter Eight contains the tables of Curvature data prepared in Chapter Four, a list of relevant notation and the bibliography.

Chapter 2

Literature Review

2.1 Introduction

The literature describing the present state of the art may be broadly grouped under three labels: that concerning empirical research to gain an understanding of the physical properties of steel structures; that concerning the design codes created to ensure safe deployment of steelwork; and that concerning the computer-based analysis methods which automate the codified design requirements. Due to the novel direction set out in the Chapter Three and following, there are additional components which do not fit this taxonomy, which are also included for reference.

2.2 Development of the Elasto-Plastic Model

The history of the elasto-plastic design method is a long and drawn-out one. The lack of mathematical tools required for analysis of statically indeterminate structures led to a compromise in the regular use of elastic design methods. The Bessemer process arrived in the middle of C.19 and provided an inexpensive means to produce ductile steel, and overcame the difficulties in producing purified non-brittle steel. Consequently, experimental work with brittle pig-iron supported the initial development of linear elastic models for failure loads. This led to formidable structures, such as the Forth Rail Bridge. Opened in 1889 following the delays in its construction caused by the catastrophic collapse during a storm of a comparable cast iron rail bridge across the River Tay, this structure features steelwork that remains within the elastic range of stress-strain behaviour and deflects very little, even in extreme winds. Clearly this design strategy is excessive and pressure to economise, in parallel with the scientific search for a better representation of the physical processes of structural steel behaviour, provided the impetus to improve the design methodology

The first analytical treatment of strut design was performed by Leon-

hard Euler (1707-1783) and published in *Mathematica* (1736) as part of the revolution he brought about in applied mathematics. Euler is credited with the first development of useful calculus methods, although rivalling Newton's method of fluxions, his approach is a closer relation to that used today.

Euler's analysis concerns a perfect strut (a straight circular column, free from material residual stresses and of homogeneous material around its loaded axis to avoid buckling along an axis containing some defect) held upright by pins at each end and subjected to a pure axial load, resulting in no lateral deflection of the member under the load. Labelling its critical buckling load P_{cr}, the member, being perfect, only shrinks in length under compression until it reaches P_{cr}. This model can be amended to describe an imperfect strut if a small lateral force is added halfway down the the member currently under consideration, ensuring that the strut has an initial lack of straightness. Euler's work has:

$$P_{cr} = \frac{n^2 \pi^2 EI}{L^2}. \tag{2.1}$$

The origin of this equation is described in Chapter 3. The value of n in (2.1) can be any integer, thus permitting an infinite number of mathematically-stable if physically impossible buckled positions (for example those described in Figure 2.1, which would have to be obtained in the same manner as the half-sine buckled state here: initial perturbing loads forcing deviation from true at the positions corresponding to the extremes of the Sine curve). Practicalities of physical systems force $n = 1$ whether by gravity effects, material imperfections, the inclusion of strain hardening, local buckling or other properties of a member.

The need to understand the behaviour of steel beyond its elastic stress-strain region was recognised by A.E.H. Love (1892) who identified the need for plastic behaviour to be included in design and construction and whose comments identify that elastic theory to be *"at [that] time behind engineering practice"*. The inclusion of this aspect of structural behaviour in design practice did not begin for almost forty years.
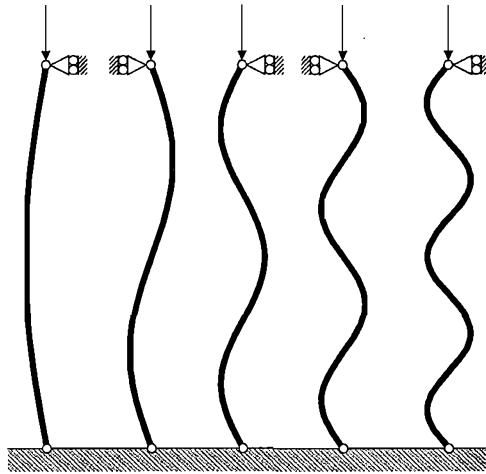
Figure 2.1: The first five modes of buckling as prescribed by Euler's strut-buckling formula
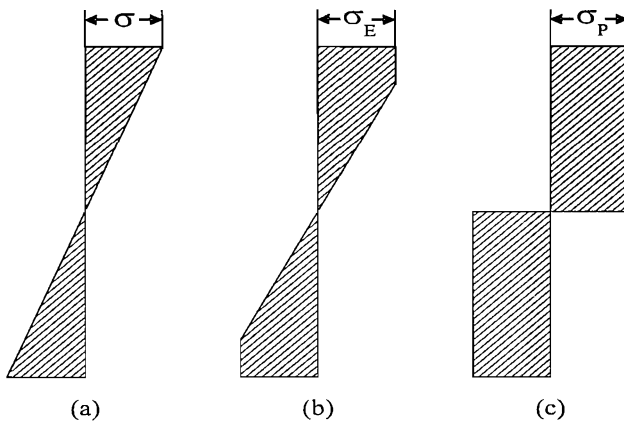
Figure 2.2: Example stress distribution across a uniform member (a) under general load – elastic behaviour; (b) with yield spreading from the extreme fibres into the cross-section at elastic limit; (c) idealised visualisation of full-plastic state for hinge in simple-plastic theory

8

A few years later J.A. Ewing (1899) suggested Figure 2.2, the enduring standard for understanding the behaviour of a member whose cross-section is under bending moment loads at the limit of elastic behaviour and beyond (see Moy, 1996, Ch. 2). The figure placed here identifies the stress distribution for a pure bending moment across a member of uniform cross-section. Applied bending moments cause flexure of the beam, which stretches one edge and compresses the other, giving rise to a stress distribution across the depth of the member (Figure 2.2(a)). When it is assumed that the material of the member follows an elastic-plastic stress-strain relationship (describing a flat stress response beyond the elastic region, as per Figure 2.3(f)), the standard description of plastic stress distribution passes a boundary where parts of the cross-section become plastic (Figure 2.2(b)) and moves on to a terminal state of bending moment, where the state depicted in Figure 2.2(c) is presented as the final, albeit impossible in practice, state which arises as the stress continues to increase with bending moments. In addition, this work advised that the bending moment which permits collapse cannot be calculated using the engineer's beam equation due to the inability of the method to support non-elastic values of stress. J.F. Baker (1956) was critical that Ewing may never have seen Figure 2.2(c) in experimental conditions; however its reasonable appearance became the standard explanation of simple plastic theory for the development of the stress distribution as bending moment increases up to its maximum (plastic hinge) value.

It now serves to qualify the stress-strain curves used in the variety of analyses surveyed here. As introduced in Figure 2.3, the six key stress-strain relationships used in analysis. Initial work assumes a linear elastic response with a fixed deflection regardless of the load (Figure 2.3(a)); "Elasto-plastic" analysis uses Figure 2.3(f), but pragmatic need to simplify calculations led to the "rigid-plastic" mode of Figure 2.3(e), which avoided additional moment behaviour caused by displacements arising from loading; Figure 2.3(b) is the "rigid-plastic-rigid" sequence of Horne and Medland (1966), which allows
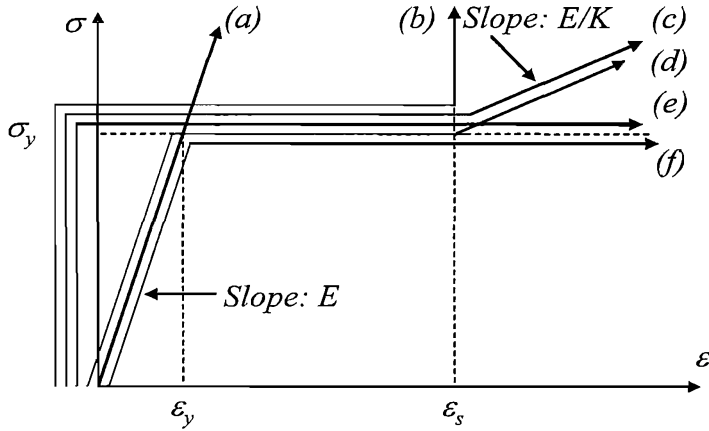
Figure 2.3: Variety of stress-strain relationships
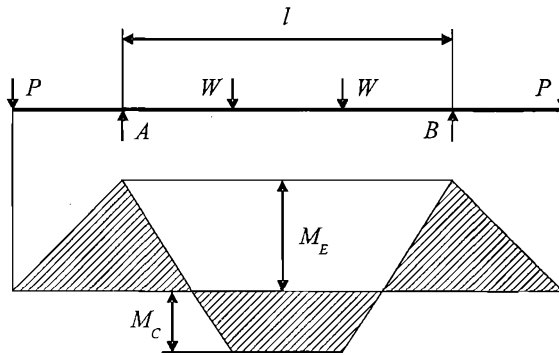
Figure 2.4: Maier-Liebnitz' overspecified beam layout above bending moment diagram

post-plastic movement approximating strain hardening while strain-locking any hinges which may form. The same work refers to a "rigid-plastic-strain-hardened" stress-strain curve of Medland (1963). The full elastic-plastic-strain-hardened relationship is Figure 2.3(d).

In the 1950s and 1960s, the inclusion of plastic and post-plastic analysis in design methods began. Baker (1956), cited the above two works of (Ewing, 1899) and (Love, 1892), and wrote of the experiments performed upon fixed-end beams by Maier-Liebnitz (1936). Maier-Liebnitz showed that a built-in beam (Figure 2.4) can support more load than elastic theory predicted.

10
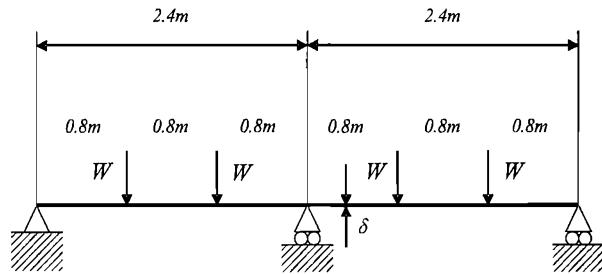
Figure 2.5: First overspecified structure tested by Baker

This featured the moments at supports for the span of the beam reaching the elastic moment, M_E and continuing to support further increases of load while not failing. The forces spread out across the beam until $M_C = M_P$, when a failure mechanism was formed. This inspired Baker to perform his pioneering investigations into the plastic behaviour of continuous beams and portal frames. First, a two-span beam was set up with its three supports on the level (Figure 2.5) and loaded to collapse. The test was repeated twice again, once with the central support raised (first, $\delta > 0$ in Figure 2.5) and once lowered (second, $\delta < 0$ in Figure 2.5) sufficiently far as to generate a moment equal to M_P. The beam was subsequently loaded to collapse, and in doing so it supported more then the predicted elastic load. Baker states that the raising or sinking of supports does not affect the ultimate strength of a continuous beam. The second round of testing focused upon portal frames and observed a second linear stage of deflection after the elastic stage (as Figure 2.6). This was assumed to be relating to the spread of a plastic hinge across the centre of the span (although work detailed in Chapter Six shows this to be strain-hardening resistance to further buckling).

Horne (1960) lays weight to the need for elasto-plastic design principles with arguments arising from the lack of attention paid to potential impact of partial plasticity on frame instability. The work moves toward the goal of estimating the elasto-plastic collapse load by examining a selection of approximate techniques for calculating the collapse load. It first explores the

11
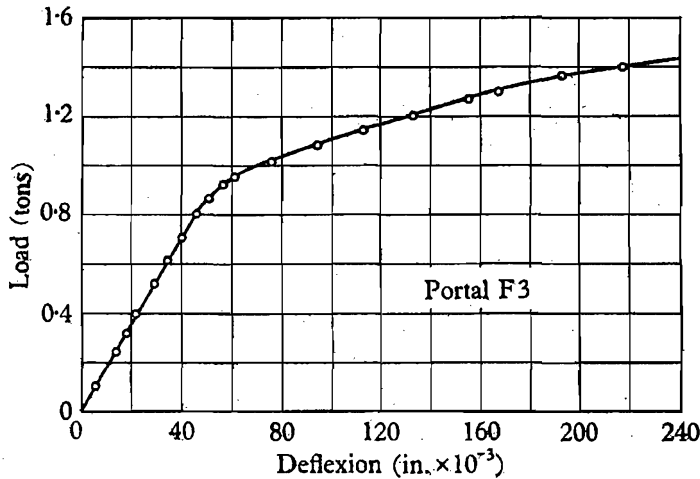
Figure 2.6: Load-deflection curve from Baker (1956) portal frame testing, with second linear section of deflection, after formation of the first plastic hinge

methods of elastic, simple (or rigid) plastic and elastic-plastic analyses (which use Figure 2.3 (a), (e) and (f) respectively) and explains their assumptions before providing graphical comparisons, such as those replicated in Figure 2.7. This figure indicates a geometrical method for ascertaining a measure, μ, of the deflection for a given load factor λ_{load} of the elastic-plastic mode of behaviour, and does so without neglecting axial loads.

The curve ODE of Figure 2.7 is an approximation to $OAFD$ of Figure 2.8 by geometric construction. The value sought is λ_F, the Merchant-Rankine collapse load. Merchant (1954) generalised the Rankine load for the collapse of a strut (from Rankine (1866)). The Merchant-Rankine load is an estimate of the lower bound of failure and was created to balance the elastic yield and elasto-plastic critical loads when it was observed that the elasto-plastic value was too conservative and the first elastic critical mode too inefficient an estimator of collapse. Horne uses this estimator in search of an optimal load factor, designated λ_H due to the later use of λ to denote slenderness.

The first search for λ_H uses a parameterisation by μ to examine the stability of the underlying energy function of a structure, and such a relationship

12
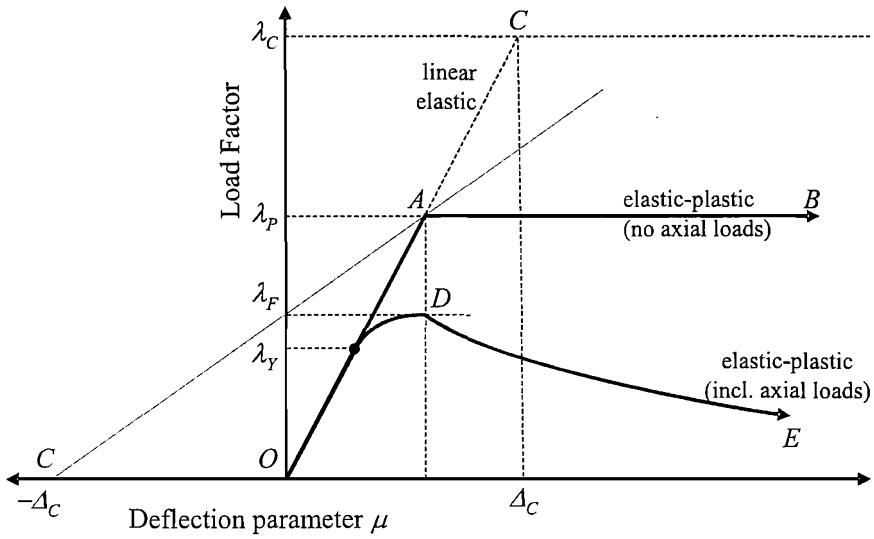
Figure 2.7: Comparison of failure modes corresponding to analysis methods and their relation to Merchant-Rankine load
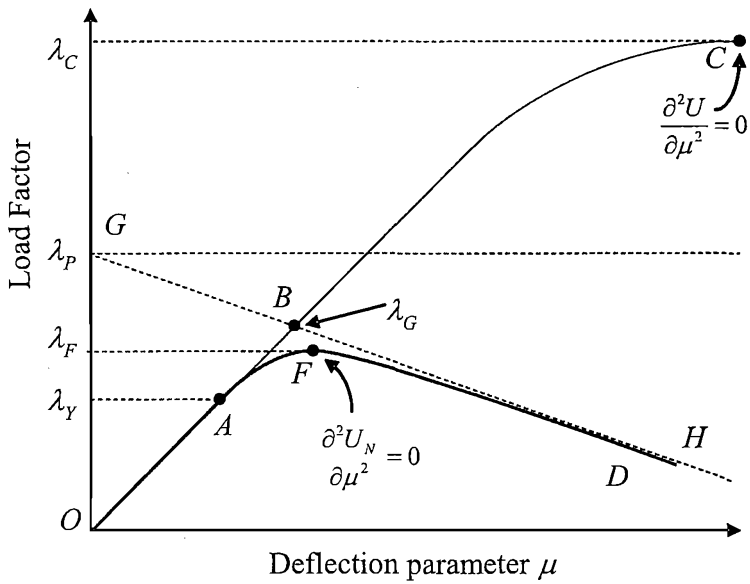
Figure 2.8: Load deflection curve for an elastic-plastic structure

provides both Figures 2.7 and 2.8; the second search, experimental observation. The line GH in Figure 2.8 comes from the assumption of a rigid-plastic stress-strain relationship (2.3(e)); ideal elastic behaviour would predict OBC, which rises to λ_C, the first elastic critical load arising from axial loading. The actual path $OAFD$ moves linearly from the origin to the start-of-yield at A, which corresponds to λ_Y, to the peak at F with corresponding λ_F, before approaching GH asymptotically. Horne notes that Merchant's claims, (Merchant, 1954, 1956) that λ_F may be a function of λ_C, λ_P and λ_Y as well as λ_G, alleviate the problem of calculating λ_F directly. Horne states that the easiest way to calculate λ_F involves the use of λ_C and λ_P.

Horne (1963) fleshes out the previous rationale for calculating an analogue to $OAFD$ of 2.8. λ_F, the Merchant-Rankine load, is the peak of the elasto-plastic curve which includes the effects of axial thrusts (in Figure 2.7). First, the deflection (Δ_c) and load factor (λ_c) corresponding to the elastic critical buckling load are calculated. The intersection of the Load Factor axis (above λ_Y) with the line from $-\Delta_c$ to OAD supplies the height on the vertical axis; the position on the horizontal axis remains the horizontal position along OAD. Horne claimed that λ_F is the maximum at D. A serious criticism of all the methods outlined in this work (Horne (1963)) is implicit in this graph (2.8): neglecting axial loads will cause significant over-estimation of the carrying capacity of critical parts of a structure.

Additionally, Horne (1963) is critical of methods neglecting the strain-hardening properties of steel, including an heuristic explanation for the spread of plasticity in a hinge. Figure 2.9 illustrates the development of this mode of thought, using the example of a simply-supported beam with a point load at its mid-span: (a) under rigid-plastic a strain-strain relationship (as per 2.3(e)); (b) an elasto-plastic stress-strain curve provides deflection before a plastic hinge is formed; (c) the inclusion of a stress-strain model featuring a strain hardening behaviour following short section of post-elastic plasticity was expected to produce a length of the beam made flexible under the

14
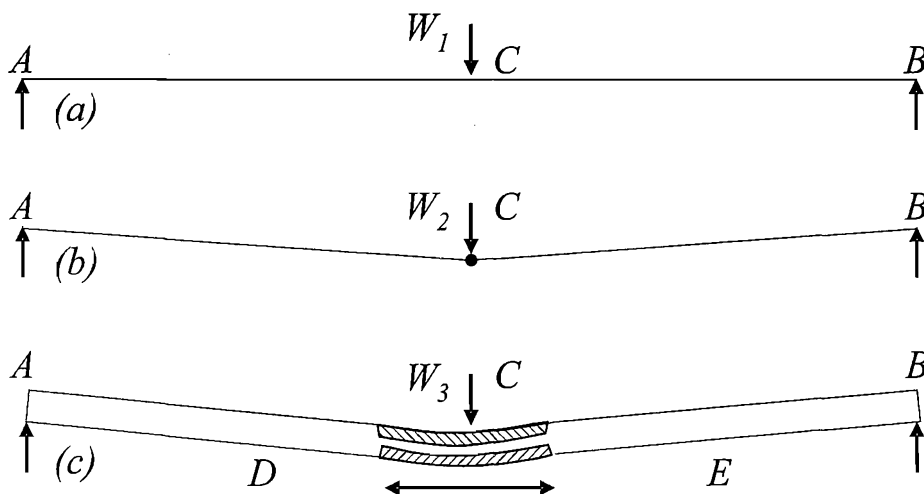
Figure 2.9: Advances in failure modelling, from the simple plastic of (a), through the single plastic hinge of (b) to the plastic section (DE) in which strain hardening spreads curvature of (c)
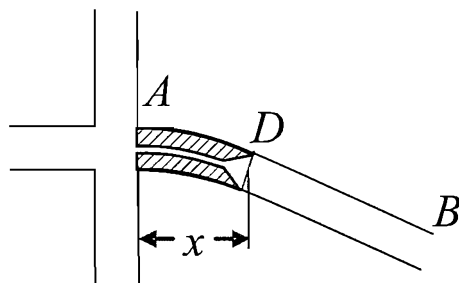
Figure 2.10: Spread of plasticity in a strain-hardened hinge mechanism

loading, which spreads as the load increases.

An example strain-hardened hinge is featured in 2.10, for which 2.11 is a graph for moment against distance x from the body of the structure (both are after figures from Horne (1960)). Horne calculates the work performed in the situation of Figures 2.10 and 2.11 to be:

$$\lambda \Sigma W s + \lambda \Sigma R \beta^2 l = \Sigma M_P \phi + \Sigma \frac{E}{k f_y} \frac{I}{hS} M_P \phi^2 \qquad (2.2)$$

under certain assumptions concerning the scale of the terms involved. The first summation may be analogous to $P - \delta$ deflections and concerns the load

Figure 2.11: Graph of moment used to calculate work absorbed in 2.10

factor λ, loads W and small-scale deflections s; the second, an analogue of $P - \Delta$ effects, with axial loads R, hinge rotations β and l for loaded member lengths; the third calculates work done against member elasticity, using M_P for plastic moment, ϕ for total rotation at a joint; and the fourth incorporates the extra work done against strain hardening: $\frac{E}{k}$ is the strain-hardening modulus; f_y, the yield stress; I, second moment of area; S, the plastic modulus; h the 'effective lever arm' of Figure 2.11; and M_P and ϕ are as before. The load factor λ will not be less than λ_P if the strain-hardening components in Equation 2.2 are not less than those of the $P - \Delta$ effects. Thus Horne shows that strain-hardening has the potential to compensate for frame instability which would otherwise lower the load-bearing capacity of a frame to less than that of a simple-plastic collapse load. Horne additionally concludes that computer modelling is the only reasonable place to include the strain-hardened behaviour due to the complexity it brings manual calculations.

Horne and Medland (1966) identifies *"strain hardening is sufficient in many cases, particularly single-storey frames, to contrast the effect of deformations on fail load"*, which is a step forward for the inclusion of strain-hardened behaviour but at the same time a step backwards in its bypassing the inclusion of second-order effects in steel design. The inclusion of the

rigid-plastic-strain-hardened method of Medland (1963) showed that strain hardening allowed the mean stress in the flanges to be considered as varying linearly with the curvature. Using a value of slope for the strain hardening section $\frac{E}{K}$, where K is the proportional strain-hardening modulus, analysis of the average curvature for mean stress permits the formation of an estimate of the length of the strain-hardened plastic hinge, along with the creation of a family of curves for members relating their curvature and loading under rigid-plastic strain-hardened deformation. The use of (another) parameter k set at the ratio of strain-hardening yield strain to strain at elastic yield has these curves underestimate the curvature and stresses. Medland found that taking a value for k just above this ratio gives good agreement with observed data, but determining exactly how large the discrepancy between these two values (K and k) requires inspection of the bending-moment diagrams for a specific structure and its loading. Medland and Horne conclude by saying that the best place to apply the phenomenon of strain hardening is in the digital computation of structural behaviour, particularly in the creation of look-up tables and interpolating functions to describe such behaviour.

Byfield et al. (2005) examine Mill Test Data in the search for k and find that S275 data supports k at 9.3; S335, 9.0; a conservative $k = 10$ is deemed a pragmatic choice for practice, both in terms of accuracy and safety. From their analysis of 50 mill tests of hot-rolled I- and H-sections, an accurate stress-strain relationship is developed and its parameters supplied. Additionally, a computer-generated moment-curvature relationship is described, a process central to the present work and fully-explained in Chapters Three and Four.

Davies (2006) identifies that the above work (Byfield et al., 2005) ignored buckling effects in creating a moment-curvature relationship and acknowledges that in the absence of either local or lateral-torsional buckling, strain hardening effects have a rationale for inclusion in structural steel design. However, these benefits disappear in the presence of local buckling of the ten-

sion flange or lateral-torsional buckling, even if these factors are accounted for in design. Additionally, the closing comments identifying the existence of a relation between strain hardening and rotation capacity are upheld in this project's computer simulations.

2.3 Design Codes

The need for safety is balanced against economy in construction, requiring legislated direction as to acceptable tolerances in design and construction. A response to this has been the development of safe guidelines in the BS449, BS968, BS5950 and Eurocode 3 standards for the use of structural steelwork. Their inception arose from the development of understanding of beam behaviour.

Euler's initial steps were augmented 150 years after *Mechanica* by W.E. Ayrton and J. Perry's work (1886), which demonstrated an alternative means for calculating the crushing stress in a strut (which is has a lower-case p symbol denoting stress while the corresponding Euler force calculated above is denoted as an upper-case P symbol).

Initially assuming a pinned strut restrained so that its sinusoidal bowing with amplitude δ is solely in one plane, purely elastic behaviour, no internal stresses and that collapse occurs when the stress on the concave side reaches p_{cr}. Then p_{cr} is the lesser root of

$$(p_Y - p_{cr})(p_E - p_{cr}) = \eta p_E p_{cr} \qquad (2.3)$$

for $p_E = \frac{\pi^2 E}{\lambda^2}$, p_y is the yield stress or chosen design strength and p_{cr} the required mean stress at failure. The other terms: η relates a non-dimensional factor measuring initial crookedness; E the stress-strain properties of the material; λ the slenderness of the beam (measured as the ratio of l, the buckled length of the member as measured on its original axis to r, the radius of gyration). Initially $\eta = \frac{c \cdot \delta}{r^2}$ from the derivation, with c being the distance

from the centroid to the extreme fibres of the beam and $\delta = \frac{l}{1000}$. Ayrton and Perry also suggested that $\eta = \alpha\lambda$, where α is an empirically-derived imperfection factor used to reduce η to accommodate the existence of internal stresses. Incorporating the internal stresses into this design approach led to the adjustment made by Robertson in 1925, which became part of the first UK code for structural steelwork, BS449 (1932, 1948). His recommendations included setting $\alpha = 0.003$ and using this value for the curves of a number of grades of steel.

BCSA-29 (1966), discussing the use of plastic design in portal frames to BS968 (1942, 1968) says: "*The effect of axial loads in the frame on the value of M_P is usually negligible, but a safe allowance may be made by calculating M_P for the highest axial load in any member*", which is a striking commentary three years after the discussion of member thrusts in structural analysis in Horne (1963) as discussed above. Unfortunately these axial loads may be hard to determine in the rafters of a portal frame, leading to the conventionally-held the assumption that the largest axial load appears in the columns. Davies (1990) examines the basis of the BS5950 (1990) requirements concerning the omission of axial load effects during the calculation of the stability of pitched-roof portal frames. In such frames the axial thrusts along rafters can be of the same order as the axial thrusts in the columns. §5.5.3.2 of BS5950, in particular, is criticised heavily, suggesting that frames are used with low axial thrusts or more-rigourous second-order analyses are performed. Alternative calculations are suggested to ameliorate these difficulties of the 1990 edition of BS5950-I.

Further developments to design code BS449 arose from G.B. Godfrey's derivation in (1962) of a curve based upon

$$\eta = \frac{3}{10}(\frac{l/r}{1000})^2 \qquad (2.4)$$

along with the suggestion in 1972 by J.B. Dwight of·a new formula to allow for the plateau at low slenderness indicated by experimental data. This newer

formula is

$$\eta = \alpha(\lambda - s_1). \tag{2.5}$$

Dwight also suggested that an appropriate value for s_1 would be one fifth of the value of λ for which the Euler P_{cr} causes crushing ($s_1 = \frac{\pi}{5}\sqrt{\frac{E}{p_Y}}$). This was chosen because it also the slenderness for which the strain-hardening Euler curve (using E_s instead of E) cuts the line $P_{cr} = P_y$. When codified in the preliminary publication of BS5950 (1985), four values of α are used in this equation to produce four curves used to classify column behaviour according to cross-section type, with four classes of cross-section having values of $\alpha = 0.0020$, 0.0035, 0.0055, and 0.0080.

BS5950 recommends calculating the compression strength for a strut from the methodology as stated above. In BS5950 (1990), Appendix C (p.98) the Perry strut formula describes the compressive strength (not the stress, despite being expressed in units of stress), appearing as

$$p_c = \frac{p_E p_Y}{\phi + \sqrt{\phi^2 - p_E p_Y}} \tag{2.6}$$

where ϕ is used here as a constant: $\phi = \frac{p_Y + (\eta+1)p_E}{2}$. This is analogous to the derivation described above. The four column curves described above, included to model different cross-sections, are as above. §7.2.6 (p.10) of BS5950 : Part 2 : 1985 describes the assumed lack-of-straightness: non-hollow sections used as beams or compression members, $\kappa_s = 3mm$ or $\frac{l}{1000}$, whichever is the greater. Any other section has $\kappa_s = \frac{l}{500}$. Eurocode 3 (EC3 (1992) Figure 5.5.1, Page 100) specifies an initial lack-of-straightness of $\frac{l}{600}$, for a member appropriate to its Class A buckling curve. Lacking perfect straightness in this way ensures that any beam will eventually buckle under critical load. The same section contains a formula for calculating the maximum moment in a beam, halfway between two points of inflexion (Figure 2.12). The formula is

$$M_{max} = \frac{\eta f_c S}{(1 - f_c/p_E)}, \tag{2.7}$$

20
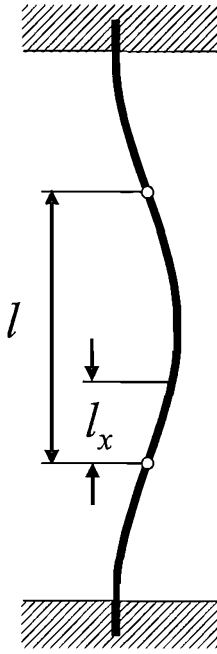
Figure 2.12: A built-in strut with deflection contributing points of curvature inflexion

and the corresponding moment in the member at a distance l_x from a point of inflexion is: $M_{max}\sin(\frac{180l_x}{l})$, inheriting a sinusoidal bowing from Euler's strut formula.

The curves were selected for BS5950 upon the previous work done for BS449 (1959 and 1969/1970), and were in line with contemporaneous recommended standards curves for the European Community (as it was then known). The mode of buckling which most influences the curves is the interactive combination of both flexural and local buckling. British Standards before BS5950 used two methods to describe this behaviour, the Effective Section Method and the Effective Yield Method. The Effective Section Method is relates the collapse load to the critical strength by disregarding an ineffective width in the column. The collapse load is then calculated from

$$W_c = P_c(\Sigma b_e t). \tag{2.8}$$

It uses the same column curve as the original section. The Effective Yield

21

Method arose in BS449 and uses a reduction in the yield stress σ_{py}, for which

$$\sigma_{py} = \frac{\Sigma b_e t}{\Sigma b t}.$$

Then

$$W_c = p_c' \Sigma b t \tag{2.9}$$

where p_c' comes from the reduced column curve of σ_{py}.

BS5950:1990 itself contains three methods for describing interactive flexural behaviour. One is called the Compact Zone method, and is in essence the Effective Section Method outlined above. The second, Effective Width, is most suited to beam-columns. When use in pure column situations it diminishes the buckling stress where it appears in the ratio for b_e referring to an element remote from the axis of buckling. These methods appear somewhat conservative when applied to columns and are better suited to beams. The third method, again, reduces the yield stress such that the given section becomes compact. Then the collapse load is acquired as for that of a compact member with this reduced yield.

Bayo and Loureiro (2001) provides a good introduction to the Eurocode 3 requirements and mechanism for buckling analysis of steel-framed structures, while providing an alternative method which avoids having to calculate an 'effective length' between points of inflexion of a buckled member. Also included is a clear flow chart describing selection criteria for picking the analysis (direct second-order, first-order with amplified moment or first-order with sway moment) most appropriate to the planned design.

The specifications in Eurocode 3 relating to compression members continue the pattern of multiple strut curves, each appropriate to the axis of buckling and the type of cross-section of the beam (Taylor (2001)). Taylor identifies the design procedures for rolled steel, stating that compression member have a relative slenderness calculated for them before the reduction factor χ is applied to the cross-sectional resistance to obtain the member bucking resistance. Taylor also identifies that combined axial force and bend-

ing make use of an interaction formula which was not finalised at the time
of publication.

§5.5 (p.97) of Eurocode 3 contains tabulated imperfection factors for uni-
form members, tabulated reduction factors and equations for describing flex-
ural buckling. Torsional and interactive torsional-flexural buckling appear in
Part 1.3 of Eurocode 3. Equation 5.45 (*ibid*, §5.5.1.1, p.97) of Eurocode 3
describes the design buckling resistance of a strut:

$$N_{b.Rd} = \frac{\chi \beta_A A f_Y}{y_{M1}}.$$ (2.10)

χ is the reduction factor, either calculated from a formula or, where appro-
priate, read from table 5.5.2 (p.99) (here as Figure 2.13). f_y is the yield
strength; β_A a scaling factor equal to 1 for cross-sections labelled 'Class 1',
'Class 2' and 'Class 3', and equal to $\frac{A_{eff}}{A}$ for beams labelled 'Class 4'. $y_M 1$
is the resistance of the member to buckling, equal to 1.1 (ibid, p.54). For a
member of constant cross-section under constant axial compression, χ may
be calculated from

$$\chi = \frac{1}{\phi + \sqrt{\phi^2 - \bar{\lambda}^2}}, \ \chi \leq 1,$$ (2.11)

for which

$$\phi = \frac{1}{2}(1 + \alpha(\bar{\lambda} - \frac{1}{5}) + \bar{\lambda}^2)$$ (2.12)

$$\bar{\lambda} = \sqrt{\frac{\beta_A A f_Y}{N_{cr}}} = \frac{\lambda}{\lambda_1}\sqrt{\beta_A}$$ (2.13)

$$\lambda = \frac{l}{r}$$ (2.14)

$$\lambda_1 = \pi\sqrt{\frac{E}{f_Y}} = \frac{939}{10}\eta$$ (2.15)

$$\eta = \sqrt{\frac{235}{f_Y}} \qquad (\text{for} f_Y \text{in} N/mm^2).$$ (2.16)

α, the imperfection factor, for curve (a) is 0.21; 0.34 for (b); 0.49 for (c); and
0.76 for (d).

Member imperfections or initial lack of straightness are covered in §5.2.4.5
(*ibid*, p.64), part of the section on internal forces and moments, indicating

23

Table 5.5.2 Reduction factors χ				
$\bar{\lambda}$	Buckling curve			
	a	b	c	d
0,2	1,0000	1,0000	1,0000	1,0000
0,3	0,9775	0,9641	0,9491	0,9235
0,4	0,9528	0,9261	0,8973	0,8504
0,5	0,9243	0,8842	0,8430	0,7793
0,6	0,8900	0,8371	0,7854	0,7100
0,7	0,8477	0,7837	0,7247	0,6431
0,8	0,7957	0,7245	0,6622	0,5797
0,9	0,7339	0,6612	0,5998	0,5208
1,0	0,6656	0,5970	0,5399	0,4671
1,1	0,5960	0,5352	0,4842	0,4189
1,2	0,5300	0,4781	0,4338	0,3762
1,3	0,4703	0,4269	0,3888	0,3385
1,4	0,4179	0,3817	0,3492	0,3055
1,5	0,3724	0,3422	0,3145	0,2766
1,6	0,3332	0,3079	0,2842	0,2512
1,7	0,2994	0,2781	0,2577	0,2289
1,8	0,2702	0,2521	0,2345	0,2093
1,9	0,2449	0,2294	0,2141	0,1920
2,0	0,2229	0,2095	0,1962	0,1766
2,1	0,2036	0,1920	0,1803	0,1630
2,2	0,1867	0,1765	0,1662	0,1508
2,3	0,1717	0,1628	0,1537	0,1399
2,4	0,1585	0,1506	0,1425	0,1302
2,5	0,1467	0,1397	0,1325	0,1214
2,6	0,1362	0,1299	0,1234	0,1134
2,7	0,1267	0,1211	0,1153	0,1062
2,8	0,1182	0,1132	0,1079	0,0997
2,9	0,1105	0,1060	0,1012	0,0937
3,0	0,1036	0,0994	0,0951	0,0882

Figure 2.13: Eurocode (EN1993) Table 5.5.2 for reduction factors χ of steel

that such arise only in second-order treatment of design stability. Figure 5.5.1 (here as Figure 2.14) describes the three approaches to analysis of a beam depending upon whether it is governed by elastic behaviour, linear or non-linear plastic behaviour, as well as modifying y_{M1} for the beam. Table 5.5.3 (Figure 2.15) describes the mechanism by which the appropriate flexural buckling curve is to be calculated. Conservative estimates abound within Eurocode 3.

The Commentary to German design code DIN 18800 (Beuth Kommentar DIN-18800) supplies Figure 2.16, which quantifies the scale of internal strains used in the simulations below. The same reference supplies the EC3 recommendations for internal strains in hot-rolled steel members.

Some of Davies' (1990) suggestions are included in BS5950 Part I (2000), and its content in this area is explained in King (2001a). The notion of frame second-order effects (termed $P - \Delta$ effects) and member second order effects (termed $P - \delta$ effects) are introduced (Figure 2.17). The work has a particular focus on in-plane stability because out-of-plane buckling can be checked as per any other beam-column between lateral restraints. In-plane buckling relies on the stiffness of members within a portal frame to resist buckling effects; the scale of the axial loads in the rafters being comparable to the columnar thrusts requires different stability checks in pitched-roof portal frames than for beam-and-column structures. King introduces the elastic critical buckling factor, λ_{CR}, for portal frames, analogous to the Euler strut formula 2.1 which appears in Figure 2.18. The use of load factors in analysis is criticised briefly, due to the impact caused to $P - \Delta$ effects by variations in loading patterns.

2.4   Analysis Using Digital Computation

Davies (1966) is heavily critical of the Merchant-Rankine load advocated above, particularly where its predictions about the failure load compromise

Cross-section		Method of global analysis	
Method used to verify resistance	Section type and axis	Elastic or Rigid - Plastic or Elastic - Perfectly plastic	Elasto-plastic (plastic zone method)
Elastic [5.4.8.2]	Any	$\alpha(\bar\lambda - 0.2)\, k_\gamma\, W_{el}/A$	-
Linear plastic [5.4.8.1(12)]	Any	$\alpha(\bar\lambda - 0.2)\, k_\gamma\, W_{pl}/A$	-
Non-linear plastic [5.4.8.1(1) to (11)]	I-section yy-axis	$1.33\alpha(\bar\lambda - 0.2)\, k_\gamma\, W_{pl}/A$	$\alpha(\bar\lambda - 0.2)\, k_\gamma\, W_{pl}/A$
	I-section zz-axis	$2.0\, k_\gamma\, e_{eff}/\epsilon$	$k_\gamma\, e_{eff}/\epsilon$
	Rectangular hollow section	$1.33\alpha(\bar\lambda - 0.2)\, k_\gamma\, W_{pl}/A$	$\alpha(\bar\lambda - 0.2)\, k_\gamma\, W_{pl}/A$
	Circular hollow section	$1.5\, k_\gamma\, e_{eff}/\epsilon$	$k_\gamma\, e_{eff}/\epsilon$

$k_\gamma = (1 - k_\delta) + 2 k_\delta \bar\lambda$ but $k_\gamma \geq 1.0$

Buckling curve	α	e_{eff}	k_δ			
			$\gamma_{M1} = 1.05$	$\gamma_{M1} = 1.10$	$\gamma_{M1} = 1.15$	$\gamma_{M1} = 1.20$
a	0.21	$l/600$	0.12	0.23	0.33	0.42
b	0.34	$l/380$	0.08	0.15	0.22	0.28
c	0.49	$l/270$	0.06	0.11	0.16	0.20
d	0.76	$l/180$	0.04	0.08	0.11	0.14

Non-uniform members:

Use value of W_{el}/A or W_{pl}/A at centre of buckling length l

Figure 5.5.1 Design values of equivalent initial bow imperfection $e_{o,d}$

Figure 2.14: EN1993 Figure 5.5.1 guidelines for initial lack of straightness and recommended path for analysis

Table 5.5.3 Selection of buckling curve for a cross-section

Cross section	Limits	Buckling about axis	Buckling curve
Rolled I-sections	h/b > 1,2: $t_f \leq 40mm$	y - y z - z	a b
	40mm < t_f ≤ 100mm	y - y z - z	b c
	h/b ≤ 1,2: $t_f \leq 100mm$	y - y z - z	b c
	t_f > 100mm	y - y z - z	d d
Welded I-sections	$t_f \leq 40mm$	y - y z - z	b c
	t_f > 40mm	y - y z - z	c d
Hollow sections	hot rolled	any	a
	cold formed - using f_{yb} *)	any	b
	cold formed - using f_{ya} *)	any	c
Welded box sections	generally (except as below)	any	b
	thick welds and b/t_f < 30 h/t_w < 30	y - y z - z	c c
U-, L-, T- and solid sections		any	c

*) See 5.5.1.4(4) and figure 5.5.2

Figure 2.15: EC3 buckling curve selection criteria

27
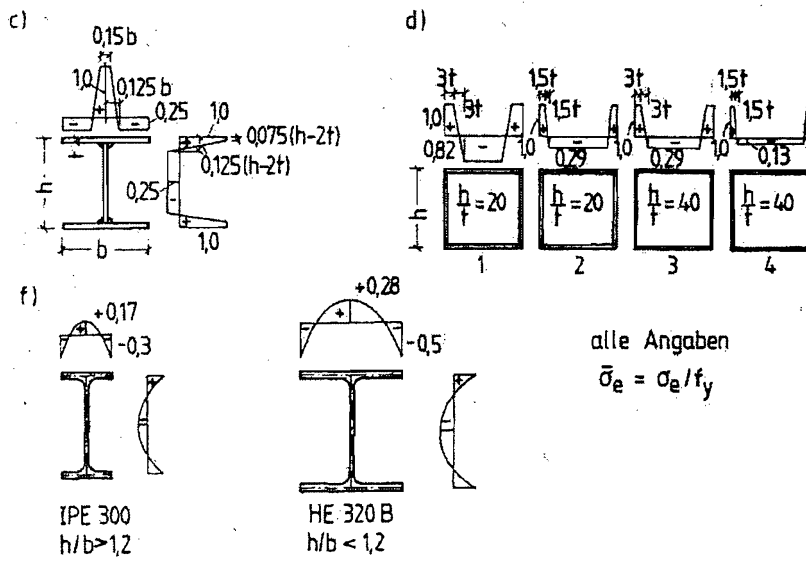
Figure 2.16: Residual Stresses as a ratio of yield stress (p_y) for welded sections, (c); tubular sections, (d) and hot rolled I- and H-sections, (f)
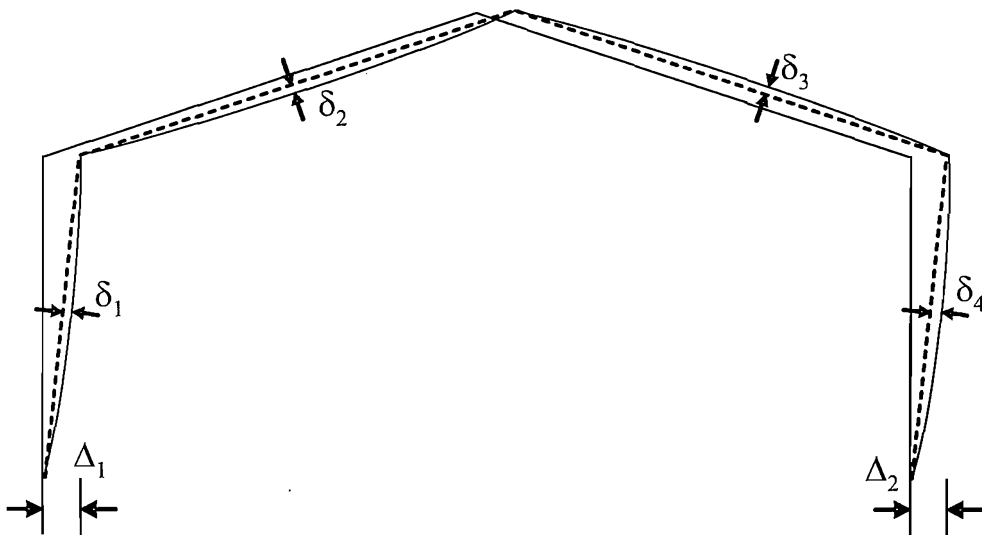
Figure 2.17: Portal frame under sway deflection showing $P - \Delta$ and $P - \delta$ effects
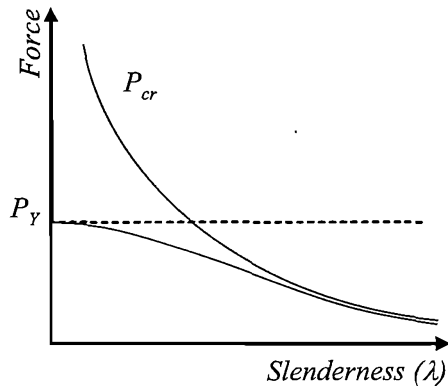
Figure 2.18: Elastic critical buckling load (P_{CR}) and squash load (P_Y) for a strut

the stability of portal frames. The work introduces the formulation and techniques involved in computer-based structural analysis using stiffness matrices. It concludes that strain-hardening behaviour can compensate for the loss of carrying capacity due to frame instability as it raises the expected value of failure load; that Merchant-Rankine remains an appropriate tool for assessing failure load despite criticism; and that the inclusion of strain hardening behaviour in computer modelling is the only reasonable place to account for the benefits of strain-hardening in tall or slender structures.

The advocacy of digital computation is continued in Davies (1967), which has particular application to shakedown loads. In contrast to overloading collapse, shakedown is the repeated loading and unloading below the calculated elastic yield load which causes plasticity in the extreme fibres of members and leads to reduced load-bearing capacity and eventual collapse. (The primary paths to collapse investigated in the 1960's were shakedown and overloading collapse; present opinion as per Davies (2002) is that failure arising from shakedown methods is far less likely than collapse brought about by overloading.) A form of analysis is explained which uses stiffness matrix methods to find points at which simple plastic hinges are found, alongside the discussion of an extension of the method to discover the stability of the structure. How-

29
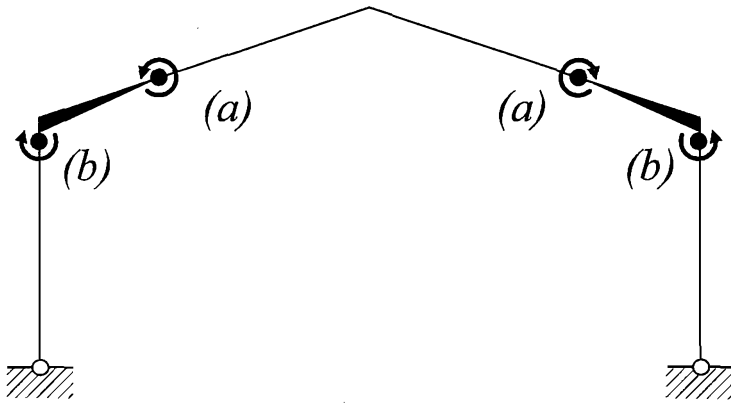
Figure 2.19: Two false fail mechanisms found by FE methods: many simulations predict hinges with opposite sign to actual bending moments such that hinge mechanisms in any combination of (a) or (b) cannot permit collapse. Correct fail mechanisms match the direction for their bending moments to that of the failure mechanism.

ever, the use of computer-bound analyses is advocated in conjunction with engineering judgement and manual calculations. Davies (1988) stated that blindly trusting the computer-based packages for safe designs is not appropriate both for safety and for the expert status of Chartered Civil Engineer. Preliminary calculations and tests of the results from computer programs are essential because many, at the time, failed to correctly predict the failure mode of certain pinned-base portal frames (Figure 2.19) precisely because the moments causing some of the predicted hinges act in the opposite direction to the motion of failure. A suggested mechanism is detailed to test if the predictions of a given computer system are correct (Figure 2.20).

Chan (2001) is in basic agreement with Davies' criticisms of unwise use of computer-based analysis tools. While establishing the need for member imperfections to be included in the initial state of a structure modelled by computer (and introducing an extension to present FEM methods which incorporates this information), Chan says: "*[The presented technique's] extension to design by elasto-plastic analysis under static and cyclic loads requires*

$$\frac{13}{10}W \qquad \frac{7}{10}W$$

(a) Geometry & Loading

(b) Elastic bending moments

0.516WL

0.756WL   0.728WL

(c) Bending moments at collapse

0.675WL

0.65WL   0.675WL

(d) Collapse mechanism

$$1.926\frac{M_P}{L} \qquad 1.037\frac{M_P}{L}$$
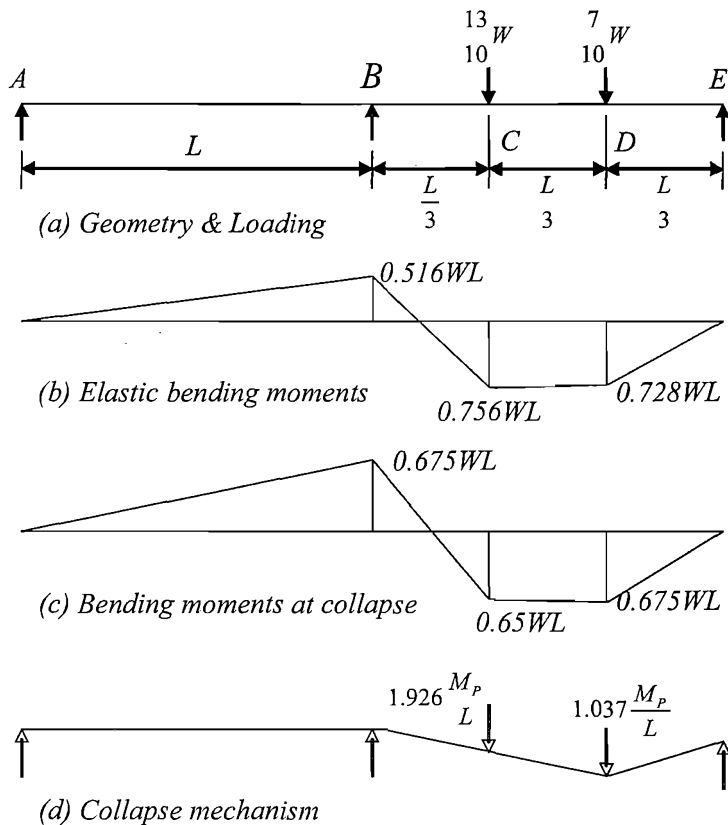
Figure 2.20: Suggested test model from Davies (1988) to evaluate correctness of supplied results from computer-based analysis

careful standardisation, codification and, most importantly, training to engineers. Benchmarked examples and software should be established for quality assurance. Before this objective is achieved, all these powerful analysis tools remain toys for experienced researchers and engineers."

One method by which justification may be found for a particular computation method could be full-scale tests of structures, against whose data computed predictions may be compared. Davies et al. (1990) explains the processes followed in constructing and testing sample frames (Figure 2.21) in order to calibrate results provided by simulation. The computer model of this structure had two gable ends and one portal frame span. The hinges were simulated as partially flexible at their links to the haunched sections

31
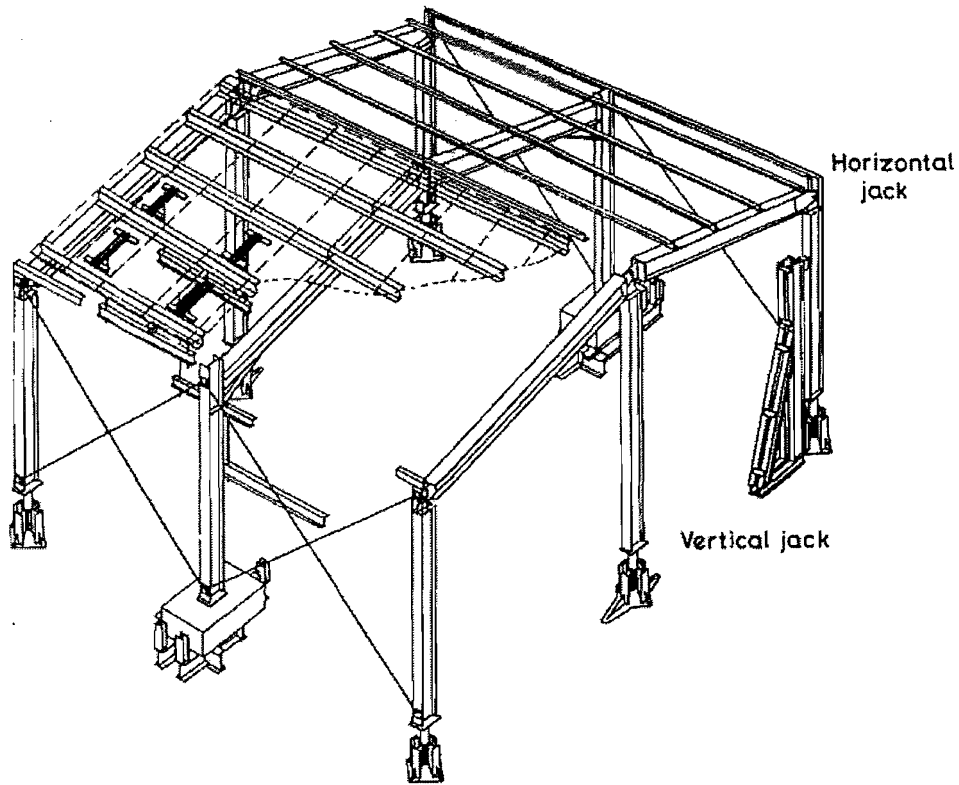
Fig 1. General arrangement for tests

Figure 2.21: Single-bay portal frame tested in Davies et al. (1990)

of the rafters. Both the simulation and laboratory tests were reported as failing due to shear distortion at the interface between the column and rafter haunches (Figures 2.22, 2.22). The conclusion that the model, calibrated by the test data, will provide accurate information about the structural behaviour under loads must face the criticism that the full-scale tests were stage-managed to alleviate potential problems related to the transfer of load via the purlins supporting the roof sections or related to the stiff end-frames not flexing when the central span was loaded and the resulting effect upon the total load carried by the portal; these effects are not mitigated in contemporary construction so further research to quantify them and include them in computer-based analysis may be beneficial.
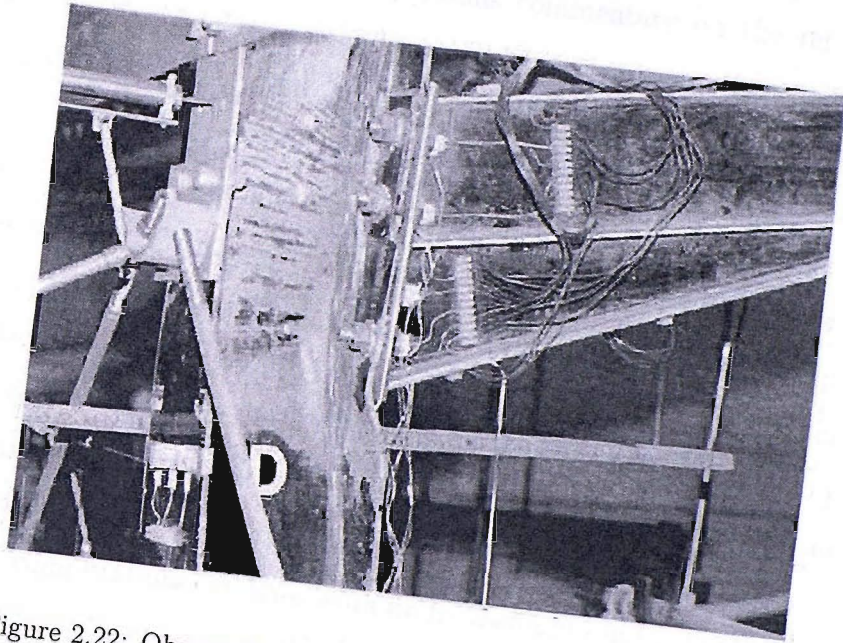
Figure 2.22: Observed Failure Mode of Test Frame in Figure 2.21

Shear hinge
distortion

Compression zone
failure
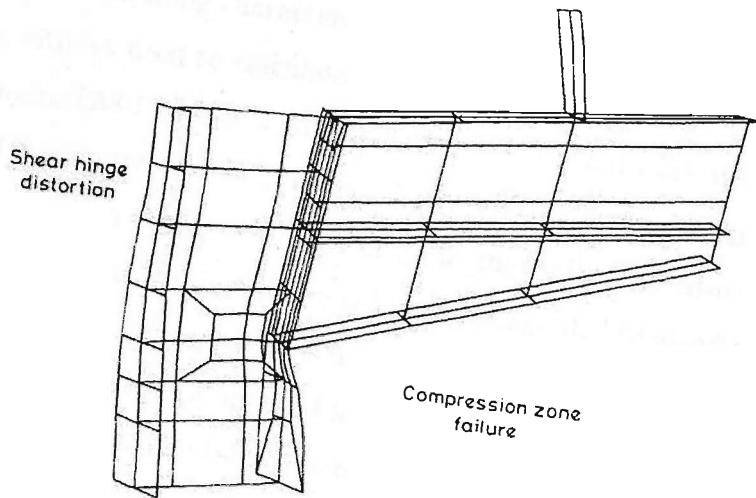
Figure 2.23: Predicted Failure Mode of test Frame in Figure 2.21

Davies (2002) qualifies the previous commentary on the reliability of computer-based analysis methods with solid explanations of correct methodology, which had been known for a number of years before this paper was submitted but withheld due to commercial considerations. Davies explains the steps taken to perform analysis by F.E.M. and Influence Coefficient methods (a computational technique arising from the special use of shakedown to predict the collapse load), with the inclusion of steps necessary to protect against the false fail methods mentioned above. Also explained are the inclusion of second-order effects, semi-rigid joints and strain-hardening in elasto-plastic frame analysis and the inclusion of semi-rigid joints and stability functions in Influence Coefficient analysis.

Most computational systems work under assumptions of elastic behaviour up to plasticity in order to predict the formation of plastic hinges and consequent collapse mechanism. Gu and Chan (2005) is no different, but seeks to unify the process of design around simulation and analysis without reference to structural design codes. As part of the journey in this direction, they provide an advanced element for finite element analysis which is able to describe the large-scale buckling characteristics of a member using a single element in analysis without need to calculate the effective length of the member. Bayo and Loureiro (2001) follow a similar path, using virtual work in contrast to Gu and Chan's direct solving of the differential equilibrium equation.

Lay and Smith (1965) were critical of the impossible curvature of Figure 2.2(c), insisting that strain-hardening has to be included to avoid the impossible discontinuity in cross-sections with fully-plastic hinges. Their investigation developed a numerical method for characterising the moment-curvature relationship which included strain hardening. The method makes use of a table of corresponding values which assist the search for valid values of moment at the end of loaded members, allowing the deflection of a structure to be calculated. Their predicted curves showed good agreement with contemporaneous results. Their recommendation to characterise the moment-curvature

34

and moment-axial-curvature relationships informed the techniques used in Chapters Three and Four.

2.5 Additional Ideas

Internal stresses within members further complicate the process of analysis. Hot rolled steel, with different portions of the cross section cooling at different rates, locks in additional stress distributions which can significantly affect the behaviour of the member under loading. Szalai and Papp (2005) extended existing work approximating internal stress distributions in I-shaped members and made it effective for structural analysis. Where previous assumed stress distributions had sought to satisfy the equilibrium of moments in both axes of a cross section and associated normal forces, Szalai and Papp recognised that torsional forces and bimoment needed to be satisfied also. Governed by five equations (one for normal forces, two for moments, one for bimoment of torsion and one for twisting forces), they selected a parabolic distribution for internal stresses and found the algebraic expression of stress distribution across the web and flange:

$$c_f = \alpha f_Y \frac{bt_f(3b^2 + 4h_0^2)}{2b^3 t_f + 8bh_0^2 t_f + h_0^3 t_w}; \tag{2.17}$$

$$a_f = -\alpha f_Y \frac{20b^3 t_f + 48bh_0^2 t_f + 5h_0^3 t_w}{b^2(2b^3 t_f + 8bh_0^2 t_f + h_0^3 t_w)}; \tag{2.18}$$

$$c_w = -\alpha f_Y \frac{bt_f(8b^3 t_f + 3bh_0^2 t_w + 2h_0^3 t_w)}{2h_0 t_w(2b^3 t_f + 8bh_0^2 t_f + h_0^3 t_w)}; \tag{2.19}$$

$$a_w = \alpha f_Y \frac{2bt_f(8b^3 t_f + 9bh_0^2 t_w + 10h_0^3 t_w)}{h_0^3 t_w(2b^3 t_f + 8bh_0^2 t_f + h_0^3 t_w)}; \tag{2.20}$$

It must be acknowledged that the distributions featuring in this work assume each member is made of infinitesimally-thin plates, which permits one-dimensional parametrisation across the width of the flange or depth of the web, an area which can be extended. However, this model shows good agreement with the previous work, with additional support for modelling lateral torsional buckling and similar modes of failure.

It is difficult to place Rolfe (2005) within this discussion. Offering an alternative framework entirely for structural work which uses series summation to continuously model structural elements, this paper requires a different kind of appreciation than given to the texts discussed above. Its main feature is an introduction to Chebyshev (or Tschebyshef) polynomials and the use of these series summations to follow the curves of known structural elements. A Chebyshev polynomial is a special polynomial series calculated for a normalised length, that is one of the range (-1,+1), whose terms are equidistant along an arc of radius one. This makes the distribution of corresponding terms of the series along the (-1, +1) axis non-uniform, guaranteeing convergence and vastly improving the rate at which convergence is obtained. The absolute maximum error is smaller than other polynomial series methods and so the use of these series to describe the deflection, shear forces, bending moments etc. of structural members is highly suited. Rolfe works through a few examples, showing that integer coefficients may be retained throughout the calculations. It must be noted that the Chebyshev polynomials are independent of the level of complexity used to model structures and that an assumption of small deviation and simple stress-strain properties can increase the errors arising in calculation. This would indicate that they are a useful tool for desk-based checking of state or the generation of initial predictions.

2.6   Summary

The aim of this chapter has been to provide an overview of the present state of steel design theory and practice. Practicality and a correspondence between theory and reality have driven the empirical research which supports developments in theory and which in turn provides the means to analyse the behaviour of structures. This is in turn tempered by the legal requirements for safe construction of real structures, expressed in structural design codes. Computer-based analyses speed the process of designing structures according

to design codes

Love (1892) identified that theory of structural steel beyond elasticity was lacking, with theory being in advance of practice; Ewing (1899) began to work towards an elastic-plastic theory. The need for consistency and safety against the pressure to economise in real structures led to the creation of design codes, including those for steelwork was not an exception. British Standards 449, 968 and 5950 have provided engineers with safe limits for practice. In the 1950's and 1960's the quest for a strong theoretical foundation resumed, with Baker, Horne and Medland contributing plastic and post-plastic analyses. Unfortunately, Horne (1963) arrived at the erroneous conclusion that strain hardening may be sufficient to counteract the effects of deflection on collapse load, providing the older theory with a reprieve. At that time a new means of analysis arose with the arrival of digital computers. Davies and others have set the standard for Stiffness Matrix methods, which have been championed for a nearly half a century. As the present work heads toward the implementation of another computer-based analysis, the words of Chan (2001) should temper the approach: "Benchmarked examples and software should be established for quality assurance. Before this objective is achieved, all these powerful analysis tools remain toys for experienced researchers and engineers."

Having identified the state of present theory and design methodology, the present work on Analytic Structures sets out in a novel direction in order to provide alternative insights into structural members and their failure. In particular, hot-rolled steel structures form the particular focus of this work. However, before these structures can analysed, a firm grounding in the mathematical methods of Analytic Structures is required. This is presented in Chapter Three.

Chapter 3

Core Mathematics
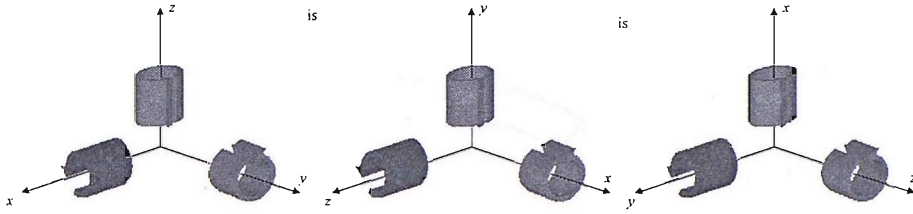
Figure 3.1: Three-dimensional Cartesian axes

3.1 Basic conventions

In this project, the standard axes and rotation convention are used, including the $Oxyz$ system of three-dimensional Cartesian axes, also known as the right-hand triple. Figure 3.1 illustrates how the triple can be applied to a set of axes. A rotation about an axis is denoted as 'positive' on appearing clockwise when viewed up the axis i.e. looking as z increases a clockwise rotation is recorded as positive. This is analogous to holding a right-hand fist with thumb extended around an axis with the thumb and fingers indicating positive motion and rotation, respectively. This convention is chosen because it maintains consistency of signs.

This chosen convention conveniently includes that of a positively-signed force acting a positive distance from the origin and has a positive value of moment (as does its counterpart in a couple: a negatively-signed force a negative distance from the same point of reference). A moment formed from such a couple brings about positive curvature; a positive moment brings about positively-signed deflection. Finally, with curvature of members being such an important factor in in-plane flexure, $\kappa = \frac{1}{r_c}$ requires that the radius of curvature (r_c) will have a sign in sympathy with that of the curvature. Both positive and negative situations are illustrated in Figure 3.2, where the $Oxyz$ triple of axes has the x-axis entering the page, with positive direction away from the reader. Figure 3.2(a) has negative moment ahead of the cross-sectional slice at the start of the section and positive moment behind, which
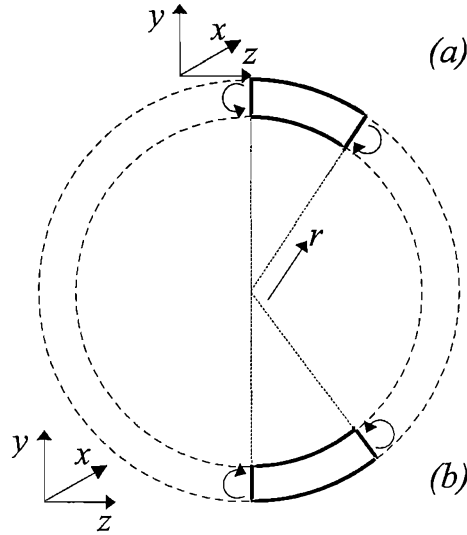
Figure 3.2: Sign convention of moments and curvature

is part of a negative overall moment. This total moment accompanies a negative measurement of r_c agreeing with negative curvature and negative value of deflection. 3.2(b) has a positive curvature from a positive value of r_c, agreeing with positive moments and positive deflection along the member.

Beam elements are an essential tool for describing and understanding structural response to load. The beam in Figure 3.3 is shown with no forces having x components and the load being applied in the y-z plane. The z-axis is used to indicate distance along the beam in its initial state; when deflected its position is parameterised by s. This s is the distance along the beam found using terms in differential geometry. Given a beam or a structure that follows a function $F(y, z)$, the function can be parameterised by s related to y and z. This s is then used to describe the distance along the beam. Although the function F may not be described or written down in simple equation terms, the process of following the path of the deformed beam follows some function with a parameter that is labelled s.

For this project, the origin of the axis is placed at ground level on the corner of the structure under investigation so that all calculation of posi-
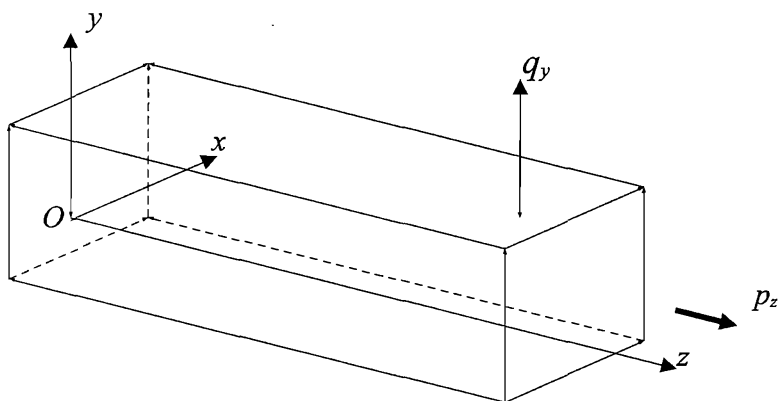
Figure 3.3: Typical loads on a beam
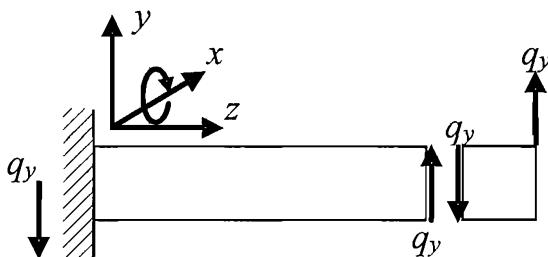
Figure 3.4: Internal action of a shear force

tion occurs in the positive-positive-positive octant of three-dimensional space. While working on the two-dimensional model of a single frame arch, the origin is placed so that the computer models it with positive x- and y-coordinates

These standard axes provide convenient shorthand while examining loaded beam systems. Figure 3.3 indicates the letter notation for various loads. A shear load will be denoted q and axial thrust p, each with subscripts indicating the direction in which they act. Torsion has not been included due to the nature of the beams under consideration: I-beam girders do not behave well under torsional forces and so every effort is made to avoid placing them under this type of load.

In addition to the Cartesian axes, the notion of a reporting surface needs
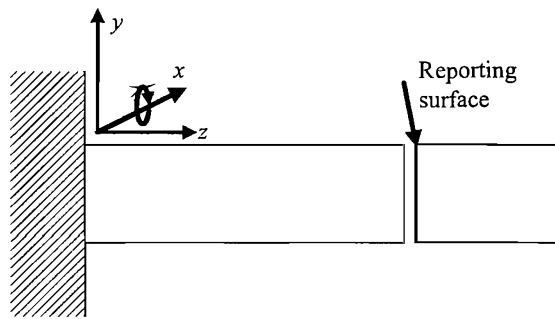
Figure 3.5: A typical reporting surface in a straight beam

introduction. The rotation sign convention informs how to record bending moments. The moment is clearly about some axis and this fact supplies an indication of how to record its sign. Figure 3.4 illustrates the internal shear forces in a section of a beam under a shear load, with a section at the end of it displayed distinct for illustration. The beam is in equilibrium, so the section at the end should have a reaction opposite to the external load, and then, at the join between the section and the main body of the beam, the force at the end of the beam is in the same direction as the external load. There are two possible forces to report as internal shear forces, one at either side of the surface between the two sections of the beam.

In this document, the term "reporting surface" will be used to describe the surface of a small cross-section whose behaviour under the load is being investigated. This surface is the one first met as progress is made along the beam away from the origin. Because the axes are usually set up to go along the beam, the reporting surface is most often that where the axis arrow "goes in" to the section being looked at. In more-complicated structures, such as the arch of a portal-frame roof, the path of the arch is followed. This is why the method is described as following the beam, progressing along it, initially moving away from the origin. The parameter s can be thought of as defining the location of the reporting surface.

Figure 3.5 indicates a reporting surface in a single beam, and Figure 3.6
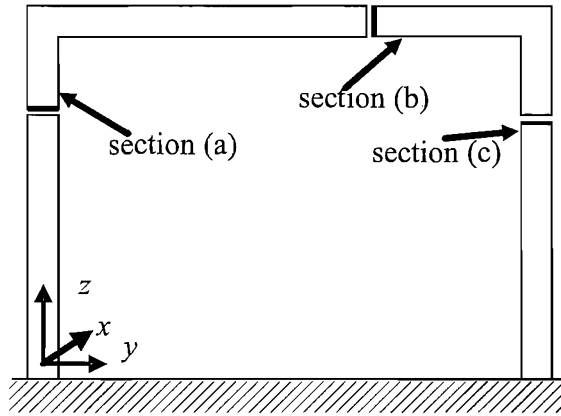
Figure 3.6: The reporting surfaces through a portal-frame

those in a portal frame, where the connected members are considered as one long curved beam. It must be noted that the bold line of section (a) in Figure 3.6 clearly is the start of a section into which the z-axis enters, whereas the bold line of section (b) is nearly at right-angles to the z-axis and the bold line at the start of section (c) apparently the wrong edge of the suggested section but remains the one to be used as it continues along the beam as described above.

3.2 Member segment parametrisation

The Engineer's Beam Equations supply

$$\frac{M}{I} = \frac{\sigma}{y} = \frac{E}{r_c},$$

(3.1)

which provides the relation

$$\kappa = \frac{1}{r_c} = \frac{M}{EI}.$$

(3.2)

This describes how the curvature, κ, depends upon the moment. Because of its reliance upon the Engineer's Beam Equations, it is complicit with the assumptions made for the derivation of those equations: linear elastic stress-strain behaviour; plane sections remaining plane and perpendicular to the

43
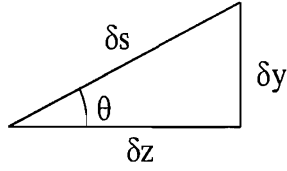
Figure 3.7: Triangle showing angle relationships that supply differential equations

beam core; and material homogeneity. Of these three assumptions, only one is kept in this project: that planar cross-sections remain planar and perpendicular to the member's core. The project's goals of simulating Steel Portal Frame structures make acceptable the assumption that shear forces can be neglected, due to the low likelihood that portal frame member failure arises from shear stresses. The core process by which the alternative mathematical derivation for structural analysis described here models members' loading and deformation follows a parameterised position along the core of its members.

Standard differential geometry results show, for a function y that depends upon z (i.e. $y = f(z)$), the arc length along that curve from a point a to a point x is:

$$s = \int_a^x \sqrt{1 + \left(\frac{dy}{dz}\right)^2}\, dz. \tag{3.3}$$

Also, from Figure 3.7, $\tan \theta = \frac{dy}{dz}$, which, when differentiated with respect to z, becomes

$$\sec^2 \theta \frac{d\theta}{dz} = \frac{d^2 y}{dz^2}. \tag{3.4}$$

This leaves

$$\frac{d\theta}{dz} = \frac{1}{(1 + \tan^2 \theta)} \frac{d^2 y}{dz^2} = \frac{\frac{d^2 y}{dz^2}}{\left(1 + \left(\frac{dy}{dz}\right)^2\right)}, \tag{3.5}$$

which, when combined with

$$\frac{ds}{dz} = \sqrt{1 + \left(\frac{dy}{dz}\right)^2} \tag{3.6}$$

44

(the differentiated form of 3.3), results:

$$\frac{1}{r_c} = \frac{d\theta}{ds} = \frac{d\theta}{dz}\frac{dz}{ds} = \frac{\frac{d^2y}{dz^2}}{\left(1 + \left(\frac{dy}{dz}\right)^2\right)}\frac{1}{\sqrt{1 + \left(\frac{dy}{dz}\right)^2}} = \frac{\frac{d^2y}{dz^2}}{\left(1 + \left(\frac{dy}{dz}\right)^2\right)^{\frac{3}{2}}}. \quad (3.7)$$

The above result differs from standard small-deflection theory, which uses

$$\frac{1}{r_c} = \frac{M}{EI} = \frac{d^2y}{dz^2} \quad (3.8)$$

This approximation relies upon assumptions of purely-elastic stress-strain behaviour and the deviation $\frac{dy}{dz}$ in Equation 3.7 to be small enough that its part in the denominator of the right-most expression in Equation 3.7 is approximately one. The implementation of the Analytic Structures method needs the additional detail provided by the denominator of Equation 3.7 and so cannot tolerate the loss of accuracy in the approximation of Equation 3.8.

However, the solutions to the system of equations under investigation here require that both elastic, plastic and strain-hardened material behaviour are described and incorporated into the structural behaviour, and that any scale of deflection is tolerated (for instance: although unlikely, slender members may be permitted to flex under loading to a degree greater than could be modelled accurately by small deflection theory). The system of equations described below side-steps the requirements of small deflection theory. The technique is able to describe members with built-in curvature (or initial lack-of-straightness such as the strut in Figure 3.8) and structures designed with flexible members.

3.3   Beam Behaviour

Figure 3.9 indicates internal bending moments arising from the load q_y. The cross-section at the left-most end is at rest. The internal bending moment can be thought of as counteracting the load on the beam-element at the left-most end of the beam. At any surface join between a beam element and main body of the beam, the bending moments cancel to ensure the beam is
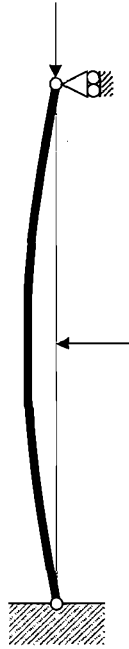
Figure 3.8: Pin-ended Euler strut with perturbation force at mid-section to ensure eventual buckling
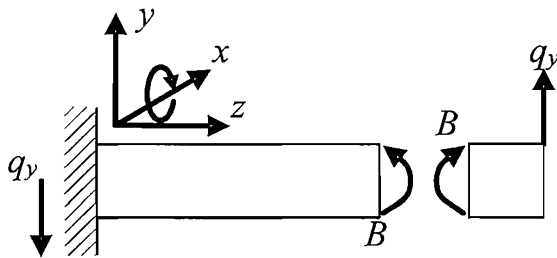
Figure 3.9: Internal shear forces in a beam

at rest. The example reporting surface shown in Figure 3.9 is a portion of the way through the member.

A built-in cantilever beam acting under the forces generated by a downward point-load at its free end and the reaction at the fixed end has its upper surface under tension and lower surface under compression. These forces cause elastic deformation and the lengthening and shortening of the upper and lower surfaces, respectively. There must remain a plane along the

46
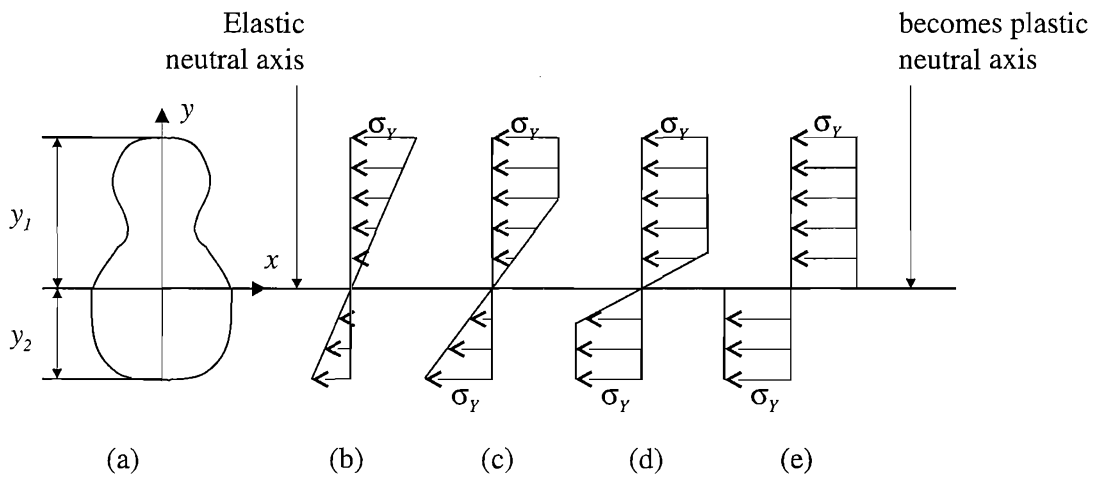
Figure 3.10: Stress distributions through a cross-section as stress increases to complete plasticity in a loaded member

length of the beam that remains unchanged in length. This plane is known as the neutral axis or neutral plane. Under bending moments alone, the neutral plane remains inside the body of the beam.

So far, the discussion of beam behaviour has been assumed to be within the elastic range of the steel material. It is important to quantify and allow for the abrupt jump to plastic (and thereafter strain-hardening) that occurs in a hypothetical 'extreme fibre' of a loaded steel cross-section. For the current discussion, it is assumed that an instantaneous discontinuity occurs at the transition point into plastic behaviour. Also assumed is an identical response to a load under both tension and compression, which may not happen in every material, and that plane sections remain plane under bending.

In order to start with a relatively simple elastic-plastic system, the loaded beam is taken as one that is symmetrical about the y-z plane. As with bending, a neutral axis emerges according to the shape of the cross-section, about which there is no stress. A beam loaded solely by moments satisfies the assumptions and allows the use of the Engineer's Beam Equation:

$$\sigma_z = \frac{My}{I}.$$

(3.9)

47

Eventually increasing M will result in σ_z reaching the maximum direct stress the beam can support, σ_Y, the point of elastic yield stress. This will happen according to the cross-sectional shape of the beam with either top or bottom (y1 or y2, respectively) of Figure 3.10 reaching the limit first. Figure 3.10 indicates the progression of yield in the material made as the moment increases to the plastic moment, M_P. This is the moment at which the entire cross-section is yielding and behaving plastically. As the moment M increases and the yield stress has been reached at one edge of the cross-section, yield spreads into the cross-section until the hypothetical end-stage is reached with the entire cross-section in plastic flow (Figure 3.10(e)). The theoretical moment which causes the entire cross-section to be in plastic flow is named the plastic moment, M_P. A beam in equilibrium that develops a plastic cross-section becomes free to flex about that point. The section becomes known as a plastic hinge, and well-placed plastic hinges will form a collapse mechanism for a system of beams. Statically determinate structures will collapse when a single plastic hinge is formed. In contrast, statically indeterminate structures are those whose behaviour under plastic flow does not necessarily allow sufficient plastic hinges to be formed to establish a failure mechanism, simply because their layout has too many supports. These require more than one plastic hinge before a failure mechanism may emerge. Figure 3.11 indicates a statically determinate structure which has a hinge forming a collapse mechanism, and includes the bending moment diagram which shows the plastic section forming the hinge and how it arises from the material being stressed so much that strains exceeding $\frac{\sigma_Y}{E}$ and the moments exceed M_E. The ratio of plastic moment to yield moment is known as the shape factor of the cross-section. Beams whose material is partly in an elastic state and partly plastic have their behaviour controlled by the elastic portions of the member, and this is referred to as "controlled plastic flow."

Among the techniques used to calculate beam behaviour for statically indeterminate systems (and a portal-frame being statically indeterminate)
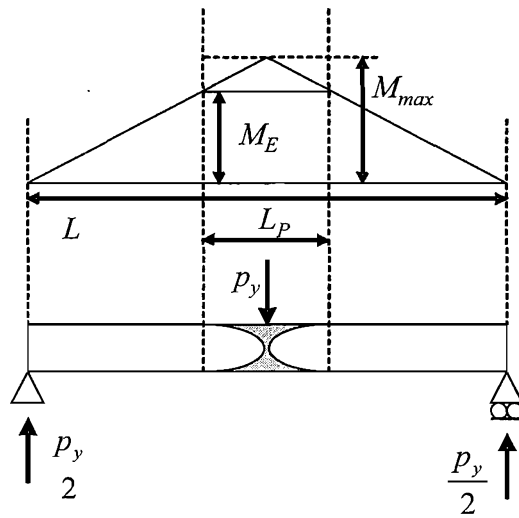
Figure 3.11: A beam with plastic hinge below its bending moment diagram (after Megson)

is the superposition method. It works by calculating the bending moments of beams, adding the factors of each force. It does not work for situations involving plastic flow. The order in which forces are applied affects the way in which plastic hinges develop. The alternative method is to apply small disturbances to a system in equilibrium. Small virtual displacements require work to be done on the system. The conservation of energy says that the sum of work done by internal forces is equal to that done by the external forces. This method allows the study of beam behaviour in both plastic and statically indeterminate situations. Ignoring these methods, computing solutions to the structure's system of equations, and making use of an accurate stress-strain curve to cover behaviour of beams under such loads that would bring about plastic and post-plastic behaviour also allows the inclusion of strain hardening behaviour to influence the stability of the structure

3.4 Strut Behaviour

The first mathematical treatment of strut behaviour was performed by Leonhard Euler (1707-1783) (published in Mechanica in 1736) as part of a revolution he brought about in the approach taken to applied mathematics. Euler is credited with the first development of useful calculus methods, although rivalled by Newton's method of fluxions, his approach is a closer relation to that used today.

If a perfect strut (one straight, free from residual stresses and homogenous around its loaded axis to avoid buckling along an axis containing some defect) is held upright by pins at each end and subjected to a pure axial load, there is no lateral deflection of the beam under the load. Labelling its critical buckling load P_{cr}, the member, being perfect, only shrinks in length under compression along the axis in which it is loaded, until the load reaches P_{cr}. The material imperfections of any other strut may be investigated by adding a small lateral force halfway down the member currently under consideration (as per Figure 3.8), which brings about a lack of straightness. Removing the lateral force at any load below P_{cr} will have the beam return to its straight position. However, when the axial load is P_{cr}, removing the lateral force does not let the beam return to its straight state, because the buckling load causes a natural state of equilibrium. In this state, the lateral deflection of the strut will grow as the load increases.

Given a particular deflection in this beam loaded at its critical load, the moment-curvature relationship under the assumption of purely-elastic behaviour has

$$\frac{M}{EI} = \frac{1}{r_c} = \frac{d\theta}{ds} = \frac{\frac{d^2y}{dz^2}}{\left(1 + \left(\frac{dy}{dz}\right)^2\right)^{\frac{3}{2}}}. \tag{3.10}$$

This links the moment, M, to the deflection y. In an infinitesimal section along the strut under load P_{cr}, the moment about the loaded axis, is $M = P_{cr}.y$. In the case where the deflection, $\frac{dy}{ds}$, is of the order of 0.1%, there is

a strong agreement in the approximation of

$$\frac{M}{EI} = -\frac{d^2y}{ds^2} \tag{3.11}$$

to Equation 3.10. This allows the rearrangement of this O.D.E. to show that it is a regular second-order ordinary differential equation of simple harmonic motion:

$$\frac{d^2y}{ds^2} + \frac{P_{cr} \cdot y}{EI} = 0. \tag{3.12}$$

This equation has solutions for $y = \mu \sin(\xi s) + \nu \cos(\xi s)$, where $\xi^2 = \frac{P_{cr}}{EI}$. The boundary conditions that supply μ and ν are $v = 0$ at $s = 0$ and $s = l$, where l is the length of the deflected beam as measured along the loaded axis. Thus $\nu = 0$, and examining μ provides information about P_{cr} (but not μ itself): a non-trivial solution to this problem requires $\sin(\xi l) = 0$. This forces $\xi l = n\pi$ where n is any whole number. The consequences of this is that, for a strut following a small deflection as per Euler's work,

$$P_{cr} = \frac{n^2 \pi^2 EI}{l^2}. \tag{3.13}$$

The value n in Equation 3.13 can be any integer, and so this solution permits an infinite number of stable buckling positions (for example those described by Figure 2.1). Using the term 'buckling points' to describe the extremes of a strut buckled into one of the later Euler buckling modes, a strut restrained to two-dimensional loading, lateral forces applied in the right pattern to match the buckling modes associated with an n larger than one and the appropriate P_{cr} load applied, the lateral forces could be removed and the crushed member would stand stable. Such unusual load patterns may permit buckled states for $n > 1$, but it is a safe assumption that nearly all load cases will buckle at the P_{cr} for $n = 1$ first. Alternatively, present practice applies restraints at the buckling points of a few low n in order to add resistance to buckling. This discussion highlights the flaws in Euler's method: it is easy to supply an n for which the physical capabilities of a beam cannot match the predictions of Euler's theory.

3.5 Algebraic Method

Previous formulaic descriptions of the limiting stresses for a compression member have relied upon curve-fitting and analytic approximation to empirical data curves. Recent developments in desktop computing have allowed the development of software that follows the codified patterns for the failure loads of beams. An alternative approach has been taken in the present work. Beginning with the equations of state for the beam and using high-precision numerical equation-solving tools, the behaviour of the system may be modelled under a number of conditions. The eventual goal is the development of equation-solving functions which enable each possible failure outcome of a structure to be considered.

Primarily, the analysis tool presented here quantifies the behaviour of an infinitesimal cross-section of a structure's members and uses equation solvers to follow through the path of the loaded and/or deflected member. The equations of state for a member under load can be synthesized to a set of differential equations which can then be solved either analytically by modern mathematical computer programs or numerically, according to the amount of information available about the system. There are three components to the method: differential geometry for following the path of the beam; solving the differential equations for the member so as to follow the deformed shape of the member and speeding up the calculation by tabulating the relationships between loading and deflection, all of which follow below. The computer modelling uses the assumptions that plane sections remain planar; local buckling is ignored; and there is no shear deformation. As this is a standard assumption with all present models of structural analysis it is justified despite the possibility that structures can be constructed whose connectors and loading defy this requirement.
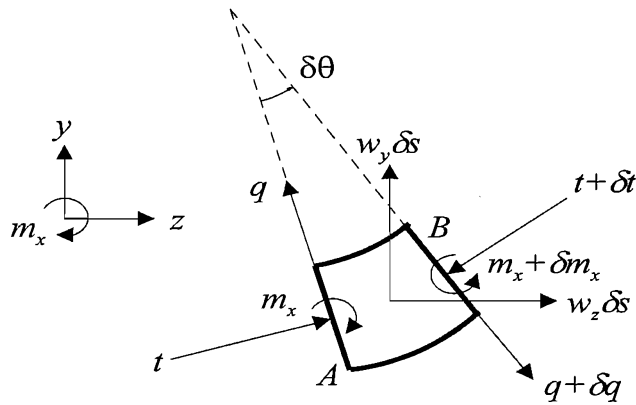
Figure 3.12: Short segment of beam and its forces
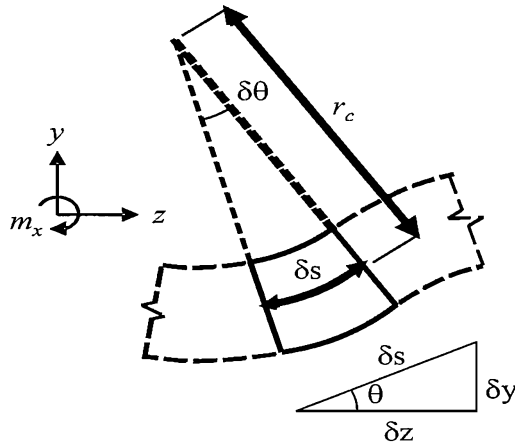
Figure 3.13: Short segment of beam and its measurements

3.5.1 Equations of State

A segment of a loaded beam, as Figure 3.12, is used to calculate the equations of state. These then can be solved to gain an understanding of the behaviour of the system. To begin, the notation is identified: the relationship between the length (δs) of an infinitesimal segment, its angle θ to reference axes and the corresponding changes in height on those axes ($\delta y, \delta z$). Additional geometric information is available from Figure 3.13. The triangle at the base of the figure, in the limits as the respective δs, δy, and δz tend to zero,

53

yields the relationships $\cos\theta = \frac{dz}{ds}$, and $\sin\theta = \frac{dy}{ds}$. Furthermore, measuring in radians permits $\delta s = r_c \delta\theta$. Consequently:

$$\kappa = \frac{1}{r_c} = \frac{d\theta}{ds}.$$

(3.14)

This allows the curvature of a given member to be specified in terms of its initial lack of straightness and the change in angle at a single cross-section generated by the forces acting upon it. The equations of state are (from Figure 3.12):

(Vertical Equilibrium)

$$f_y - f_y - \delta f_y + w_y \delta s = 0$$

(3.15)

(Horizontal Equilibrium)

$$f_z - f_z - \delta f_z + w_z \delta s = 0$$

(3.16)

When the limits of the δ's are calculated, 3.15 and 3.16 render the differential relationships between forces in the x- and y-directions as

$$\frac{df_y}{ds} = w_y$$

(3.17)

and

$$\frac{df_z}{ds} = w_z.$$

(3.18)

Taking moments about the surface marked B in Figure 3.12, using small angle approximations where appropriate and considering the limits of the δ's, the following ODE's are formed:

$$-w_z(\frac{\delta s^2}{2})\sin(\frac{\delta\theta}{2}) - w_y(\frac{\delta s^2}{2})\cos(\frac{\delta\theta}{2}) + q_y \cos(\delta\theta)\,\delta s - t_z \sin(\delta\theta)\,\delta s + M_x - M_x - \delta M_x = 0$$

(3.19)

$$-\frac{w_z \delta s}{2} - \frac{w_y \delta s}{2} + q_y - t_z \frac{\delta s}{r_c} = \frac{\delta M_x}{\delta s}$$

(3.20)

$$\frac{\delta M_x}{\delta s} = q_y.$$
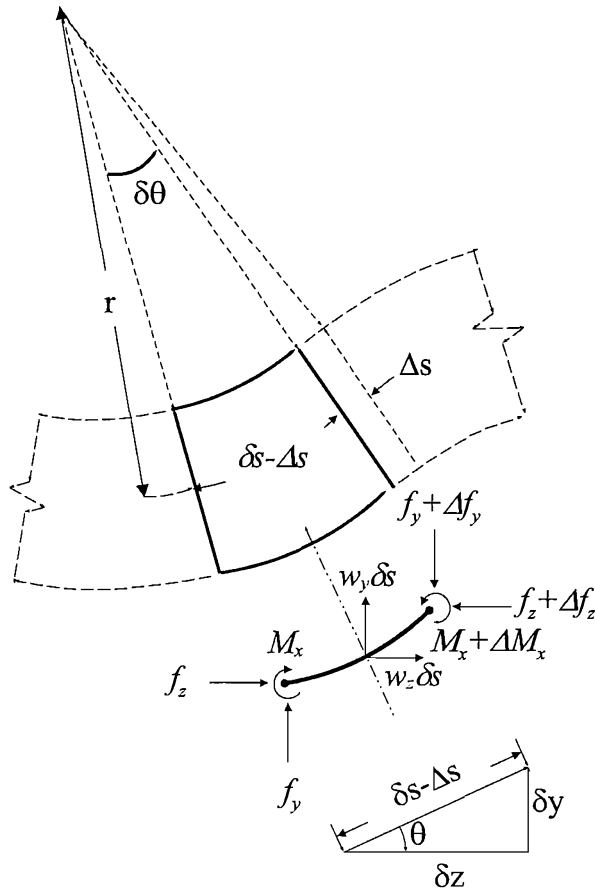
Figure 3.14: Beam segment under compression, including force diagram and relationship between δs, δy, δz, and $\delta\theta$

3.5.2 Length Contraction Under Axial Load

The initial mathematical model of beam-segments is inaccurate, failing to include any changes in length that occur when an elastic material is squashed or stretched. A steel beam or strut, when loaded, will change in length as it follows its stress-strain curve. To model this, the equations need to be altered to allow for this change in length. In constructing these equations, again, a small segment of the member is being considered so that small-angle approximation is appropriate. The situation and the trigonometric

relationship appear in Figure 3.14.

$$\epsilon = \frac{\Delta s}{\delta s} = \epsilon_\sigma \left[\frac{f_z \cos\theta + f_y \sin\theta}{A} \right] \qquad (3.21)$$

describes the relationship between the strain and the load, via the stress-strain relationship, when the beam segment is at angle θ to the $x - z$ plane. If the segment in question, originally δs in length, contracts by length Δs to become $\delta s - \Delta s$ long, the relationship to $\cos\theta$ as described by Figure 3.14 is , and use, as indicated in the Notation section of the Resources, $\epsilon_\sigma[]$ to indicate a strain calculated from its associated stress:

$$\cos\theta = \frac{\delta z}{\delta s - \Delta s} = \frac{\delta z}{\delta s}\left(\frac{1}{1 - \frac{\Delta s}{\delta s}}\right) = \frac{\delta z}{\delta s}\left(\frac{1}{1 - \epsilon}\right). \qquad (3.22)$$

Using the same logic for $\sin\theta$, the equations become:

$$\sin\theta = \frac{\delta y}{\delta s - \Delta s} = \frac{\delta y}{\delta s}\left(\frac{1}{1 - \epsilon}\right). \qquad (3.23)$$

The same 'squashy factor' appears in the shearing forces exactly as Equations 3.19 and 3.20 when the length 'δs' is replaced by '$\delta s - \Delta s$':

$$-w_z(\tfrac{\delta s}{2})(\delta s - \Delta s)\sin(\tfrac{\delta\theta}{2}) - w_y(\tfrac{\delta s}{2})(\delta s - \Delta s)\cos(\tfrac{\delta\theta}{2}) \qquad (3.24)$$

$$+q_y \cos(\delta\theta)(\delta s - \Delta s) - t_z \sin(\delta\theta)(\delta s - \Delta s)$$

$$+M_x - M_x - \delta M_x \qquad\qquad = 0$$

$$-\frac{w_z \delta s}{2} - \frac{w_y \delta s}{2} + q_y(1 - \frac{\Delta s}{\delta s}) - t_z \frac{\delta s}{r_c} = \frac{\delta M_x}{\delta s} \qquad (3.25)$$

$$\frac{dM_x}{ds} = q_y(1 - \epsilon). \qquad (3.26)$$

The differential equation relationships are found in the limit case as δy, δz and δs tend to zero:

$$\frac{dz}{ds} = (1 - \epsilon)\cos\theta = \cos\theta\left(1 - \epsilon_\sigma\left[\frac{f_z \cos\theta + f_y \sin\theta}{A}\right]\right) \qquad (3.27)$$

$$\frac{dy}{ds} = (1 - \epsilon)\sin\theta = \sin\theta\left(1 - \epsilon_\sigma\left[\frac{f_z \cos\theta + f_y \sin\theta}{A}\right]\right). \qquad (3.28)$$

3.5.3 Differential Equations of State

These six equations form the Differential Equations of State:

$$\frac{dz}{ds} = (1 - \epsilon) \cos \theta \qquad (3.29)$$

$$= \cos \theta \left(1 - \epsilon_\sigma \left[\frac{f_z \cos \theta + f_y \sin \theta}{A} \right] \right) \quad .$$

$$\frac{dy}{ds} = (1 - \epsilon) \sin \theta \qquad (3.30)$$

$$= \sin \theta \left(1 - \epsilon_\sigma \left[\frac{f_z \cos \theta + f_y \sin \theta}{A} \right] \right)$$

$$\frac{d\theta}{ds} = \frac{1}{r_c} + \kappa(s) \qquad (3.31)$$

$$\frac{df_y}{ds} = w_y \qquad (3.32)$$

$$\frac{df_z}{ds} = w_z \qquad (3.33)$$

$$\frac{dM_x}{ds} = q_y (1 - \epsilon) \qquad (3.34)$$

$$= (f_y \cos \theta + f_z \sin \theta) \left(1 - \epsilon_\sigma \left[\frac{f_z \cos \theta + f_y \sin \theta}{A} \right] \right) .$$

The variable s parameterises the member, indicating length along it through some central point and avoiding the use of x-, y- or z-coordinates. 'ϵ_σ []' is a function supplying a value of strain for a given value of stress, allowing a variety of stress-strain relationships to be included in the analysis. The loads, w_y and w_z can themselves be parameterised. The inclusion of θ allows the member to positioned and loaded at any angle; the $\frac{d\theta}{ds}$ permits modelling of curved members with a parametric function of curvature, $\kappa(s)$. All this may be included in the structure and the loads will yet deform it sensibly.

3.6 Shooting

Finding solutions to the six equations of state, above, requires a mathematical technique called 'Shooting'. Often it is assumed to be impossibly complicated while, in fact, it is deceptively simple. While this project the has a

large number of mathematical equations that need solving, the consistency of the system of equations is used to extract from known values the initial conditions which permit these values. Key to this method of analysis is the computer-based mathematics package used: Wolfram Research's *Mathematica*. Alternative software, such as Maplesoft's *Maple* or Mathworks' *Matlab* may be used but may not have the sophisticated algorithms of *Mathematica*.

3.6.1 Introducing Mathematica

Simulations in this project were designed and run on Mathematica 4.1 under the 32-bit edition of Microsoft's *Windows XP*. Mathematica is a powerful mathematics package combining algebraic and numerical tools for computation. It is presently at version 6.0 which supports 64-bit numerical accuracy and larger memory configurations where available and will run on Microsoft Windows, Apple Mac OS X and GNU/Linux platforms. The algebraic tools include symbolic differentiators and integrators, which can calculate sums such as

$$\Phi(x) = \frac{1}{2\pi} \int_{-\infty}^{x} e^{\frac{s^2}{2}} \, \mathrm{d}s. \tag{3.35}$$

The numerical tools provide algorithms for calculations where algebraic tools will not suffice. Many systems of ODE's and PDE's are not solvable by algebra alone, and numerical integration or numerical differentiation provide accurate alternatives. The standard numerical error within the 32-bit edition of *Mathematica* used, for a result x, $10^{-8} + |x|10^{-8}$.

In *Mathematica*, the commands to differentiate and integrate, solve a set of equations and solve a family of differential equations in symbolic or algebraic form are D, Integrate, Solve and DSolve. Differentiation has a numerical counterpart in the decimal fraction expression N$\left[\frac{a}{b}\right]$ (because in *Mathematica* simple fraction remains an algebraic statement unless explicitly forced to become a decimal expression); integration in the function NIntegrate; equation-solving in FindRoot; and differential equation-solving

in `NDSolve`. Due to the non-linear state of the full-detail stress-strain relationship, `NDSolve` and `FindRoot` are the key tools for solving the equations of state and discovering the unknown initial conditions that match the known boundary conditions. The numerical differential·equation solvers in *Mathematica* require initial conditions rather than general boundary conditions due to their use of iterative methods to find solutions.

3.6.2 Shooting for the area under a parabola

An example of shooting may be finding the relationship between the area below an upside-down parabola and coefficients of the parabola. The equation is known:

$$y = f(x) = -(ax^2 + bx + c). \tag{3.36}$$

Additionally the calculations are simplified if the parabola is centred on the y-axis, which makes $f(-x) = f(x)$ and $b = 0$. Also, when $x = 0$, $y = -c$. There is some number d which represents the area enclosed by the parabola and the x-axis. Suppose that a project requires knowledge of a in terms of the other constants. Some simple calculus may be performed at this point to discover that $a = \frac{64c^3}{9d^2}$. Alternatively, the same equations may be programmed into the computer system to discover the value for a. The exact command for Mathematica would be `Solve[d==Integrate[-(a x^2 + c),{x,`$-\sqrt{(c/a)}$,$\sqrt{(c/a)}$`}],a]`, where `Solve` is used because this remains purely algebraic and has no differentials.

3.6.3 Shooting for Solutions to the Equations of State

The simplest deployments of the equations of state are columns, built-in or simply-supported members, structures which feature a single member. Figure 3.15 show a cantilevered beam under UDL and the six known boundary conditions that permit the overall solution to be found - the boundary conditions are each paired with one of the six equations of state, showing that

Figure 3.15: Cantilevered beam indicating which boundary values are known at each end (a) and (b)

solutions can be found. Often the collection of column-beams, members and struts comprising a given structure is more complicated than a column or simply-supported beam. Each additional member brings information about joins and adds boundary conditions to the equations. These arise in multiples of three, being information about the forces, moments, positions and slopes at particular positions throughout the structure. As an example, Figure 3.16 features a network of beams, for which positions (a) and (c) supply information about the position (x, y) and the moment (M_x); position (b), conservation of both moments about that point and horizontal and vertical forces; and position (d) information about the position (x, y) and the curvature (κ) at that point. Another example, the system of Figure 3.16 has nine bounding values which permit the associated set of three conservation equations (moments about the join, horizontal and vertical forces) and the six differential equations to be solved. Examining the examples of Figure 3.15 and Figure 3.16 in greater detail should provide necessary clarity to this simple technique.

Figure 3.15 features a built-in cantilevered beam under UDL (acting vertically rather than perpendicular to the member surface). At the start-point for the member, the ys-position, z-position and built-in angle (θ) are known. At the end of the member, the horizontal and vertical loading and end-
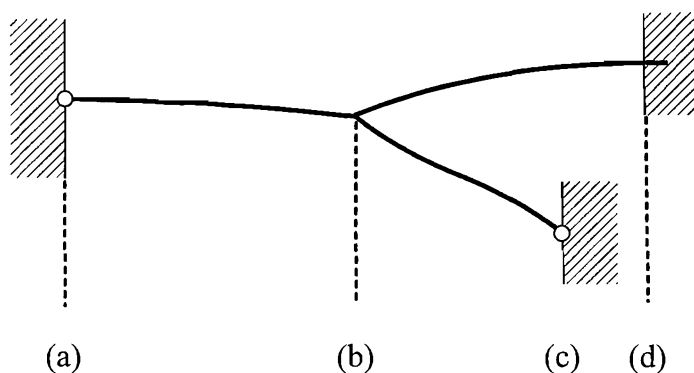
Figure 3.16: Network of beams with two pin-jointed ends and one fixed-in end

moment are known, information which is required for the initial conditions. The equation solver is asked what initial values of horizontal/vertical loading and moment will supply the known end-values, and the result obtained fed in to the initial conditions.

Figure 3.16 is more complicated, having the network of members split around a fixed join. Knowing that the conservation laws of force and moment still hold, the structure can be divided into constituent parts and dealt with in stages. Shooting will need to follow from (a) to (b) and then branch as the structure does to incorporate the effects of lengths BC and BD, shooting for each from their respective start points and iteratively incorporating the results to find the required initial conditions.

Although each structure has its own particular known final conditions which will permit the essential initial conditions to be found by numerical equation solvers, there remains a heuristic rule for solving any final points of a structure: built-in ends of members have known angle (defined by geometry) and unknown moment; pinned ends of members, known moment (usually zero) and unknown angle. It is the loading condition of each member-end within the structure, along with how each member's loading is conserved and transferred, which is key to finding a set of initial conditions for the Equations of State.

61

3.7   Program Flow-Chart

Having described the core Equations of State and the method by which known information about a structure undergoing analysis will provide a path to full simulation, it is important that these two core components are tied together well. The flow chart of Figure 3.17 shows the pattern followed, namely, unknown initial conditions used in the Differential Equation Solver to find solutions to the Equations of State are found by repeated improvements to guesses of those initial values. A complete set of known boundary conditions is essential for the mathematics of the equation-solvers to complete their function; a broad range of such boundary values will permit the shooting program to find the necessary unknown boundary values.

3.8   Additional Components

Non-linear physical factors of the material of structural steelwork add a challenging numerical layer to the process of modelling and simulation. For the cross-sections under consideration in this document, the stress-strain curve and the internal strains arising from the hot-rolling fabrication process are highly important. The following paragraphs document their inclusion in this project.

3.8.1   Stress-Strain Relationships

Using the information supplied by Byfield et al. (2005) , the elastic-plastic-strain-hardened stress-strain curve can be defined. 50 sets of mill tests data provide an accurate understanding of the stress-strain response of S275- and S335-grade steel from 0 to 4% strain. The lower bound of the 95% confidence interval for the S275 samples provides the detail of Figure 3.18: ϵ_y is at the end of the elastic range and has value $\epsilon_y = \frac{\sigma_y}{E}$. $\epsilon_{sh} = 6\epsilon_y$, and the slope of the strain-hardened section, $E_{SH} = 2700N/mm^2$, in contrast to the slope
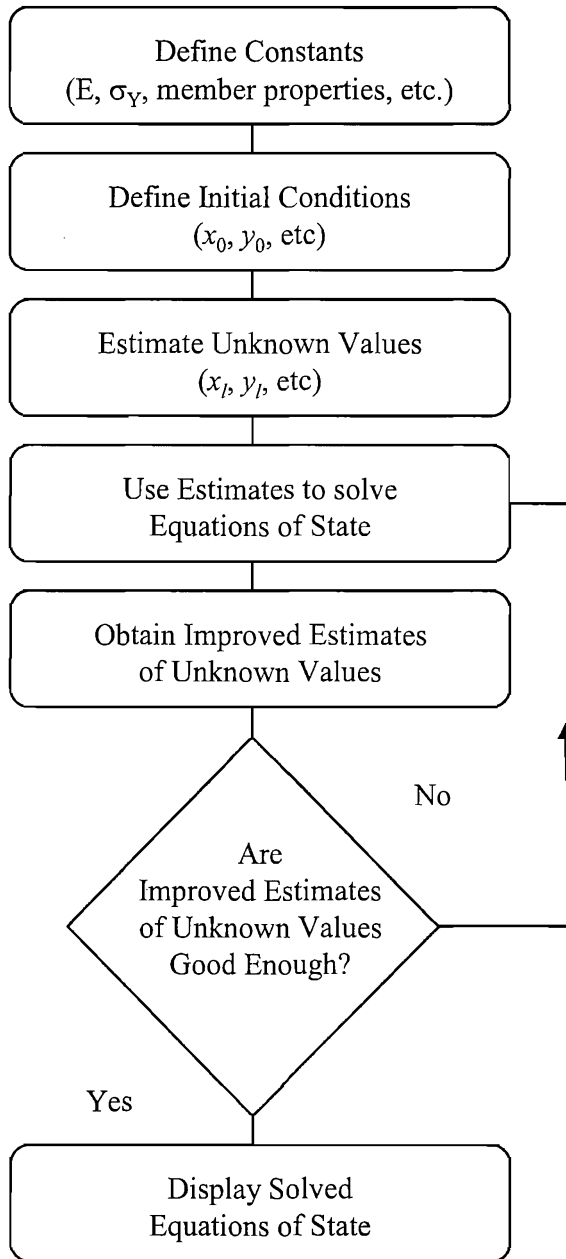
Figure 3.17: Core Program Flow-Chart for Analytic Structures
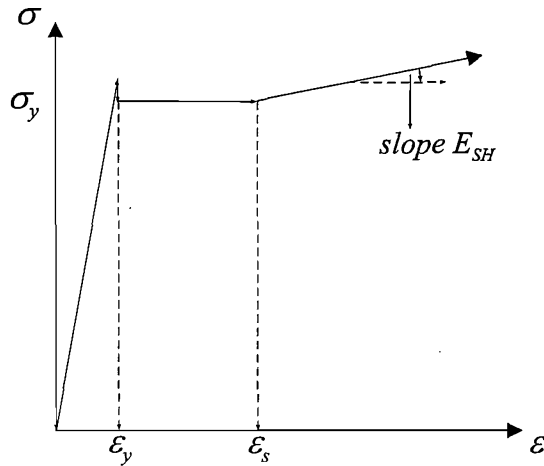
Figure 3.18: Mild steel stress-strain curve as per Byfield et al. (2005)

of the elastic section, $E = 20500 N/mm^2$. This stress-strain curve provides accurate details for mild steel up to 4% strain. An accurate model of the stress vs. strain relationship is not supported by experimental testing of Byfield and Nethercot (1998). The stress-strain curve is not required beyond 3% strain because local buckling has been shown to lead to a rapid decline in strength where the maximum strain exceeds 3% in the plastic hinge and because deflections are very large in frames with such high degrees of strain. Due to this scale of deflection, destabilising $P - \delta$ effects will again lead to overall frame buckling (in sway frames). It is assumed that the tensile and compressive stress response of S275 steel is identical (albeit for different sign and directions). Where convenient for subsequent computation, such as in the creation of Chapter Four's Curvature Look-Up Tables, modelling assumptions included allowing the strain-hardening behaviour to continue indefinitely at a rate of E_{SH} as all the member material acts as in a strain-hardened mechanism.

The precise implementation of the stress-strain curve in *Mathematica* bears discussion. In order to ensure that there is bijective mapping between a value of stress and a value of strain (that is to say that every σ is associated

with only one ϵ), an insignificant slope was added to the plastic range. For all of the simulations using an elastic-plastic-strain-hardened stress-strain curve, the plastic region is modelled by the relation

$$\sigma_{pl} = \sigma_Y + E_{pl}(\epsilon - \epsilon_Y), \qquad (3.37)$$

using $E_{pl} = 10^{-9}$. This has the side-effect of sliding the strain-hardened region so that a given stress predicts a smaller strain and a given strain will predict a larger value of stress. To combat this, the position at which the plastic 'plateau' meets the strain hardened section can be moved so that the strain-hardened section lies along the original position. Rather than following line (a) of Figure 3.19, which is clearly distinct from line (c), the dashed line (b) is followed from the plastic range below $\epsilon = \epsilon_{sh}$ until it meets the strain hardening. Finding the place where σ_{pl} (of Equation 3.37) meets $\sigma_{sh} = \sigma_Y + E_{sh}(\epsilon - \epsilon_{sh})$ shows a marginal difference between this method and a flat plastic plateau:

$$\begin{aligned}
\sigma_{join} &= \sigma_Y + 5\frac{\sigma_Y}{E}\frac{E_{sh}E_{pl}}{E_{sh} - E_{pl}} && (3.38) \\
&= \sigma_Y + \frac{1485}{221399999999918} \approx \sigma_Y + 6.70732 \times 10^{-12} && (3.39) \\
\epsilon_{join} &= \frac{\sigma_Y}{E}\frac{6E_{sh} - E_{pl}}{E_{sh} - E_{pl}} && (3.40) \\
&= \frac{178199999999989}{22139999999991800} \approx \epsilon_{sh} + 2.48419 \times 10^{-15}. && (3.41)
\end{aligned}$$

3.8.2 Incorporation of Residual Stresses

The uneven cooling of hot-rolled steel sections leaves residual internal stresses through the cross-section of the profile. The internal stresses affect the structural performance of the steelwork, most notably in the moment-curvature relationship. These are incorporated in the calculation of the stress from the strain throughout the member, with scale of these components suggested by J.B. Dwight (see Figure 6, 1978 – note the sign convention: the negative

65
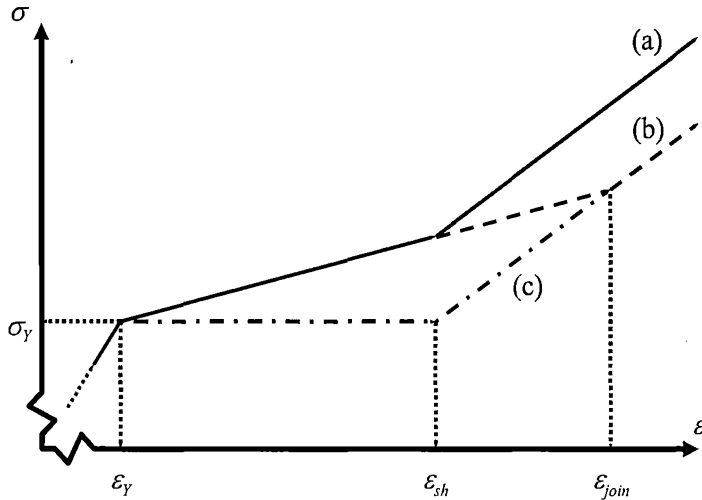
Figure 3.19: Minor alterations to the plastic range of a stress-strain relationship allow for a one-to-one relationship between stress and strain as well as accurate values of stress and strain in the strain-hardening region. (a) is typical of the relationship when programmed into a computer; (b) meets halfway between (a) and the ideal, (c)

sign is a compressive force) copied to figures Figure 3.20 and Figure 3.21, comparable with German DIN 18800 code (from the commentaries edited by H. Schmidt, 2004). The Deutsche Industrie Normale (DIN) 18800 (German steel design codes) indicates that building practices incorporate as much as $\frac{f_y}{2}$ extra compressive load in the tips of an I-section or H-section. Beams whose dimensions have a ratio of $\frac{D}{B}$ below 1.2 are expected to contain half the yield load locked in to the internal stresses while those whose $\frac{D}{B}$ ratio is more than 1.2 hold 30% of the elastic yield load. The detail of this is shown in Figure 3.22 and Figure 3.23, and these residual stresses inspired the values incorporated into EC3. The differences between the linear residual stress curves suggested in Figure 3.22 to those suggested by Figure 3.23 are minimal (Byfield and Ofner (2004)). The extra compressive forces in the flange tips of I-Beams will result in their yielding under stress lower than that expected affecting the moment-curvature relationship. This is a reaction particularly

66
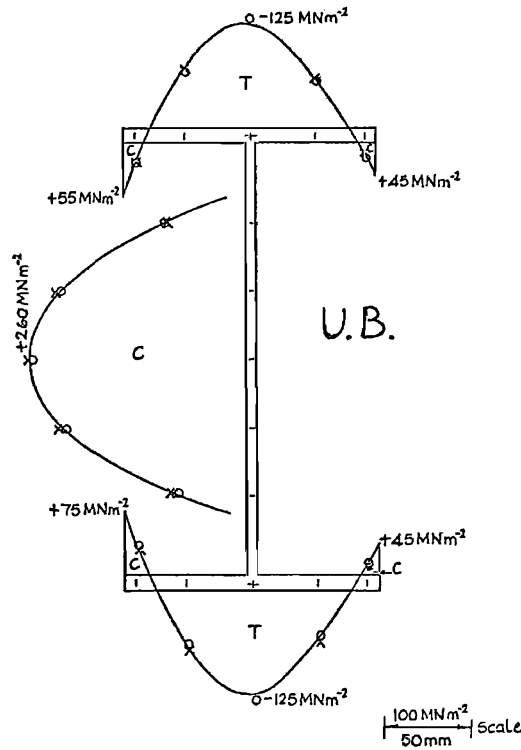
Figure 3.20: Typical patterns of internal stresses in a Universal Beam (Figure 6, Dwight (1978))

important while the member is prone to flexural buckling instability. The method of their inclusion is documented in Chapter Four.

3.9 Conclusions

The task so far has been to identify and describe the core tools of the project. The standard conventions for signs and axes are stated and the existing theory used for beam and column behaviour is outlined. The six Differential Equations of State, which form the core mathematics of this project, are derived for a cross-section of a member, from first principles, with allowances for moment-, shear- and thrust-loading, arbitrary positioning and angles. A method is outlined to provide solutions to these equations over the length of

67
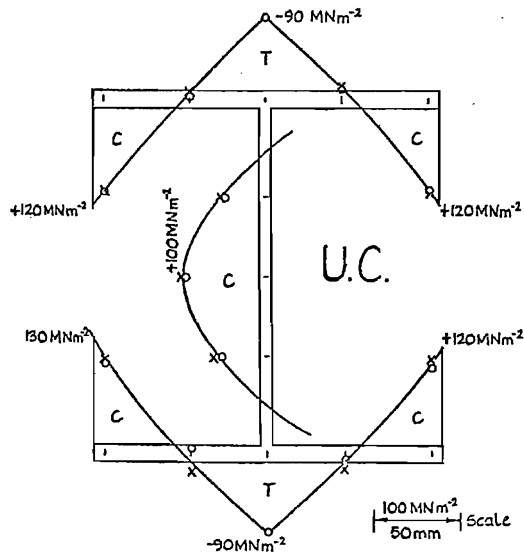
Figure 3.21: Typical patterns of internal stresses in a Universal Column (Figure 6, Dwight (1978)) Grade 43 Steel, now S275
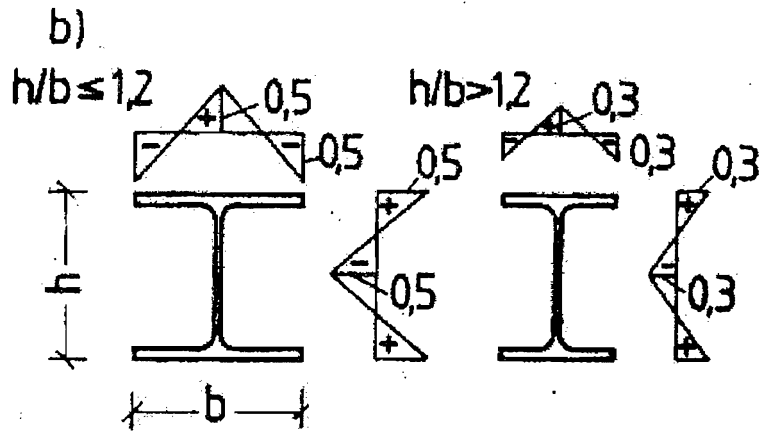
Figure 3.22: Beuth-Kommentar DIN18800 Bild 2 - 1.6 (b) with linear residual stresses in terms of p_y
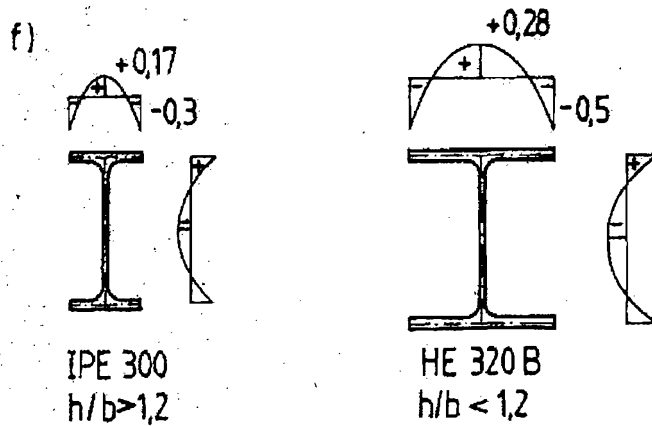
Figure 3.23: Beuth-Kommentar DIN18800 Bild 2 - 1.6 (f) parabolic residual
stresses in terms of p_y

a member or multi-member structure, making use of known boundary con-
ditions to provide the needed initial conditions for computer-based numer-
ical equation-solvers. Finally, implementation-specific behaviour regarding
stress-strain responses and locked-in strains from I-Section fabrication are
introduced.

Chapter 4

Curvature Look-Up Tables

4.1 Introduction

The large displacement beam equations presented in Chapter Three have the potential to provide extremely accurate predictions of elastic deformations. This is because curvature can be accurately predicted in elastic structures. Predicting the curvature for a given moment and axial thrust is more problematic for non-elastic structures. Lay and Smith (1965) considered the problem of non-linear moment-curvature relationships and suggested the creation of look-up tables of pre-calculated data. This chapter develops a technique to quantify this non-linear relationship for use in Chapter Three's Differential Equations of State. The technique is an advance on previous methods (Byfield et al. (2005)) because it includes the effects of axial thrusts and residual stresses on curvature. One table needs to be created for each cross-section used in Chapter Three's Equations of State (Page 57). Each load combination, as usual, causes a deflection, and inherent in this deflection is curvature. Such a value of is used in Equation 3.31 to avoid repeated shooting to find the amount of curvature associated with the load.

The Ultimate Limit State predictions of load capacity for many portal frame structures rely on elastic-plastic reserves of strength. These structures are especially sensitive to sway deformation and so it is important to accurately predict structural displacements if the full elastic-plastic reserve of strength is to be utilised. This chapter seeks to address the problem, creating look-up tables of cross-sectional curvature. Moreover, the relationship between curvature, axial thrusts and moment is quantified for cross-sections with a given residual stress distribution. The fully-analytical approach used is an advance on existing techniques for the analysis of portal framed structures because of the inclusion of the complex effects of axial thrust and residual stresses on cross-sectional curvature. Since the inclusion of these effects increases curvature and consequently frame displacements, negligence of these effects could, in some circumstances, lead to an overestimate of the
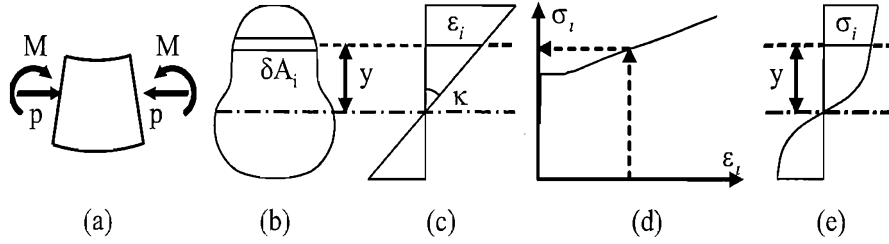
Figure 4.1: Beam segment (a) with cross-section (b), its strain distribution (c), the stress-strain curve (d) used to calculate stress distribution (e)

load-carrying capacity of sway-sensitive frames.

In the search for solutions to the Differential Equations of State (3.29 to 3.34), tabulated values for the Curvature Function $\kappa(s)$ in Equation 3.31 avoids repeated calculation of the expected cross-sectional curvature caused by a given load. The path taken to development of this tabulated data, referred to hereafter as Curvature Functions or Curvature Look-Up Tables, is explained in this chapter, starting with the simple elastic model and extending it to meet the needs of accurate simulation.

4.2 Relating Moment and Curvature

All the work presented in this chapter follows the pattern of Figure 4.1. This figure describes the overall process relating curvature and moment: for a particular thin slice cross-section of beam (e.g. that in Figure 4.1(b)) an infinitesimal strip across the cross-section with area δA_i can be taken, for which its strain ϵ_i is known and related to the curvature as in Figure 4.1(c). The stress is calculated via a stress-strain curve (Figure 4.1(d)) and the sum of the stress across the entire cross section is used to relate the loading to the cross-section's curvature.

The standards for sign remain as at the start of the previous chapter. The same right-hand triple of axes is employed, which couples a positive moment
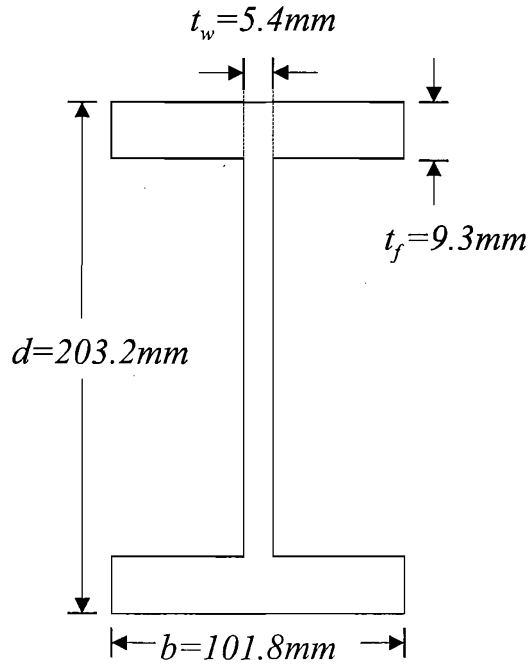
Figure 4.2: Dimensions of sample 203x102x23 I-section for which Curvature Look-Up Functions are created

with positive curvature and also with a positive angular measurement, as at the start of Chapter 3. If Equation 3.2 holds (Page 43, reiterated here: $\kappa = \frac{1}{r_c} = \frac{M}{EI}$), then r_c must be positive with positive curvature, and so is measured from the member to the centre of curvature such that a positive value of r_c occurs relative to the axes of the cross-section. Also, the assumptions discussed in Chapter 3 hold: that plane cross-sections remain planar under load and that no shear deformation occurs.

The work begins by selecting a reasonably representative I-Section suitable for use in Portal Frame structures: 203x102x23 I-section (seen in Figure 4.2) from Table B-4 of SCI P202 (6th Ed., 2001). Steel is modelled as per S275, using detail from the Mill Test Data of Byfield et al. (2005). The internal strains arising in the steel from the 'hot-rolled' fabrication process take values from Schmidt (2004). The Curvature Look-Up Tables created here use these properties throughout to enable comparisons. The process
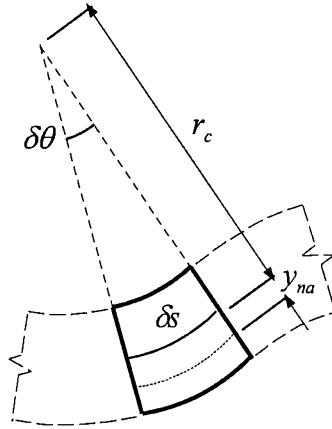
Figure 4.3: Geometry for the calculation of the strain distribution across a member

of creating a Curvature Look-Up Table begins with the Engineer's Beam Equations, which supply a relationship between moment and curvature (a reiteration of Equation 3.2):

$$\kappa = \frac{1}{r_c} = \frac{M}{EI}. \tag{4.1}$$

Since portal frame design relies upon the elastic-plastic reserve of strength, plastic and strain-hardened modes of steel behaviour will be included.

Knowing that planar slices through the material remain planar under loading provides the reassurance that the strain distribution will be linear. Figure 4.3 indicates the dimensions and symbols used to calculate the strain distribution in a cross-section with curvature κ whose neutral axis is r_c from apex with angle $\delta\theta$. Without any axial loading, the neutral axis and centroid coincide. The arc length of the neutral axis is $\delta\theta r_c$, and that at distance y from the neutral axis is $\delta\theta(r_c + y)$. This establishes that $x = r_c\delta\theta$, $\Delta x = \delta\theta y$ and:

$$\epsilon = \frac{\Delta x}{x} = \frac{\delta\theta y}{\delta\theta r_c} = \frac{y}{r_c} = \kappa y. \tag{4.2}$$

Knowing this strain distribution and the stress-strain properties of the steel under simulation, a stress distribution can be calculated. If a certain infinitesimal slice of area δA_i has stress σ_i (as in Figure 4.1), then the thrust

74

through this slice is

$$P_i = \sigma_i \delta A_i \qquad (4.3)$$

and the sum of these P_i provides the thrust through the cross-section:

$$
\begin{aligned}
P &= \sum_i P_i = \sum_{\delta A_i} \sigma_i \delta A_i \\
&= \lim_{\delta A_i \to 0} \sum_{\delta A_i} \sigma_i \delta A_i = \int \sigma \mathrm{d}A.
\end{aligned} \qquad (4.4)
$$

Taking the moments of each strip about the centroid of the cross-section, using y to denote the lever arm from the centroid:

$$
\begin{aligned}
M &= \sum_i P_i y = \sum_{\delta A_i} \sigma_i \delta A_i y \\
&= \lim_{\delta A_i \to 0} \sum_{\delta A_i} \sigma_i y \delta A_i = \int \sigma y \mathrm{d}A.
\end{aligned} \qquad (4.5)
$$

The relationship between curvature and moment in Equation 4.5 allow Curvature Look-Up Tables to be drawn up so that the curvature of a cross-section can be calculated from its moment load. This saves an enormous amount of work solving the Differential Equations of State, particularly Equation 3.31, where the inverse of this relationship would have to be discovered, by additional shooting, at every step of the search for solutions.

Figure 4.4 shows example moment-only Curvature Look-Up tables using (a) elastic, (b) elastic-plastic-strain-hardened and (c) elastic-plastic stress-strain relationships, respectively. There is very good agreement between the elastic line and the elastic ranges of both the elastic-plastic and higher-order curve. This is to be expected when the strain is converted to stress by $\sigma = E\epsilon$ in Equation 4.5:

$$
\begin{aligned}
M &= \int \sigma y \mathrm{d}A = \int E \kappa y^2 \mathrm{d}A \\
&= \kappa E \int y^2 \mathrm{d}A = \kappa EI.
\end{aligned} \qquad (4.6)
$$

The shape of the knee at M_E, the elastic moment, of the two plastic-capable curves (Figure 4.4(b) and 4.4(c), respectively) indicates good agreement
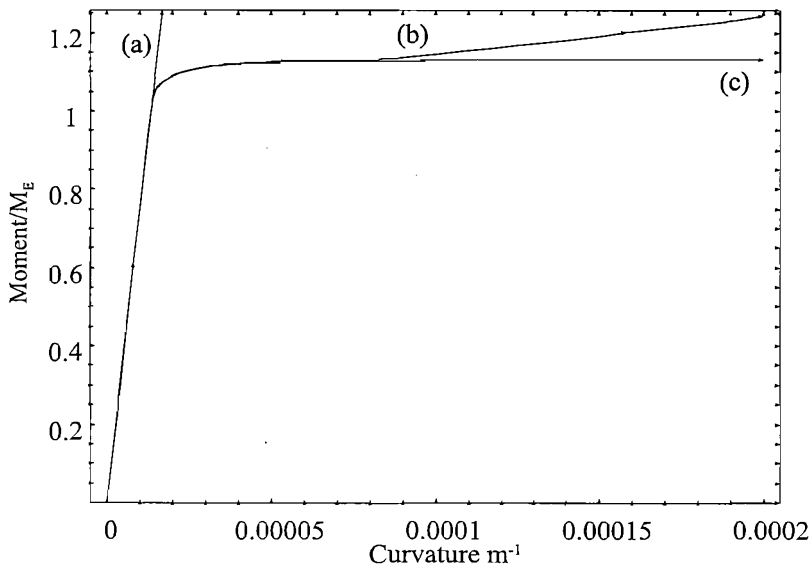
Figure 4.4: Moment-curvature relationships: (a) elastic, (b) elastic-plastic and (c) elastic-plastic-strain-hardened

between the Curvature Look-Up tables produced using elastic-plastic and elastic-plastic-strain-hardened stress-strain curves. The limited influence of strain hardening before 110% of M_E indicates that the particular cross-sections used for this graph are influenced by the onset of strain hardening behaviour only after a large amount of deflection.

4.3 Building a Moment-Curvature Look-Up Table

Prepared with reasonable guesses of curvature, the equation solver is asked to find the appropriate values of Curvature that produce a known value of moment. In *Mathematica*, the table of values was created using the `Table` command for values of Moment between 0 and 120% of the elastic Moment, M_E for the chosen I-Section. The process was performed with repeated use

of the *Mathematica* command:

$$\texttt{FindRoot}[\int_{(x,y)\in A} \sigma\,[\kappa y]\,\mathrm{d}A == M, \{\kappa, \{90\%\frac{M}{EI_{xx}}, 110\%\frac{M}{EI_{xx}}\}\}], \quad (4.7)$$

where σ is a function which provides the stress from a known value of strain. The method was sufficiently robust to use guesses for κ of 90% and 110% of $\frac{M}{EI}$ to find the Curvature, κ, associated with Moment, M, between 0% and 120% of M_E. This tabulated data, using an elastic-plastic-strain-hardened stress-strain curve and depending solely on moment loading, will be hereafter referred to as Curvature Look-Up Table (a).

4.4 Relating Moment and Axial loads to Curvature

With the impact of axial loadings already included in the Chapter Three's member equation, and it is a natural progression to examine the impact of axial thrusts upon the curvature of a loaded cross-section. Under combined axial and moment loading, the curvature of the cross section is influenced by the axial loading altering the dimensions of the thinly-sliced cross-section. (Given that this project's goals are the simulation of Steel Portal Frames, neglecting shearing forces is acceptable due to the low likelihood of portal frame member failure caused by shear stresses. The creation of a Curvature Look-Up Function including shear stresses is proposed future work.) At the very least, this new model will need to accommodate the impact of axial forces advancing the arrival of plasticity at the extremes of the cross-section. Additional care is taken to incorporate the stress distribution of the axial forces and to build a look-up table of κ for a range of values of M and P. Finally, the locked-in strain of hot-rolled steels are included in the generation of a surface of curvature.

In a cross-section of a member loaded under both moment and axial forces, the cross-sectional stress or strain distributions may be separated into
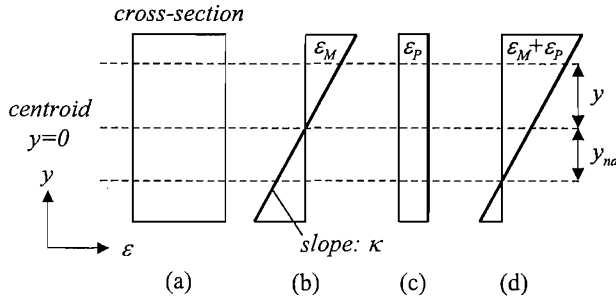
Figure 4.5: Combining strains from moment (ϵ_M) and thrust (ϵ_P) to calculate total strain and strain neutral axis position

components arising from thrusts or moments. Figure 4.5 indicates that the neutral axis under moment and thrust loading occurs when the respective strains caused by the moment and axial loads cancel each other out as $\epsilon_M + \epsilon_P = 0$. If the simple moment-curvature model is extended to include the effects of axial loads, the formation of Equation 4.2 may be kept so long as the notation records that $y = 0$ at the neutral axis:

$$\epsilon = \kappa_{na} y. \tag{4.8}$$

If the centroid occurs at some position y_c under these new coordinates, the strain at y_c is:

$$\kappa_{na} y_c = \epsilon_P. \tag{4.9}$$

Alternatively, the same statement has:

$$y_c = r_{na} \epsilon_P, \tag{4.10}$$

where r_{na} is the radius of curvature to the neutral axis. This helps the move from these new coordinates to ones which place $y' = 0$ at the centroid. The radius of curvature to the centroid, r_c can be obtained from r_{na}:

$$r_c = r_{na} - y_c = r_{na}(1 - \epsilon_P) \tag{4.11}$$

$$\Rightarrow \kappa_c = \frac{\kappa_{na}}{(1 - \epsilon_P)}, \tag{4.12}$$

78

where $\kappa_{na} = \frac{1}{r_{na}}$ and $\kappa_c = \frac{1}{r_c}$ denoting respective curvatures associated with the distance to the neutral axis and centroid. If y_c is replaced by y_{na} and y by $y' = y + y_{na}$, then the expression for the strain distribution of Equation 4.8 becomes:

$$\epsilon = \kappa_{na}y = \kappa_c(1 - \epsilon_P)(y' - y_{na}). \tag{4.13}$$

Equation 4.4 still provides the axial loading, with stress calculated from $\epsilon = \kappa_c(1 - \epsilon_P)$. As can be seen in the presence of ϵ_P, axial loads provide an additional component in the Moment sum $M = \int \sigma y dA$. However, this can be neglected for one of two possible reasons: either because axial forces are conceived as a point-load through the $y = 0$ and have no moment generating capability; or because St Venant's principle and long-beam theory say that the entire cross-section carries a proportion of the axial load (i.e. there is a part of the thrust acting on each component δA_i to be included). If the latter case, moments about the centroid sum to zero in the symmetric cross-sections of I-beams:

$$\begin{aligned} M &= \int (\sigma + \frac{P}{A})y dA \tag{4.14} \\ &= \int \sigma y dA + \frac{P}{A} \int y dA \\ &= \int \sigma y dA. \end{aligned}$$

Including axial loads forces the measurement of the position of zero strain (y_{na}) and so needs two equations to find the two unknowns κ and y_{na}. Fortunately the strain distribution of Equation 4.13 can be used in both Equations 4.4 and 4.5. These two equations in two unknowns are then supplied to *Mathematica* in order to discover the relationship between moment, axial thrust and curvature.
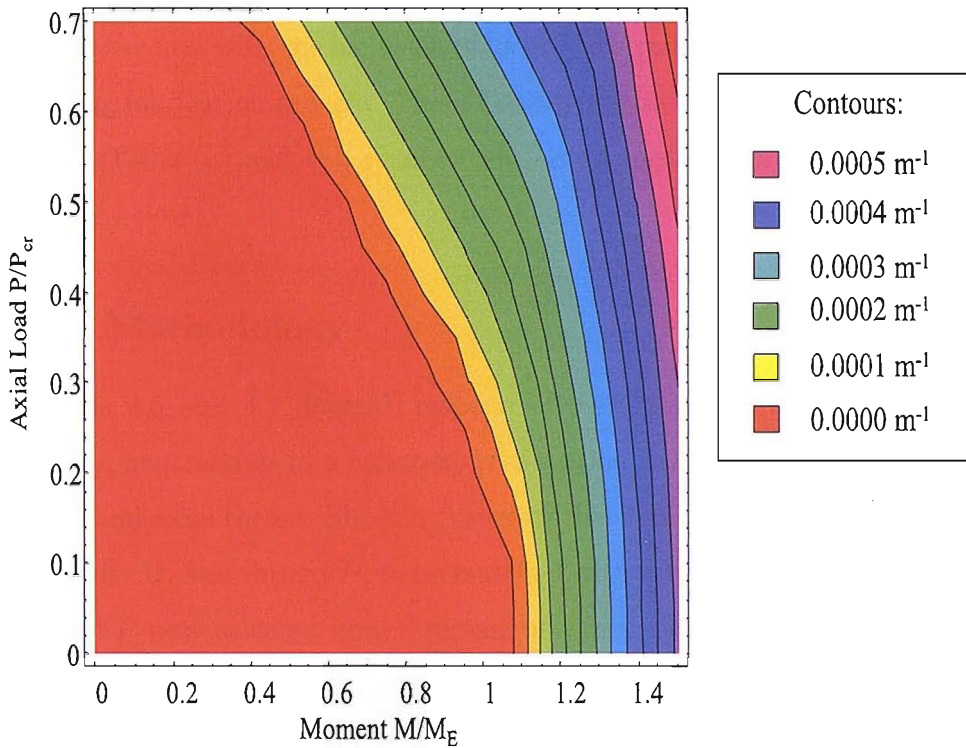
Figure 4.6: Moment (normalised), Thrust (normalised) with contours of Curvature (m^{-1}) for the cross-section of Figure 4.2

4.5 Building a Moment-Axial-Curvature Look-Up Table

When the full-detail stress strain relationship is engaged in the moment sum, a curve such as that in Figure 4.4 is produced. Extending the curve-generating program to include axial thrusts generates another non-linear graph of curvature. Figure 4.6 shows the contours of curvature for a Moment-Axial Curvature function. This work makes for enormous improvements in the efficiency of any program solving the Differential equations of state, as Equation 3.31 ($\frac{d\theta}{ds} = \kappa(s)$) may now use a look-up table instead of direct calculation.

Two Curvature Look-Up Tables were created: one that reliably predicts the curvature associated with a moment- and thrust-loading; the second that

builds on the first with the inclusion of locked-in strains brought about by the hot-rolling fabrication process. These Look-Up Tables are labelled Curvature Look-Up Table (b) and (c), respectively. Both methods are described and evaluated below.

4.5.1 Methodology

Equations 4.5 and 4.4 depend, respectively, upon the values of curvature and strain neutral axis in a member cross-section to calculate the associated moment and axial thrust. Shooting reverses this dependence, allowing values of moment, M, and thrust, P, to be matched with values of κ and y_{na}. Values of M and P were selected from a rectangular grid, and a table of values of κ was assembled. Values of M and P between those on the grid were provided by interpolation. This triplet of values for (M, P, κ) make up the Curvature Look-Up Table. $\pm$ 120% of M_E formed the extremes for M in order to cover the elastic and extend into the strain-hardened ranges. The values of P ranged between $\pm$ 70% of P_{cr} as, at higher increments of load, shooting failed to find smooth curves. This provides a broad-enough range of moment and axial loads for use when shooting with the Differential Equations of State in models of portal frame structures.

4.5.2 Initial Guesses for Shooting

Key to the process of finding values of curvature and neutral axis for a given moment- and thrust-loading are the initial guesses supplied to the numerical equation solvers. Good guesses vastly speed up the process of finding valid results; bad guesses may never find suitable results. The grid of M and P values was covered by iterating over values of moment while holding constant the values of axial load. Once the upper limit of M was reached, P was increased. The initial guesses of curvature, κ, and neutral axis location y_{na} used in building Curvature Tables lend themselves to following increments of

the moment, because they are calculated by iterating a proportional increase of the supplied results from the previous step of the algorithm. To do this, the output for the previous two iterations of κ and y_{na} are needed to predict the next. The difference between the last two known steps (being, at some i^{th} position along the way, $\kappa_{(i)} - \kappa_{(i-1)}$ and $y_{na(i)} - y_{na(i-1)}$) supply the guesses for the next iteration. Shooting will easily find solutions from initial guesses of:

$$\kappa_{(i)} + 80\%(\kappa_{(i)} - \kappa_{(i-1)}) < \kappa_{(i+1)} < \kappa_{(i)} + 120\%(\kappa_{(i)} - \kappa_{(i-1)}) \quad (4.15)$$

$$y_{na(i)} + 80\%(y_{na(i)} - y_{na(i-1)}) < y_{na(i+1)} < y_{na(i)} + 120\%(y_{na(i)} - y_{na(i-1)}).$$

Where there was no previous step, such as the first step after p has been incremented and $m = 0$, educated guesses predicting values for κ and y_{na} are needed. These can be easily supplied from Elastic theory, with

$$\kappa = \frac{M_E(\frac{M}{M_E} + \frac{P}{P_{cr}})}{EI}, \quad (4.16)$$

which scores the loading as a proportion of the elastic limits for each and uses that in Equation 3.2, and a good prediction for the position of the neutral axis using the predicted κ in:

$$y_{na} = \frac{\epsilon_P}{\kappa(1 - \epsilon_P)} \approx \frac{P}{\kappa(AE - P)}. \quad (4.17)$$

Additionally, the following short cuts avoid evaluating integrals known to be zero: when $\kappa = 0$, $m \equiv 0$; when $y_{na} = 0$, $p \equiv 0$.

4.5.3   Including internal stresses

If M and P are calculated from the overall stress in a member according to its position through the cross-section, then the built-in strains of hot-rolled steel members can be added into the equations for M and P. Using the internal stress values from Schmidt (2004), as shown in Figure 2.16, Figure 3.22 and Figure 3.23, a parabolic strain distribution was calculated for flange and web internal strains. It is important to note that the expansion of hot metal

82
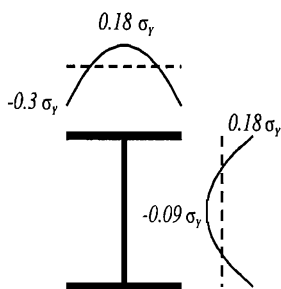
Figure 4.7: Internal stress diagram for hot-rolled steel member

and consequent internal displacements of a hot-rolled member cooling disproportionately create internal strains which are most-often acknowledged by their associated internal stresses. These locked-in strains cause no additional deflection to a given cross section, so their overall impact upon the stress distribution - the sum over the whole of a web or flange and entire cross-section - is assumed to be zero. This allows the parabolas to be calibrated to the member, retaining local built-in stresses without compromising the shape of the cross-section. The parabolas are assumed to follow the mid-line of the web and flanges and be uniformly spread across the cross-section, in similar fashion to Szalai and Papp (2005), who assumed that their web and flanges behave as line elements with zero width. Figure 4.7 shows the initial model used here, dividing up the I-section into three rectangles with appropriate parabolic internal strain distributions.

4.5.4 Program Outline

The program written to create each Curvature Look-Up Table followed the same pattern of: predict initial estimates for curvature; shoot for curvature; store values. The program loop, incrementing values of load while the load was within predefined limits. In the cases where Look-Up Tables use both moment and axial loadings, the iteration held constant the thrusts while the moments stepped up to their limit, before the thrust was incremented and a

new value used.

The procedure used to shoot for the required values of curvature is an extension of that explained in Figure 3.17 (Page 63). With known physical constants from the material and cross-section dimensions input, the process of shooting inherent to Figure 3.17 is followed until sufficiently accurate results are obtained, and the results graphed. The key differences between Curvature Look-Up Tables (a), (b) and (c) are outlined in Figure 4.8 which also functions as an outline of the shooting process used to derive each set of data.

Define constants: π, E, E_{sh}, etc.

Define member by $\{d, b, t_w, t_f, p_y, \lambda\}$

Calculate: $\{A, I_{xx}, M_E\}$

Curvature Look-Up Table (a)

Shoot for κ which provides M

$$M = \int \sigma_y y \, dA; \quad \sigma_y \text{ from } \varepsilon_y = \kappa y$$

- M in range of:

  $(-120\% \, M_E, 120\% \, M_E)$

- At each step use guesses for κ:

  $(99\% \, M/(EI_{xx}), 101\% \, M/(EI_{xx}))$

Curvature Look-Up Table (b)

Shoot for κ predicted by M & P

$$\begin{cases} M = \int \sigma_y (y - y_{na}) dA \\ P = \int \sigma_y dA \end{cases} \quad \sigma_y \text{ from}$$

$$\varepsilon_y = \kappa(y - y_{na})$$

- M in range:

  $(-120\% \, M_E, 120\% \, M_E)$

- P in range: $(-70\% \, P_{cr}, 70\% \, P_{cr})$

- Initially: $\quad \kappa = \dfrac{M_E(\frac{M}{M_E} + \frac{P}{P_{cr}})}{EI_{xx}}$

$$y_{na} = \frac{\varepsilon_P}{\kappa(1 - \varepsilon_P)} = \frac{P}{\kappa(AE - P)}$$

Or subsequently: $\quad \kappa = \kappa_i - \kappa_{i-1}$

$$y_{na} = y_{na(i)} - y_{na(i-1)}$$

in guesses: $\quad (\kappa_i + \frac{80}{100}\kappa, \kappa_i + \frac{120}{100}\kappa)$

$$(y_{na(i)} + \tfrac{80}{100} y_{na}, y_{na(i)} + \tfrac{120}{100} y_{na})$$

Curvature Look-Up Table (c)

Shoot for κ predicted by M & P

$$\begin{cases} M = \int \sigma_y (y - y_{na}) dA \\ P = \int \sigma_y dA \end{cases} \quad \sigma_y \text{ from}$$

$$\varepsilon_y = \kappa(y - y_{na}) + \text{int } \varepsilon[y]$$

- M, P and (κ, y_{na}) guesses as per Curvature Look-Up Table (b)

Figure 4.8: Constants, Equations and Initial Guesses used in Shooting Program for Curvature Look-Up Tables (a), (b) and (c)

4.6 Reliability Testing

Figure 4.9 shows that the increased strains in a cross-section due to axial thrusts advances the arrival of the 'knee' of plasticity. This plasticity occurs as

$$\frac{M}{M_E} + \frac{P}{P_{cr}} = 1. \tag{4.18}$$

The line marked (a) is the elastic moment curvature relation, from Equation 3.2; (b) is the curvature predicted by the elastic-plastic-strain-hardened stress-strain curve and the internal strains through each cross section when no axial load is supplied (contrast the 2D equivalent in Figure 4.4, Page 76); (c) adds 10% of P_{cr}; (d), 20%; (e), 30%; (f), 50%; and (g), 70%. A more-clear edition of this graph appears in Figure 4.10. Their divergence from the straight line of elastic curvature occurs in total agreement with Equation 4.18, which is also appears in Equation 5.23, §5.2 of Megson (1987).

The data for Curvature Look-Up Tables (a), (b) and (c) have been appended in the Resources section (on pages 171 to 185), facilitating comparisons of the predictions of curvature against existing theory. The tables on pages 171 to 178 provide insight into the effect of progressive increase in Axial Thrusts for fixed values of Moment, while pages 179 to 185 show curvature increasing with Moment at fixed values of Axial Thrust. Due to the way that the shooting simulations run in *Mathematica* and way that the data has been stored, the tabulated values here come via interpolation. Their comparison against $\frac{M}{EI_{xx}}$ while in the elastic range is one path to their validity; outside that range, comparisons are made against a round of Direct Shooting for the given value of Curvature associated with the given values of Moment and Thrust. This indicates that an interpolated surface using the data of Curvature Look-Up Table (c) is an accurate and appropriate way to find intermediary values of the calculated known points.

In the first series of tables, it can be seen at a glance that the fixed values of Moment, the Moment-only Curvature Functions ('Elastic Curvature' and

86
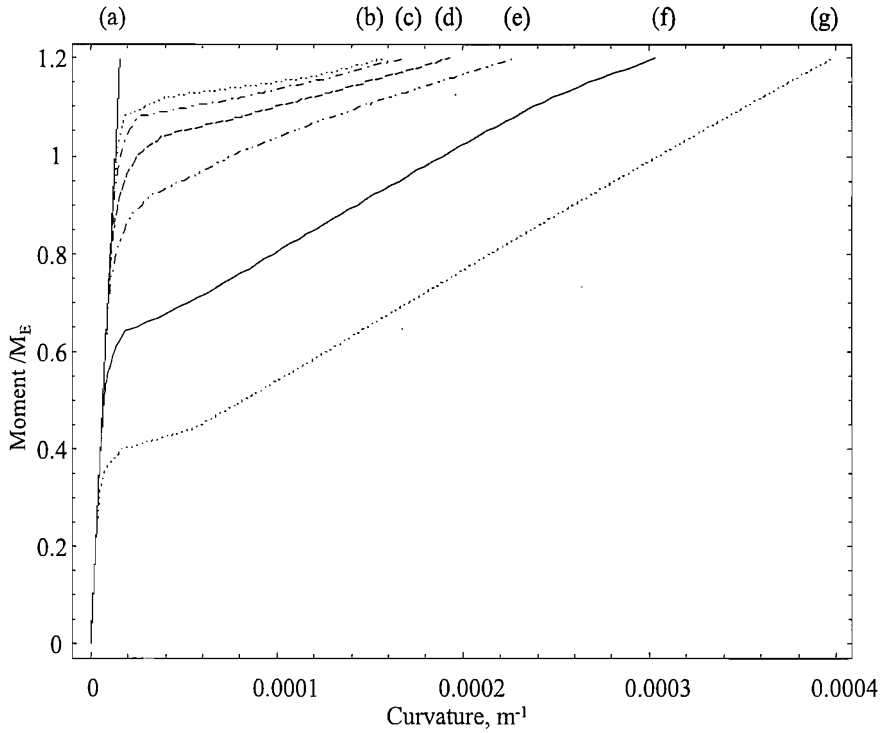
Figure 4.9: Moment-Curvature graph of Curvature Look-Up Table (c) with increasing values of Axial Load, compared to the elastic (a), $P = 0$ in (b); 10% of P_{cr} in (c); 20% in (d); 30% in (e); 50% in (f); and 70% in (g)

Curvature Look-Up Table (a)) do as advertised: remain fixed. With the Thrust-aware Curvature functions (Curvature Look-Up Tables (b) and (c)), additional curvature is recorded as the Thrust increases. There is a drastic increase in curvature when the Moment and Thrust work together to bring about post-elastic portions of the cross-section. This can be seen throughout both sets of tables, with Curvature Look-Up Table (c) beginning the 'knee' of increased curvature when the proportional contributions from Moment and Thrust,

$$\frac{M}{M_E} + \frac{P}{P_{cr}},\tag{4.19}$$

is 90%. This difference must be seen in proportion – it is never larger than 5% – and must be attributed to the presence of Internal Strains caused by Hot-Rolled fabrication.

87
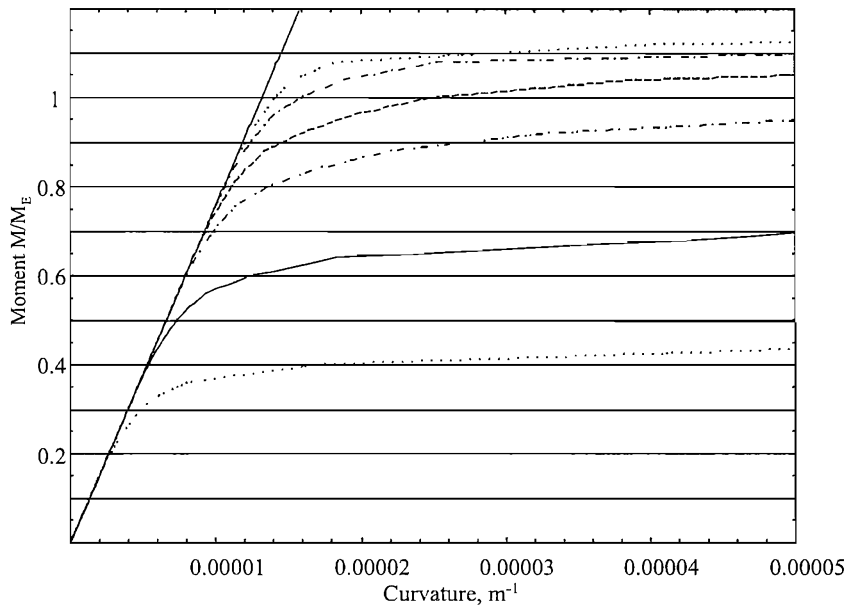
Figure 4.10: Moment against Curvature as per Figure 4.9 with additional detail to show where each level of Axial Load departs from the elastic curvature

The second series of tables clearly shows the deviation of the Curvature Table (a) from the predicted Elastic Curvature as the Moment rises above M_E. Curvature Look-Up Tables (b) and (c) differ in their post-plastic state, with (b) being lower in the plastic region before growing to larger curvature for less moment than (c) as the loading increases (Figure 4.11). There is also an earlier onset of plasticity in for Curvature Data (c) which arises from the presence of internal strain data in the computer model. The internal strain also accounts for Curvature (c)'s increased stiffness after plasticity, which is noteworthy for its potential to aid the stiffness of heavily-laden structures, later in this thesis.

4.7   Conclusions

The introduction of an important segment of the Analytic Structures system is completed above, with the description of the mathematical relationship
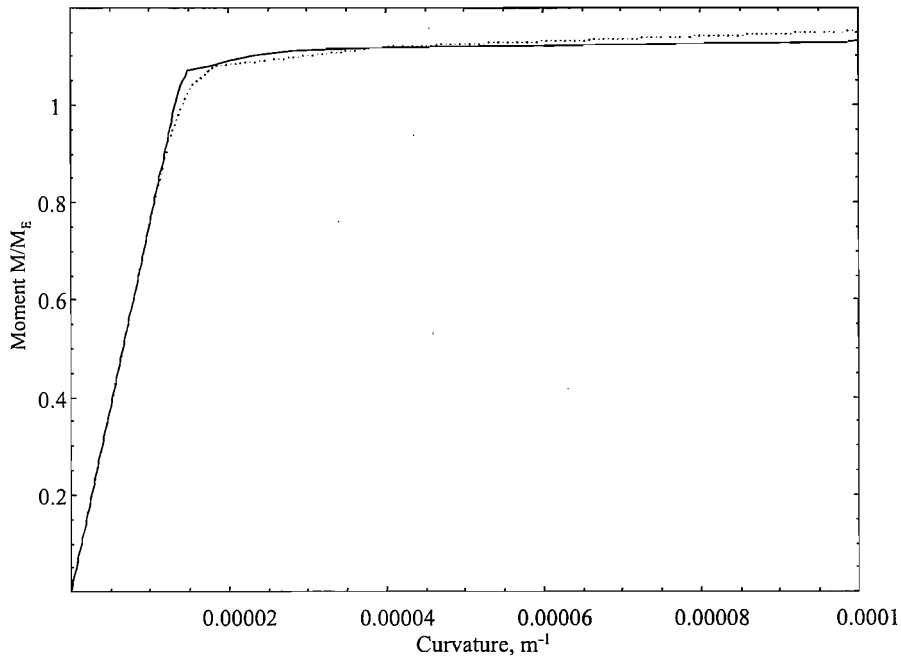
Figure 4.11: Moment against Curvature comparing Look-Up Tables (b) (solid line) and (c) (dashed line) into post-elastic behaviour

between Curvature and Moment in the cross-section of a structural member. The goal of producing Look-Up Tables of Curvature is achieved for three variations of input data: Moment-only loading, Moment and Axial loading and the same but for the inclusion of Internal Strains arising from the fabrication of Hot-Rolled Steel Cross-sections. These sets of data are labelled, respectively, Curvature Look-Up Tables (a), (b) and (c).

Within the data produced by Shooting with Equations 4.4 and 4.5, predictions below the Elastic boundaries of M_E and P_{cr} correlate in all cases, showing that

$$\kappa = \frac{M}{EI} \qquad (4.20)$$

is an appropriate descriptor of the curvature of a member while its cross-section is deflecting within the elastic range of steel behaviour, i.e. when

$$\frac{P}{P_{cr}} + \frac{M}{M_E} \leq 1. \qquad (4.21)$$

Figures 4.4, Page 76 and 4.9, Page 87 are both good indicators of this agree-

89

ment. The surface formed from the data points of Curvature Look-Up Table (c) correlates well with direct scoring of the data. This supports the recommendation that an interpolated 'blanket' surface be used to predict the curvature of a cross-section loaded between known points.

At present the method suffers from the shortcomings of being unable to predict the curvature for axial loads above 70% of the crushing stress of the cross-section used, or that it does not cater for shear stresses in the cross-section. Neither of these issues impact the behaviour of Portal Frame structures and so do not harm the use of this method in the analysis of the next few chapters. Among the results sought in Chapter Five are the limits of applicability of these Curvature Look-Up Tables to columnar members, and further comment is made there. The issue of shear deformation in cross-sections is suggested further work.

With a whole system for Structural analysis outlined, its application to two test scenarios continues in this document. One test case is the development of a Strut-Buckling curve after BS5950-2000 Table 24(a) and appears in Chapter Five. Chapter Six then continues to test this structural modelling system as applied to a 30m Portal Frame span, comparing the Analytic Structures method against the design code results for BS5950 and simulated result from CSC UK's *Fastrak Portal Frame* Steel Design Software.

Chapter 5

Simulated Struts

5.1 Introduction

This chapter sets out to simulate structures which implement the mathematical models outlined in the preceding pages, to quantify the accuracy of these computer models and lend support to the reliability and accuracy of the structural modelling system introduced in this work.

In Chapter Two, the background for computer-based Structural Steelwork Analysis was discussed. Chapter Three saw the introduction of the Core Mathematics of Analytic Structural Steelwork Design, including the method of discovering initial conditions from boundary values, known as Shooting, as well as the six Equations of State for a cross-section of a member (as on Page 57).

Chapter Four introduced important optimisations to the Program outlined in Figure 3.17, where the $\frac{1}{r_c}$ of Equation ?? is supplied by a precalculated table relating Axial Thrust, Moment and Curvature, hereafter known as a Curvature Look-Up Table. Three Curvature Look-Up tables were created using the methods outlined in Chapter Four: Table (a) relates Moment to Curvature via a full-range (elastic, plastic and strain-hardening) stress-strain curve; Table (b) matching a Moment and Axial Thrust to a Curvature using the full-range stress-strain relationship of Figure 2.3(d); and Table (c) supplying a value of Curvature from Moment and Axial Thrust loads taking into consideration both the Internal Strains of Hot-Rolled Steel members and the fullest stress-strain relationship.

The computer program models struts of uniform cross-section in simulations of increasing complexity to qualify the behaviour of a simple, pin-ended Euler strut against the predicted strut-buckling loads from BS5950. The series of strut simulations builds from an infinitely elastic strut through the elastic-plastic-strain-hardened strut using Curvature Look-Up Table A to using Curvature Look-Up Table B and Table Curvature Look-Up Table C which incorporate internal strains of Section 3.8.2. These simulations were

then extended to include improved initial guesses, built-in curvature and self-load, with the intent to compare Curvature Look-Up Tables A and C.

5.2 Mathematical Framework

The most effective method of building a complex simulated model of structural behaviour will start with what is known and easily verifiable — albeit with inherent assumptions which limit deployment in design practice — before extending the model to include behaviour which removes the reliance upon assumptions and extends the applicable scope of the simulations. For this reason, the models used here start with assumptions of elastic behaviour and no axial component in the relationship between loading and curvature.

The primary assumptions remain: that of plane sections remaining plane; the members deflect within the plane of their loading; and that no shear strain occurs. Given that the simulations concern a pin-ended strut, the assumptions are reasonable, and loads in practice can be applied via pinned joints so that the load is transferred to the entire cross-section of the strut from the pin. Localised strains may emerge from a pin which is not in contact with the entire cross-section, but such behaviour is assumed not to happen (by St Venant's principle). Neglecting deformation arising from shear strain is appropriate to Steel I-sections but would deem this modelling method inadequate for other materials; the required mathematical adaption is discussed in the chapter on Proposed Further Work.

5.3 Buckling of a Pinned Strut

Megson (1987) and Moy (1996) comment that struts, following the derivation of Euler's Buckling Load and its application in the elastic small-deflection equation (3.8, $\frac{M}{EI} = -\frac{d^2y}{ds^2}$), predict a sinusoidal deflection pattern. The first mode of a strut whose ends are fixed in position and has ends free to rotate

is a half-sine curve; constraining the angle by building-in the ends of the strut forces deflection into a full-phase sine curve, as predicted by solutions to Euler's Strut-Buckling formula (Equation 3.12, $\frac{d^2y}{ds^2} + \frac{P_{cr}\cdot y}{EI} = 0$).

The pin-ended strut was selected in order to qualify simulations of this model due to Euler's original derivation of the strut-buckling curve. Euler's formula provides a good starting point for comparison of known theory to results produced by the system of equations and curvature look-up tables explained in this document. The single input variable – axial thrust – and the single member lend themselves to quick calculation and analysis.

5.3.1 Development and Methodology

Having introduced the mathematics of the system of structural modelling above, in Section 5.2 which features Figure 3.17, the specific details of modelling a pinned strut can be filled in. As identified above, the path to a full detail model started from a simple and verifiable beginning with infinitely-elastic properties, before advancing onward.

The simulations were performed in *Mathematica* using a pre-calculated curvature look-up table in the six equations of state, 3.29 to 3.34 (repeated on Page ?? as Equations ?? to ??), and shoots to discover the initial rotation, axial load and load in the plane of buckling. A strut of length l is held horizontally and pinned at each end, and compressed by a force w_y applied at the top. The shooting uses the knowledge of the axial loading at the top of the strut ($f_y(l)$), that the upper pin remains directly above the lower pin ($z(0) = z(l)$) and that the moment around the upper pin is zero ($M_x(l) = 0$) because the pin cannot provide resistance to moment. The unknown sought by the shooting process is the initial angle of the strut to its base pin. An overview of the layout is in Figure 5.1.

The member tested throughout the range of simulations was a 203x102x23 I-section from table B-4 of SCI P202 (6th Edition, 2001), whose radius at

94
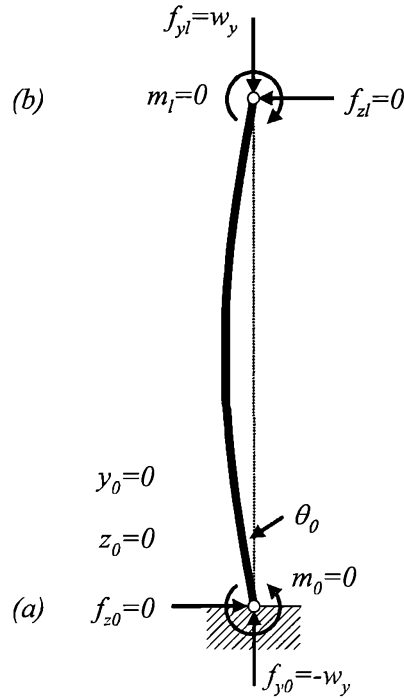
Figure 5.1: Shooting for the base conditions at (a) of a pinned strut using known boundary conditions at (b)

the web-flange intersection was neglected in order to simplify the method by which internal stresses of hot-rolled steel sections were included in the simulations. The tests calculated the mean stress at collapse for a range of values of slenderness, from a near-zero value up to $\lambda = 300$. The use of a very small but non-zero lowest value for λ is essential to avoid a zero value of height when the slenderness is used to calculate the length of the strut as per Equation 5.1,

$$\lambda = \frac{l}{\sqrt{I/A}} \iff l = \lambda\sqrt{I/A}, \tag{5.1}$$

which also defines the initial lack of straightness, as per BS5950:2:1985 §7.2.6 (p.10): the larger of 3mm or $\frac{l}{1000}$ for Class A sections. It is important to note that inserting nonsensical values (such as a near-zero λ which creates a strut of height < 1mm with initial midpoint deflection 3mm as per design guidelines) into the computer simulation will result in nonsensical output

95
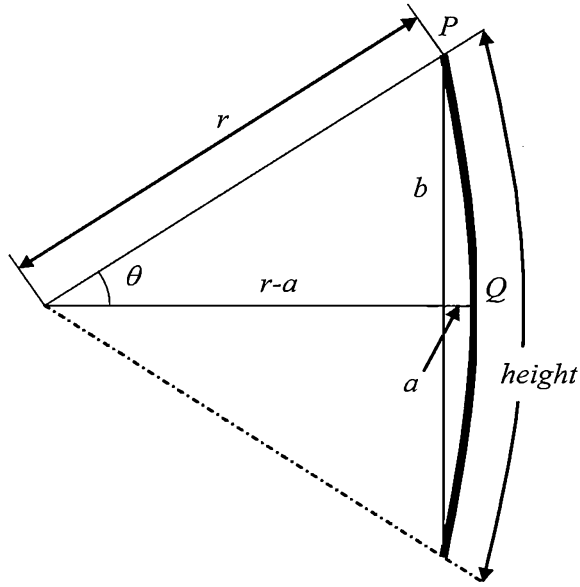
Figure 5.2: Geometry of the relation between initial lack of straightness and radius of curvature in pinned struts Series A–D

from the computer program.

5.3.2 Infinitely Elastic Strut

The first iteration of the simulations, labelled Series A (key details: elastic, moment only), held to the elastic stress-strain response throughout the full range of load. As identified above this assumption of unending elastic behaviour permits the use of a moment-curvature derived from the Engineer's Beam Equations (Equation 3.2): $\kappa = \frac{1}{r} = \frac{M}{EI}$. The built-in curvature for this set of simulations followed the arc of a circle, with a constant value for κ_s added to Equation 3.31. This was derived from the geometry of Figure 5.2. Further, the tangent at the base provides a good guess of θ when $s = 0$, the angle of the strut to the base pin.

A few methods were available for calculating the radius of this circle, denoted r in Figure 5.2, the first and simplest being adopted for use in this family of equations. There are three paths to calculating a built-in

curvature arising from the initial lack of straightness, one using a small-angle assumption, another assuming that PQ is a straight line of length $\frac{l}{2}$, the third using a numerical equation-solver. In the first case $b = r \sin \theta$, and, via Pythagoras' Theorem and the arc length $r\theta = \frac{h}{2}$:

$$r = \frac{r^2 \sin^2 \theta + a^2}{2a} \approx \frac{r^2 \theta^2 + a^2}{2a} = \frac{h^2/4 + a^2}{2a} = \frac{h^2 + 4a^2}{8a}. \tag{5.2}$$

Alternatively, using Pythagoras twice (on $a^2 + b^2 = PQ^2 = (\frac{h}{2})^2$ and $(r - a)^2 + b^2 = r^2$):

$$r = \frac{h^2}{8a} \tag{5.3}$$

The differences between the curvature calculated from these two guesses are of the order of 10^{-12} throughout the range of λ used in these simulations. The final method uses

$$\cos \theta = \frac{r - a}{r} \iff r = \frac{a}{1 - \cos \theta} \tag{5.4}$$

and

$$r\theta = \frac{h}{2} = \frac{a\theta}{1 - \cos \theta} \tag{5.5}$$

from which the right-hand equality is input into an equation solver to discover a value for θ (typically around -0.004 for $a = \frac{h}{1000}$) which can be substituted into

$$\kappa = \frac{1}{r_c} = \frac{1 - \cos \theta}{a}, \tag{5.6}$$

thus providing a direct path to the built-in curvature arising from the initial lack of straightness. θ is also a good guess for the angle at the base of the strut, due to the similar triangles to the tangent of the arc. The alternative of stating r as a function involving inverse cosines, with Equation 5.5 rearranged to the form

$$r\theta = r \cos^{-1} \left(\frac{r - a}{r} \right) = \frac{h}{2}, \tag{5.7}$$

is equally correct and saves a step in calculation only to incur the expense of checks on the input to the inverse cosine function so that $-1 \leq \frac{r-a}{r} \leq 1$. The difference between the first two methods against the third is consistently 0.001%.

5.3.3　Non-Elastic Behaviour

As identified in Chapter Four, the choice of stress-strain distribution informs the behaviour of the moment-curvature relation, so great care was taken to include non-elastic behaviour accurately throughout the second phase of simulation development. A new stress-strain response brings a new moment-curvature relation that of Byfield et al. (2005) with an improved relation between moment and curvature, as per Chapter Four:

$$M = \int \sigma_y.y\mathrm{d}A \qquad (5.8)$$

This was the only change to this family of simulations, although it must be noted that dropping the assumption of elasticity influences the 'squashy factor' of $(1 - \epsilon)$ in Equations 3.29, 3.30 and 3.34.

A complication arose from use of an elastic-plastic stress-strain response curve (Figure 2.3(f), Page 10) makes for a limiting plateau in the Curvature Look-Up Table created using this stress-strain relationship, and is shown in the Moment-Curvature graph of Figure 4.4(c) (see Page 76). This causes the inability to solve the Differential Equations of State for the member. There is no full data set completed for an elastic-plastic strut due to these difficulties. Such simulations are planned future work because it is believed that the information provided will give insight into the plastic and post-plastic behaviour of cross-sections in columns.

A full elastic-plastic-strain-hardened stress-strain curve (Figure 2.3(d)) provides the defining shape for Curvature Look-Up Table (a). Figure 4.4(b) illustrates this, showing a knee as partial plasticity through the cross-section permits more flexure to occur before stiffening and strain-hardened behaviour governs increases in deflection. For this series of simulations, no changes were made to the built-in curvature of the member or the initial angle guess $(\theta(0))$, and this data were denoted Series B (with the key details: full stress-strain; moment-only).

5.3.4 Combined Axial and Moment Loads in Deflection and Curvature

This next phase of simulations also saw the incorporation of axial loading behaviour upon the curvature of the strut. The equations governing this interaction are outlined in Chapter Four, and the most-significant changes made to the system were the alteration of Equation 3.31 (appears as $\frac{d\theta}{ds} = \frac{1}{r_c} + \kappa(s)$ on Page ??) to make use of the interaction of moment, thrust and curvature values in Curvature Look-Up Table (b). Also, while it must be noted that the presence of internal strains are modelled, their inclusion arrives later, with simulations using Curvature Look-Up Table (c). This allowed the reliability and stability of the initial conditions to be confirmed for the simulations using the more-complicated Curvature Look-Up Table (b). At this stage, the same series of assumptions about initial lack-of-straightness and built-in curvature were applied from the previous families of simulations and the data are identified as Series C (key details: full stress-strain; moment and axial forces).

5.3.5 Internal Strains from Cooling of Hot-Rolled Steel

With an established family of simulations using Curvature Look-Up Table (b), the next step included the effect of internal strains from cooling of hot-rolled steel cross-section. As described in Chapter Four, Curvature Look-Up Table (c) uses the predicted values of internal strains (ϵ_{int}) supplied in Schmidt (2004) added to the strain arising in Equations 4.4 and 4.5. The differences between Curvature Look-Up Tables (b) and (c) are compared in Chapter Four. Curvature Look-Up Table (c) was included in a family of simulations which appear as Series D (with the key details: full stress-strain; internal strains; moment and axial forces).
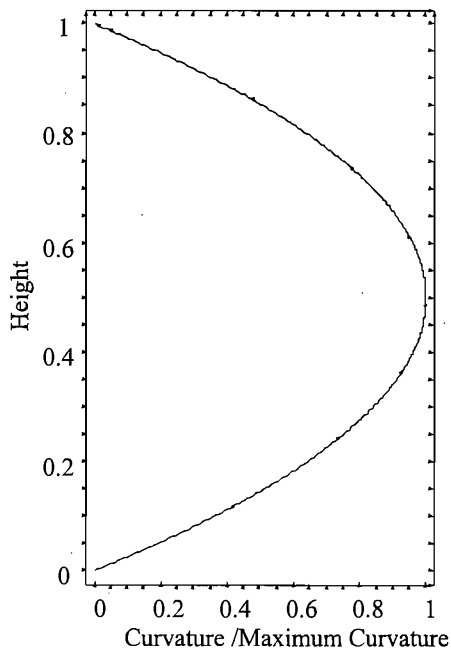
Figure 5.3: Simulated Strut Showing Sine Pattern Caused by Curvature

5.3.6   Fully-Loaded Simulations

Having previously assumed that the member itself has no impact upon the
load, efforts were made to include the weight of the member in the simulation.
The weight was applied from a look-up table which matched the height up the
strut to the weight from the mass of steel above it, and supplied to Equation
3.32 (as $\frac{df_y}{ds} = w_y$ on Page ??) as a function parameterised by s, the distance
along the member. With the tables of cross-section properties of SCI P-202
supplying a value for mass per metre length, this was an easy feature to
add, calculated from the initial member data. Including this behaviour was
deemed essential for future use in modelling portal-frame arches.

Additionally, while initial simulations assumed that the curvature of the
strut follows the arc of a circle, which simplified calculating the built-in cur-
vature arising from the initial lack of straightness, progressive simulations
adopted a built-in initial-lack-of-straightness supplied by a sine curve sub-
stituted into Equation 3.7. The Sine curve was chosen because the in-plane

deflection of struts appear to follow a Sine curve (Figure 5.3). Parameterising $z = s$ and $y = \delta \sin \left[\frac{\pi s}{l} \right]$, where $\delta = \max(\frac{l}{1000}, 3mm)$ as before, permits:

$$\kappa_s [s] = \frac{-\delta \left(\frac{\pi}{l} \right)^2 \sin \left[\frac{\pi s}{l} \right]}{\left(1 + \delta^2 \left(\frac{\pi}{l} \right)^2 \cos^2 \left[\frac{\pi s}{l} \right] \right)^{\frac{3}{2}}}, \qquad 0 < s < l. \tag{5.9}$$

This has the additional benefit of providing an accurate estimate for the value θ_0 for shooting, making use of the tangent at zero to the parameterised function of curvature:

$$\frac{dy/ds}{dz/ds} \big|_{s=0} = \frac{\frac{\delta \pi}{l} \cos \left[\frac{\pi s}{l} \right]}{1} \big|_{s=0} = \frac{\delta \pi}{l}. \tag{5.10}$$

This combination of stress-strain relationship, Curvature Look-Up Table, loading patterns and initial curvature are included among the data as Series E. The key details of Series E are: full stress-strain; internal strains; self-weight; curvature incorporating moment and axial loads. A final data series was created, using the same details as Series E but for no axial thrust component in the Curvature Look-Up Table.

5.3.7 Summary of simulations

Table 5.3.7 summarises the key details in each family of pinned-strut simulations run and Figure 5.4 shows the path followed in the strut simulations.

Series Name	Stress-Strain Type	Curvature Function	Built-in Curvature	Loading
Series A	As per Figure 2.3(a)	$\kappa = \frac{M}{EI_{xx}}$	$\kappa_s = \frac{8\delta}{h^2}$	$w_z(s) = w_y(s) \equiv 0;\ f_z(s) \equiv 0;\ f_y$ is upper-pin point load
Series B	Figure 2.3(d)	Look-up Table (a)	$\kappa_s = \frac{8\delta}{h^2}$	$w_z(s) = w_y(s) \equiv 0;\ f_z(s) \equiv 0;\ f_y$ is upper-pin point load
Series C	Figure 2.3(d)	Look-up Table (b)	$\kappa_s = \frac{8\delta}{h^2}$	$w_z(s) = w_y(s) \equiv 0;\ f_z(s) \equiv 0;\ f_y$ is upper-pin point load
Series D	Figure 2.3(d)	Look-up Table (c)	$\kappa_s = \frac{8\delta}{h^2}$	$w_z(s) = w_y(s) \equiv 0;\ f_z(s) \equiv 0;\ f_y$ is upper-pin point load
Series E	Figure 2.3(d)	Look-up Table (c)	$\kappa_s\,[s] = \dfrac{-\delta\left(\frac{\pi}{l}\right)^2 \sin\left[\frac{\pi s}{l}\right]}{\left(1 + \delta^2\left(\frac{\pi}{l}\right)^2 \cos^2\left[\frac{\pi s}{l}\right]\right)^{\frac{3}{2}}}$	$w_y(s)$ is weight of column above position s; others as above

Table 5.1: Summary of Key Details for Each Strut Simulation

5.4 Results of Strut Simulations

Having run the above families of simulations, two classes of data arise: the initial conditions for a given loading pattern, provided by Shooting, and the Look-Up Tables of y- and z-position, y- and z-loading, moment and angle throughout the member. With five families of simulations tested at 21 or 22 values of λ with incremental loading of between 25-50 stages, a large amount of digital data was created. Each test was deemed to have 'failed' when it was clear that the limiting boundaries of the computer simulation fail to contain the loading pattern. Typically, this appeared as extended time to complete a given simulation, with physically impossible initial conditions found by shooting, or with graphs of the resulting strut showing an unlikely physical deflected position.

Due to the logic of the system of equations and absence of intelligence, the program will try to simulate impossible loading patterns, which prompts the warning appropriate to all computer systems: Garbage In, Garbage Out. This is to say that bad assumptions and incorrect implementations input to the computer will create useless output. The following sections seek to show that the system described here is not garbage input and does not produce garbage output. One such point is the in-plane deflection of the struts: unless constrained, a strut will flex about its weakest axis – unfortunately not the one not tested here.
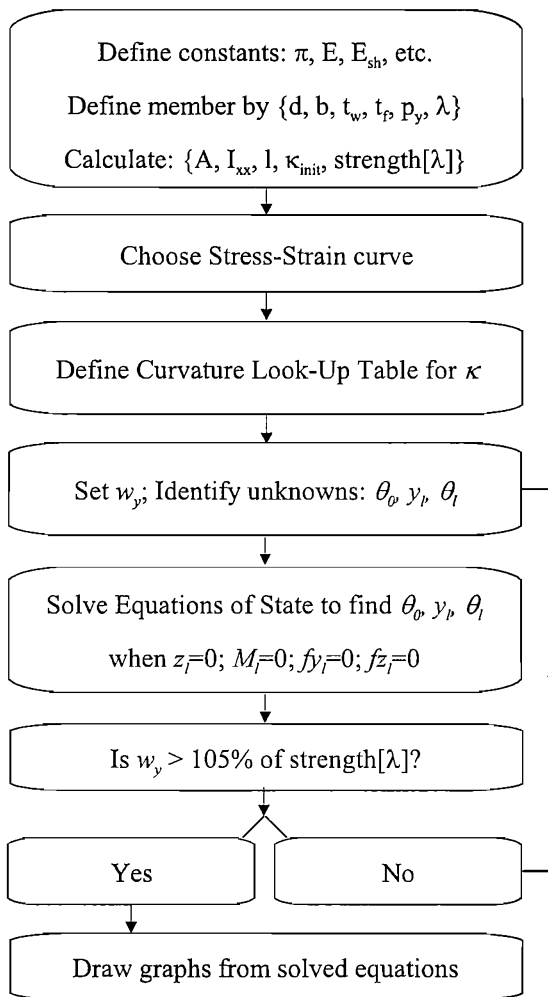
Figure 5.4: Flowchart Summarising the Program Used in Chapter Five's Strut Simulations

Pinned Strut Buckling Stress against Slenderness
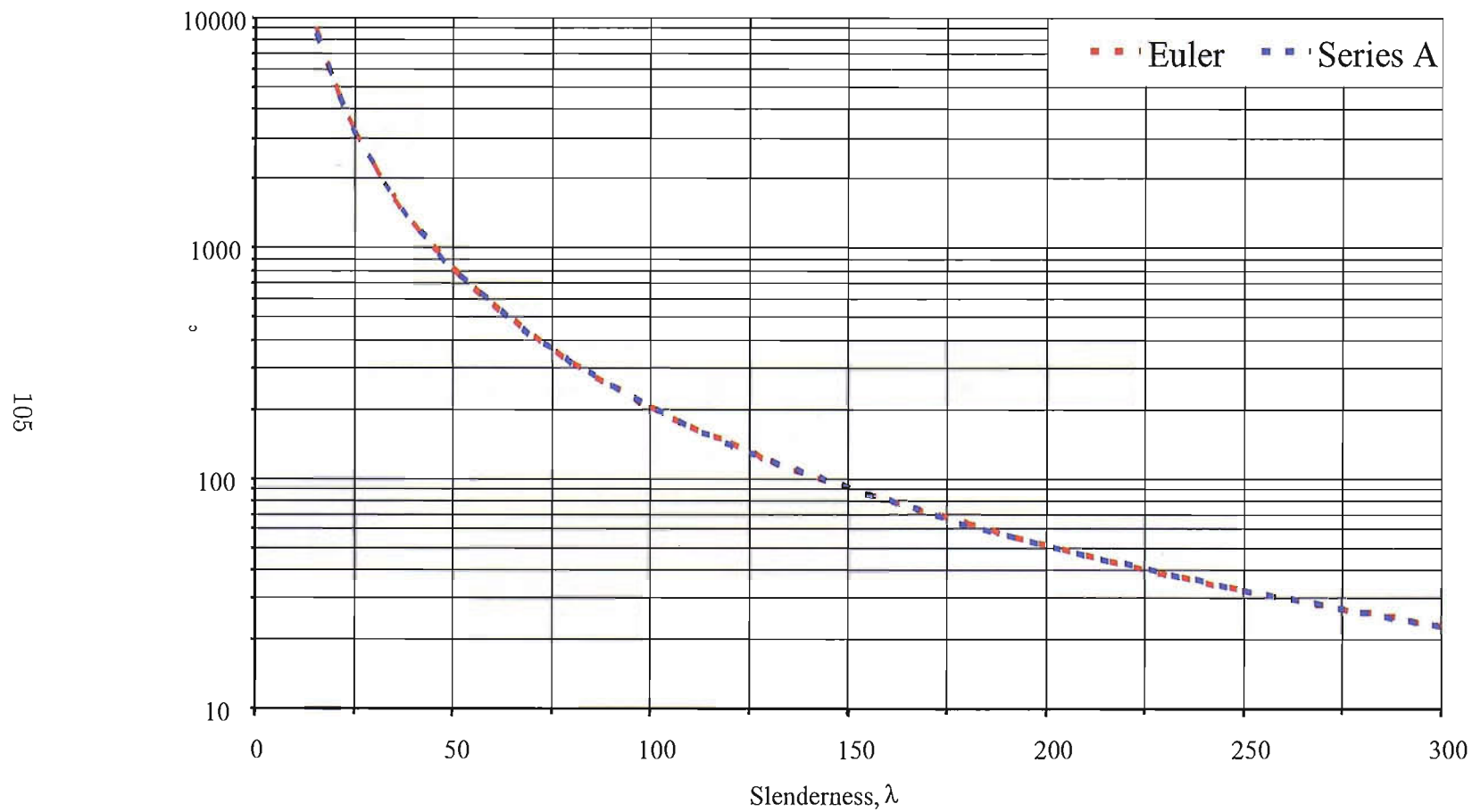
Figure 5.5: Series A simulation data plotted next to data generated by Equation 3.13

**Percentage Error of Series A against
Euler Formula Buckling Strengths**
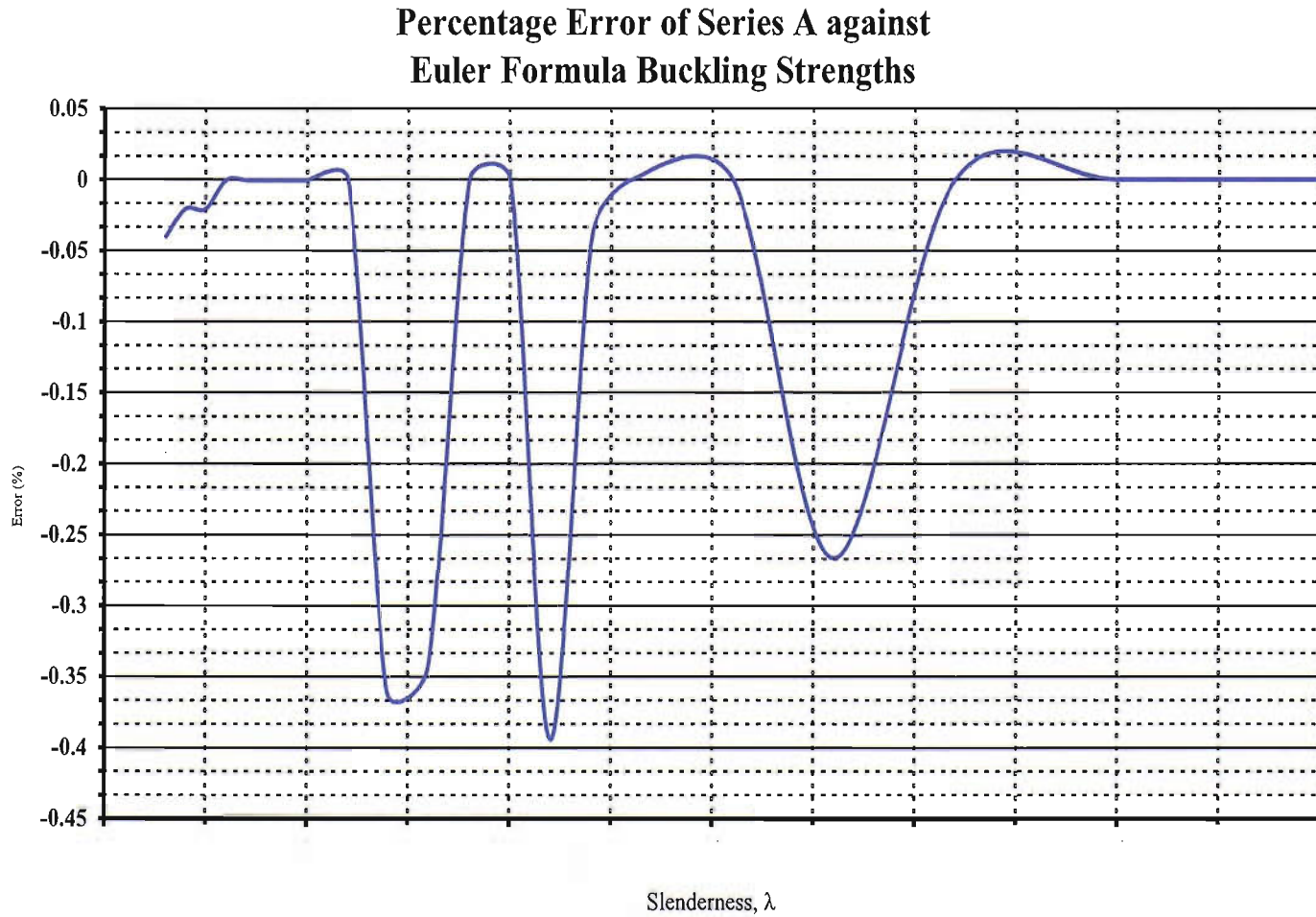
Figure 5.6: Percentage difference Between data from Series A and data generated by Equation 3.13

5.4.1 Elastic Simulations against Euler Buckling Loads

The comparison of the elastic-only simulation family, Data Series A, with
the predictions of

$$P_E(\lambda) = \frac{\pi^2 E}{\lambda^2} \qquad (5.11)$$

is of tremendous importance in establishing whether the methods introduced
in this document are appropriate to structural analysis. Figure 5.5 shows
that, for a large range of values of λ, from 15 to 300, the data in Series A
is a tremendously good fit to the Euler Crushing Load. Figure 5.6 shows
that the percentage proportional error of Series A is never more than 0.4%
from the Euler Crushing Load. For further qualification of the quality of
Series A as a model of a pinned-end crushing strut, the Pearson Product-
Moment Correlation Coefficient, used to show how well-related are two tables
of numbers, has $r_{\text{pearson}} = 0.99990690$ in its first eight significant digits.
In the context of a perfect positive correlation having $r_{pearson}=1$, this is a
remarkable result. Additionally, performing a two-tailed significance test of
the correlation of this data provides a p-value probability that the association
is a random coincidence of 5.00×10^{-35}.

It may be of note to show Figure 5.7 of a sample Series A simulation
over-loaded far past the Euler crushing load, behaving in a similar manner
to a family of curves known as the Elastica. It is not possible to examine the
midpoint deflection of the strut, as will be done below for other simulations,
because of the undefined parameter in the solution $y = \mu \sin\left[\sqrt{\frac{P_{cr}}{EI}}s\right]$ to
Euler's Strut Bucking Equation (also seen as Equation 3.12):

$$\frac{d^2y}{ds^2} + \frac{P_{cr}.y}{EI} = 0. \qquad (5.12)$$

5.4.2 BS5950 against Series E

As with Series A, a comparison of Series E against the BS5950 Table 24(a)
failure stress shows an exceptional similarity between these values of failure
stress. The data of Series E are not available for the full range of λ as seen
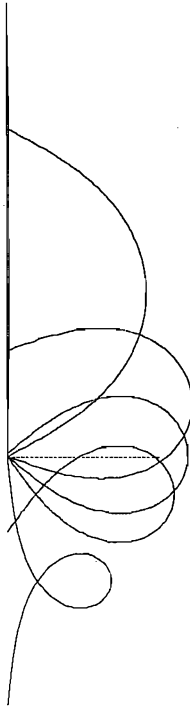
Figure 5.7: Elastic strut continuing to buckle as its pin passes through the simulation's 'floor'

in previous families of simulations due to difficulties in creating entries for Moment-Curvature Look-Up Table (c) at high values of axial load and low values of moment. Further work would seek to include the flexure of local buckling which is manifest in high-thrust and low-moment loading patterns.

Pinned Strut Buckling Stress against Slenderness
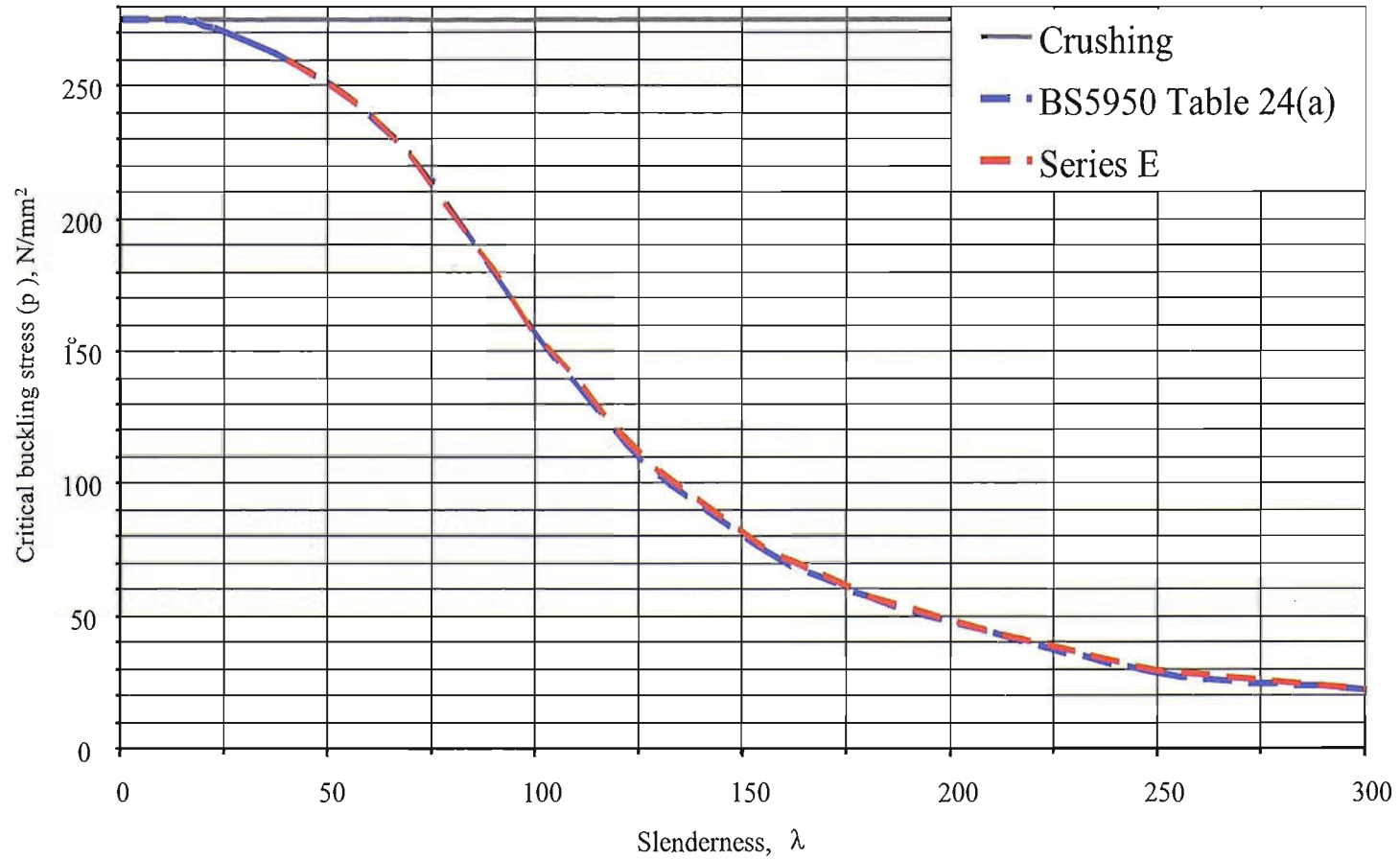
Figure 5.8: Series E data plotted next to BS5950 Table 24(a) data

Figure 5.8 is a side-by-side comparison; Figure 5.9 shows how small the deviation is between these two sets of data. Again, the Pearson Product-Moment Correlation Coefficient is invoked as a measure of similarity between the two sets of data, and is calculated to be 0.99994780 in its first eight places, with the two-tailed significance test having p-value 2.87×10^{-30}.

Figure 5.9: Percentage Error of Series E against BS5950 Table 24(a) data

5.4.3 The Impact of Internal Strain

Computer simulations of thrust-dependent buckling struts should make necessary the inclusion of thrust in the Curvature Look-Up tables of the simulation. Less obvious is the need for the internal strains arising from the hot-rolling fabrication process. Series C and D share the same initial factors of stress-strain response, loading patterns, initial curvature. Their only deviation is in their Curvature Look-Up Tables, with both using the interaction of Moment and Curvature loading to follow the curvature of a cross-section in the Equations of State. Series C neglects, while Series D includes, the additional internal strains found in hot-rolled members. Figure 5.10 shows the respective Strut-Buckling Curves of Data Series C and D.

Pinned Strut Buckling Stress against Slenderness
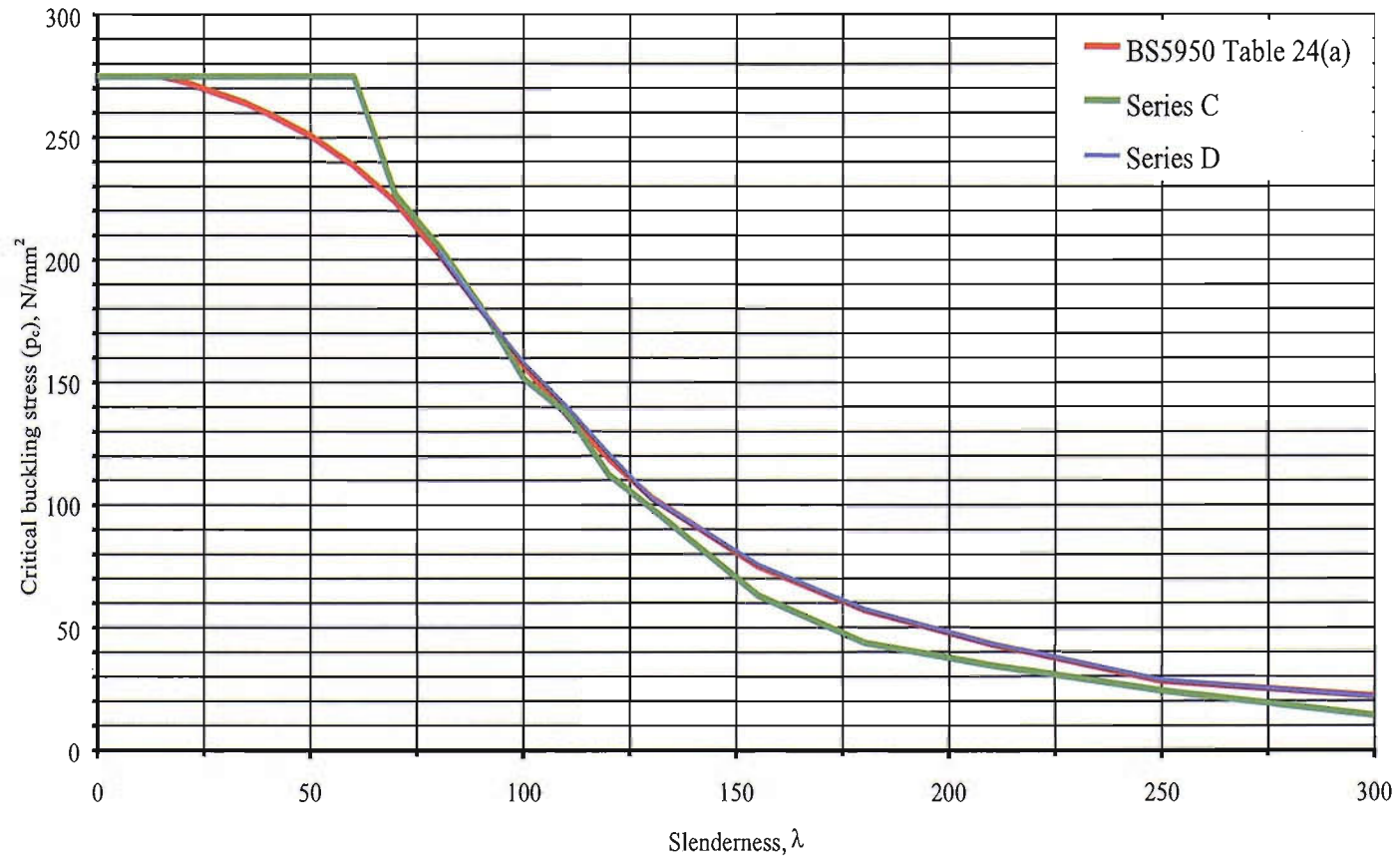
Figure 5.10: Series C, D and BS5950 Mean Stress at Failure
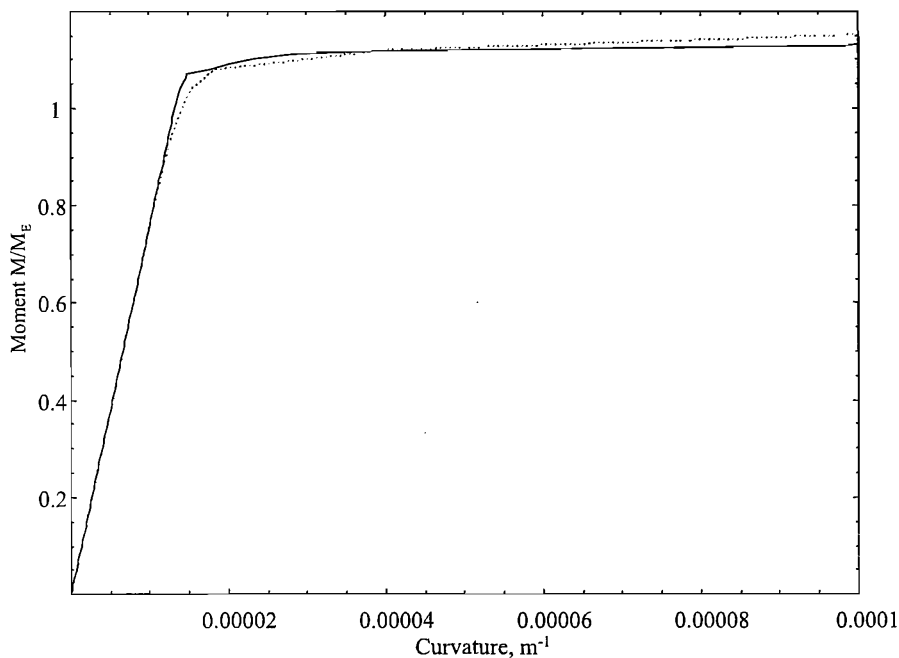
Figure 5.11: Moment against Curvature comparing Look-Up Tables (b) (solid line) and (c) (dashed line) into post-elastic behaviour

Series D and BS5950 are so close as to be indistinguishable above $\lambda = 70$, in Figure 5.10, while Series C is only able to closely predict the BS5950 Crushing Load between $70 \leq \lambda \leq 120$. The additional resistance to crushing failure of Series D above $\lambda = 125$ comes from the increased strain capacity around the web-flange junction in the lower half of the I-Section, that is the portion of the cross-section under tensile forces from the Moment load which has increased compressive strain from the Hot-Rolling fabrication process.

As remarked in Chapter Four (particularly Figure 4.11, Page 89, reproduced here as Figure 5.11), the presence of internal strains in the computer model alters the Curvature Look-Up Table such that Series C will be stiffer before abrupt onset of plasticity with lower post-plastic resistance to deflection where Series D has a smoother 'knee' into plastic behaviour and stiffer post-plastic response. This provides the interpretation of the differences of the respective Data Series' Strut-Buckling curve: where C and D fail at sim-

114

ilar loads $(70 < \lambda < 130)$, little post-elastic behaviour occurs, and where their fail loads diverge $(130 < \lambda < 300)$, the difference in post-elastic behaviour generates the difference in failure loads. In the more-slender struts, the increased flexure is associated with increased curvature, which is shown in Figure 5.11 to match larger values of curvature to lower values of moment for Series C than D. This increased curvature results in larger deflections and consequent lower failure load. It is clear that Internal Strain behaviour is important in slender struts to counteract their increased flexure compared to stocky struts.

5.4.4   Increasing the Accuracy of Computer Models

The failure load differences between Series D and E are minimal. This is a testament to the Curvature data created in Chapter Four. The results that D and E provides an additional quality which should not be overlooked: that Series E has a higher-fidelity model of a strut and consequently is able to provide results close to the BS5950 curve for lower values of λ than D does (5.2). Even though the series do not have a full set of data for the whole range of λ, among Series E's additional data is a call to more-detailed computer models for a higher degree of accuracy.

5.5   Conclusions

This chapter developed a computer model of a buckling strut according to the mathematical model developed in Chapters Three and Four. A pin-ended strut, loaded axially and constrained to the major axis of its 203x102x23 I-Section, was simulated and five families of simulations were run at a range of values of strut slenderness from $\lambda = 0$ to $\lambda = 300$, combining variations of stress-strain response, Curvature Look-Up Table (from Chapter Four) and cross-section internal strain. Each simulation presented data points of the mean stress at failure, which are analyzed, compared and discussed.

λ	BS5950 Failure Load	Series D	Series E
30	260		
40	260		259.948
50	251		250.7
60	239		240.258
70	224		224.121
80	203	203.5	202.541
90	180	179.846	181.345
100	157	158.172	156.219
110	137	140.458	139.213
120	119	120.834	119.875
130	103	102.959	104.695
155	75	75.7936	75.0912
180	57	57.4508	57.1361
210	43	43.2098	43.6268
250	28	28.4876	28.4876
300	22	21.745	21.745

Table 5.2: Failure loads comparing numerical results of Series D and E to BS5950

The agreement between the elastic-only strut and the predictions from Euler's Strut Formula are exceptionally well correlated and provide an impressive base-line for the reliability of the method developed here. This baseline is bettered by the fullest-detail strut simulations in the chapter matching the BS5950 Table 24 Strut-Buckling for Class A sections. This simulation used a full-range stress-strain function and a Curvature Look-Up Table built from the interaction of moment, thrust and member internal strains. The small differences between a few of the series of data serves both to describe the iterative development of the strut-buckling simulation and to highlight the causes of previously unidentified member behaviour. In particular, the

impact of internal strains in Data Series D in comparison to its predecessor, Series C, shows the importance of internal strains to increase the post-plastic stiffness of slender ($\lambda > 130$) members.

Overall, this chapter achieves its aim to show that Analytic Structures' mathematical model is suited to structural analysis, being a highly-reliable means to model structural elements. The next step is to show the reliable simulation of structural elements within a whole structure.

Chapter 6

Simulated Portal Frames

6.1 Introduction

Due to its economy and versatility, the steel portal frame is the most common structural form in pitched-roof buildings. Its typical loading pattern consists primarily of large moments but relatively low axial thrusts and it is ideally suited to the modelling system developed and described in this project. With the mathematics of the system, the development of Curvature Look-Up Tables described, a real-world application is an ideal place to compare existing design practice and an existing computer design package.

6.2 Methodology

An in-plane two-dimensional model of a single-bay portal frame was developed in the Analytic Structures system and progressively-loaded until failure. The structural model is, in principle, similar to that used in Chapter Five. As before, the physical constants and member properties are defined. The loading pattern was also created, and the initial guesses prepared. The six Differential Equations of State remain the same as those laid out in Chapter Three. The Curvature Look-Up table follows the same principles as described in Chapter Four. The looped search for solutions is the same, in principle, as that used in Chapter Five. It differs in using four steps, one for each member in the span. This can be most easily achieved by solving the Different Equations of State for each component member of the structure, supplying the final state of each member to the next. The general program outline appears in Figure 6.1; the path taken within the Shooting stage of the Portal Frame simulations is summarised in the flow-chart of Figure 6.2.

The first iterations of the computer model used the same cross-sections in both the columns and rafters to check that the guesses used in Shooting could find suitable initial conditions. The dimensions of the frame simulated are sketched in Figure 6.3 and adopt the convention of measuring to the member

119
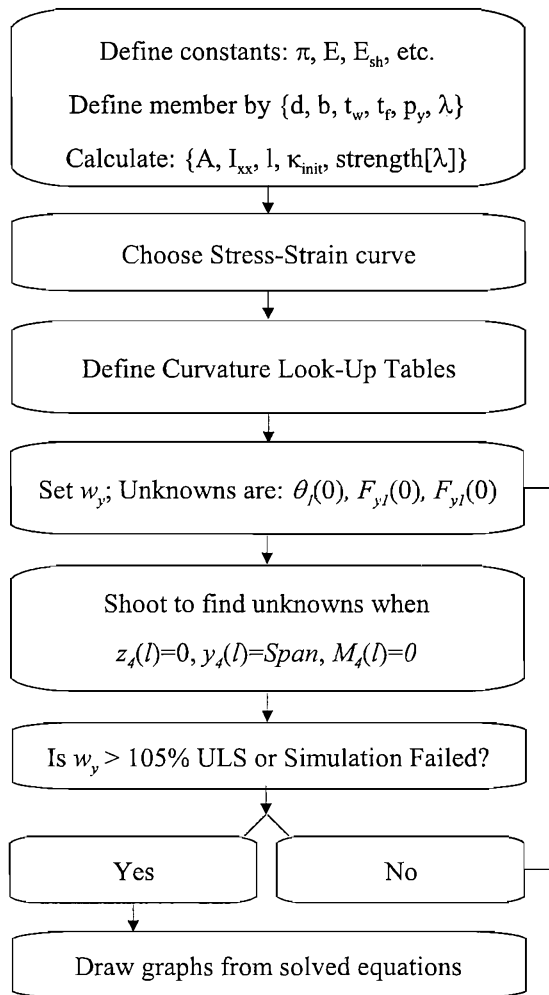
Figure 6.1: Flowchart Summarising the Program Used in Chapter Six's Portal Frame Simulations

centrelines. This first round of simulations only depended on the Moment loading, using Curvature Look-Up Table (a) in S275 Steel. It provided results which justified the development of further models. Subsequently, the behaviour of Moment and Thrust loading and the internal strains of hot-rolled cross-section was included, via Curvature Look-Up Table (c), along with adaptations for differing I-Sections in the column and rafters (Column: 533x210x101 UB; Rafter: 457x191x67 UB), both in S275 Steel. These simulations, again, delivered behaviour in line with experimental results.
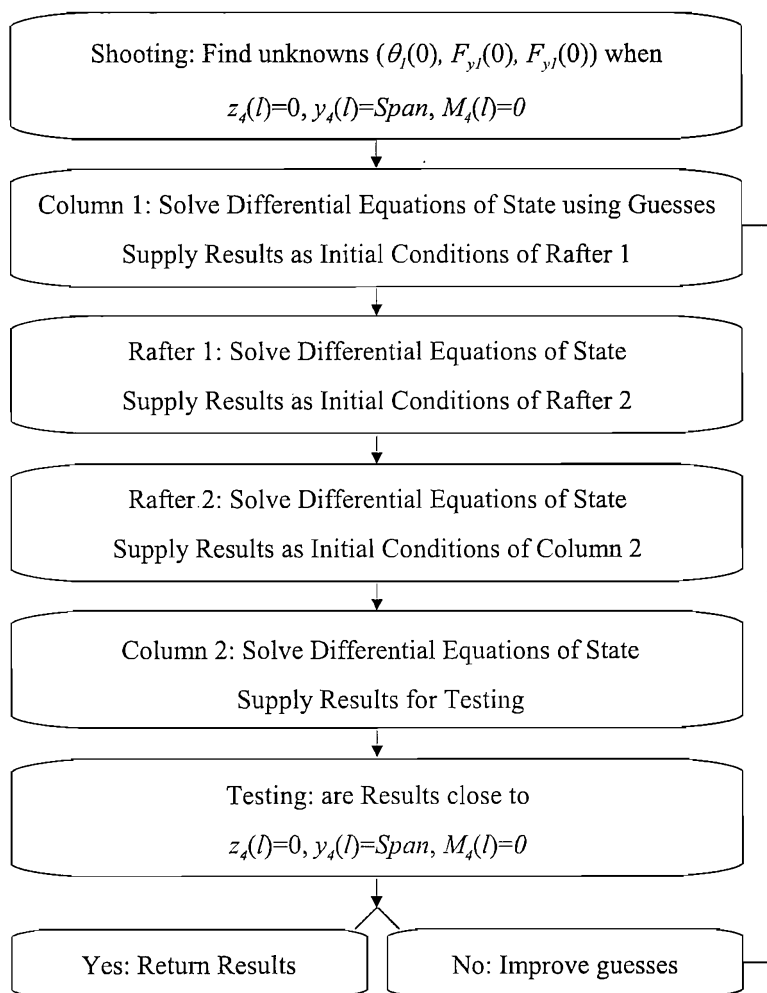
Figure 6.2: Flowchart Summarising the Shooting Process for Four Members of the Portal Frame

121
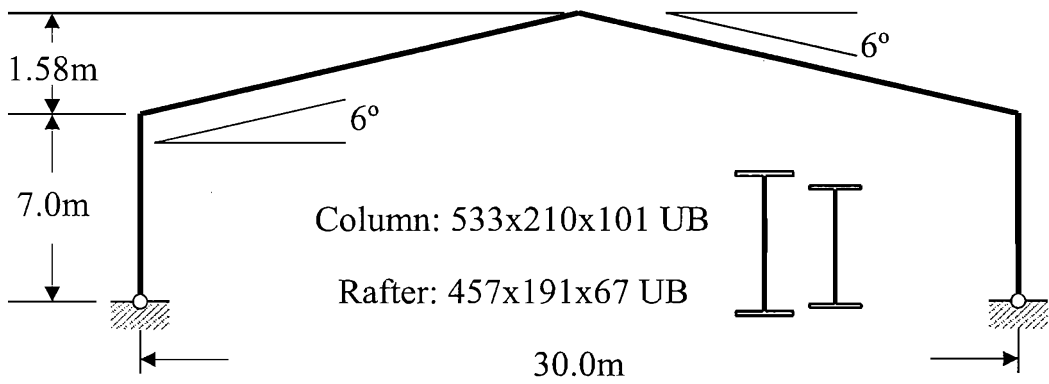
Figure 6.3: Dimensions of the Portal Frame tested here

The figure shows a portal frame with the following labeled dimensions and members:

1.58m

7.0m

6°

6°

Column: 533x210x101 UB

Rafter: 457x191x67 UB

30.0m
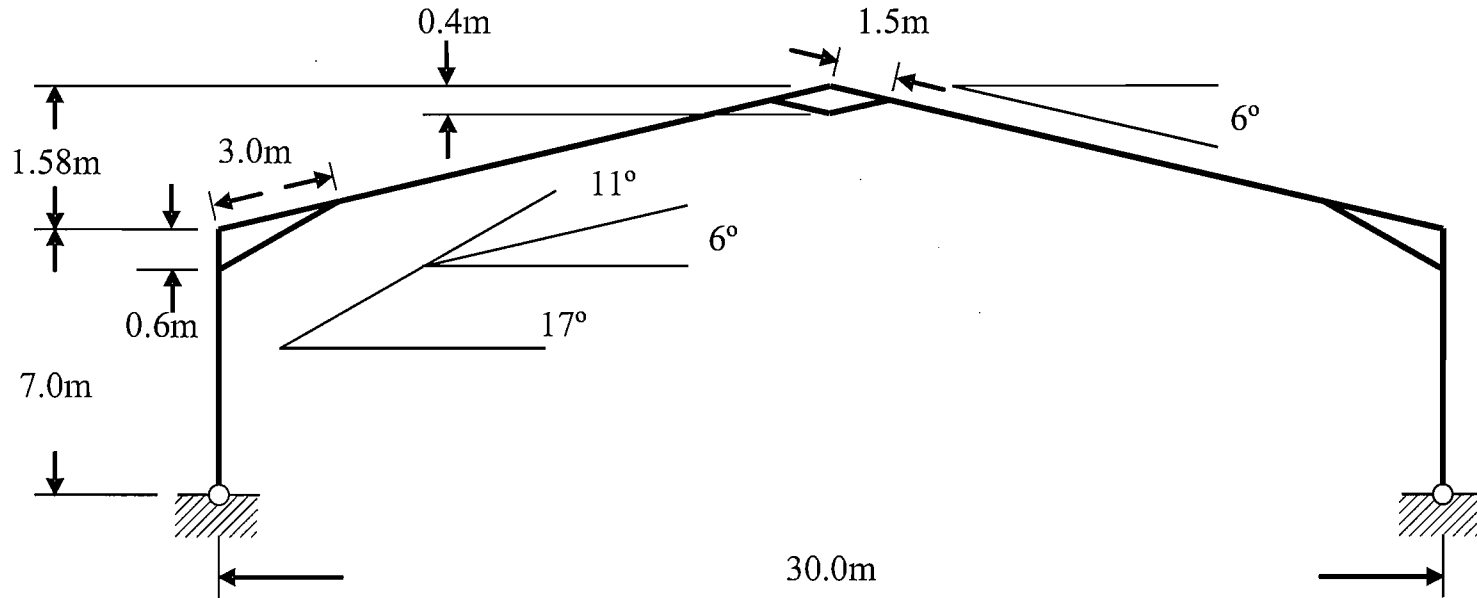
Figure 6.4: Dimensions of the full Portal Frame with additional haunches

The third iteration of the model included haunches at each joint. The specific details are shown in Figure 6.4 Under the assumption that haunched cross-sections would remain elastic and, as ever with portal frames, that axial loads are minimal in contrast to moment loads, the Curvature Function for the haunches used an adapted form of Equation 3.2, varying according to the I_{xx} of the cross-section. Throughout the Analytic Structures method, there is a dependence upon the position along the member, s, and as a result it was simple to calculate the second moment of area of the I-Section plus its haunch:

$$I_{xx}^H = \frac{b(d+x)^3}{12} - \frac{(b-t_w)(d+x+t_f)^3}{12} + \frac{(b-t_w)t_f^3}{12} + t_f(b-t_w)(\frac{x-d-t_f}{2})^2.$$

(6.1)

This version of the calculation – one of many possible alternatives – uses an I-Section of height $d + x$ and adds to it the flange of the original non-haunched cross-section, shown in Figure 6.5. Converting the position s in the haunched section of a member to the depth x is a linear equation:

$$x = \frac{s}{L_{\text{haunch}}} d_{\text{haunch}}$$

(6.2)

for appropriate values of the length (L_{haunch}) and depth (d_{haunch})of the haunched section. In this instance it is assumed that the length of the Haunch (L_{haunch}) is the length in the direction of the member and that d_{haunch}, the haunch depth is the total extra depth added, from the lowest point of the original cross-section's web to the base of the haunch web.

In order to extend the existing four-member model of a portal frame, a considerable time-saving approximation was made: the haunched parts of each member were added as highly-resistive sections at their respective ends of the columns and rafters (as in Figure 6.6). This will cause the resistance to motion of the eave haunches to count twice in resisting bending – once at the top of the column and also at the start of the rafter. Although this amendment did not harm the simulation's reliability (as is shown below), this method of haunch inclusion is inadequate. Plans for its replacement,

124
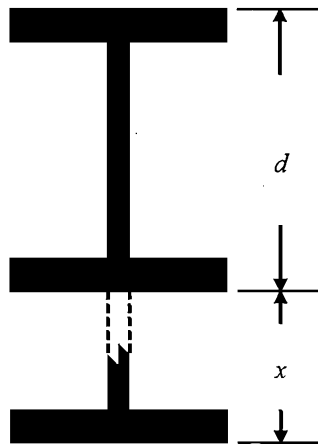
Figure 6.5: Dimensions of I-Section Haunch for use in Equation 6.1
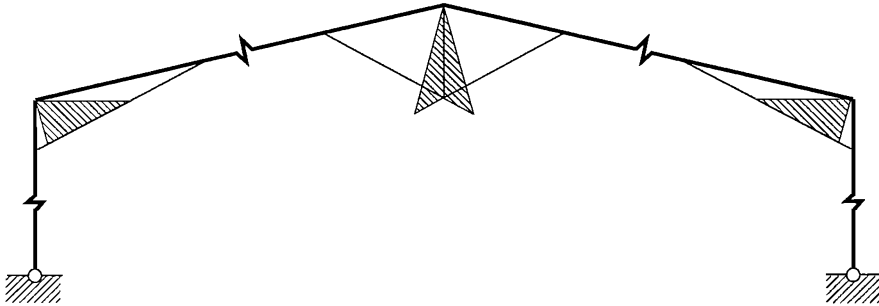
Figure 6.6: Simple implementation of Haunches has overlapping sections, which
are highlighted

simulating each of the haunched sections as distinct members, is outlined
among the further work.

The final amendments included altering the cross-section data for the
portal frame to use different members for column and rafter and to include
in the loading pattern the self-load of the frame. From the data provided
by each completed simulation, four key figures were drawn: First is the
displacement diagram, scaled 1:1 for the deflection; second, the ubiquitous
Bending Moment Diagram; third, showing the strains at each extreme of the
member's fibres; and fourth, a figure showing the reduced stiffness of the
member. These measures are discussed in greater detail below.
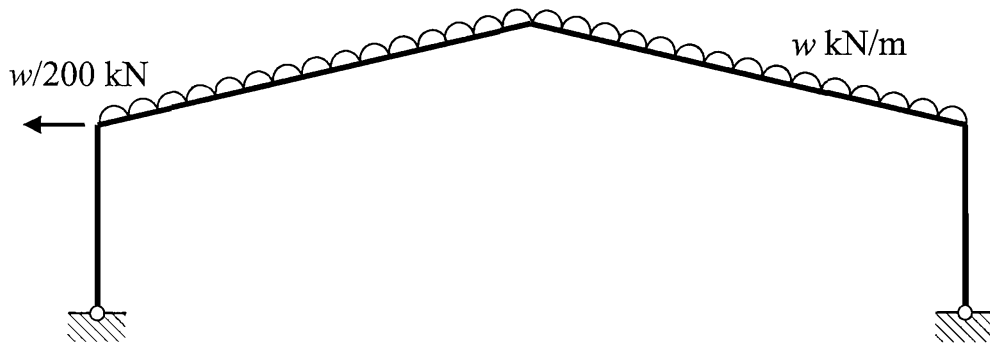
Figure 6.7: Loading pattern for the Portal Frame under examination

6.3 Testing

The model of Portal Frame selected for testing was that of a 30m span with 7.0m eaves height and rafter angle 6° (Figure 6.3). This was selected to match the hand calculations presented in the worked example by Salter et al. (2004) (SCI Publication No252). This calculation of collapse load was repeated using the *Fastrak Portal Frame* programme developed by CSC Ltd in conjunction with Professor J.M.Davies of Manchester University. This programme uses the elasto-plastic design methodology and is marketed specifically for portal frame design. Thus the predictions of collapse load provide a good benchmark for the predictions from the methodology developed herein.

The cross-sections used were input to the frame simulation in *Mathematica*, and Curvature Look-Up tables were calculated for the column and rafter cross-sections. The load pattern is as Figure 6.7, with a uniformly distributed load w working vertically across the rafters and a horizontal load of $w/200$ at the left-side eaves-rafter join providing the Notional Horizontal Load. The loading w does not include the forces from self loading due to their whole-frame context in contrast to the uniform loading of w across the rafters. As assumed in SCI-P252, the gravity load case is dominant in this analysis.

The predictions made by the elastic-plastic simulation from *Fastrak* in-

clude an overview of the members and their positioning, haunch and restraint positioning, varied load cases as per the detailed design stage, graphs of the position of plastic hinges, the frame bending moment diagram and examinations of frame stability. Again, it is the frame bending moment diagram and collapse load calculations which provide insight into the predicted behaviour and consequently assist qualification of the Analytic Structures method.

Among the most significant of the contributions from the Analytic Structures method is the ability to examine the ongoing process of post-elastic behaviour. Where other analysis methods break each member into discrete chunks, continuity is retained because of the analytic properties of the six core differential equations of state. The creation of a sufficiently-detailed Curvature Look-Up Table is essential to this process, and the final results of these simulations are to be investigated below.

The admission must be made that these simulations are intended to be provisional indications of the applicability of the method to portal frame analysis. Not all of the results replicate those in Salter et al. (2004) – some of the results diverge from methods used for comparison which is to be expected in the situations where existing analysis makes assumptions which have no corollaries in Analytic Structures. The differences between empirical observation and behaviour predicted by Analytic Structures also offer indicators of the potential for fine-tuning of the simulations used here.

6.3.1 Measuring the Formation of Plastic Hinges

The early stages of yielding do not cause significant loss of stiffness in a member because the majority of the section remains elastic and therefore stiff. Conversely, significant yielding throughout a cross-section leads to a substantial loss of stiffness which will then be referred to as a plastic hinge. The progression of the plastic hinges has been recorded herein by a percentage loss of stiffness, which is defined as the second moment of area of the elastic

region of the section divided by the full second moment of area. If there the two points within the cross-section at which the plastic boundary occurs are labelled y_1 and y_2 which are measured from the centroid and which adopt the convention $y_1 < 0 < y_2$, Analytic Structures calculates the reduced I_{xx} from:

$$I'_{xx} = I_{xx} + I'_{xx.2} + I'_{xx.2} \qquad (6.3)$$

$$I'_{xx.1} = \begin{cases} 0 & y_1 < -\frac{d}{2} \\ -b(y_1 + \frac{d}{2})(\frac{y_1-d}{2})^2 & -\frac{d}{2} < y_1 < -\frac{d}{2} + t_f \\ -bt_f(\frac{-d-t_f}{2})^2 - t_w(y_1 + \frac{d}{2} - t_f)(\frac{y_1-d+t_f}{2})^2 & -\frac{d}{2}f < y_1 < 0 \end{cases}$$
$$(6.4)$$

$$I'_{xx.2} = \begin{cases} 0 & \frac{d}{2} < y_1 \\ -b(\frac{d}{2} - y_2)(\frac{d+y_2}{2})^2 & \frac{d}{2} - t_f < y_2 < \frac{d}{2} \\ -bt_f(\frac{d+t_f}{2})^2 - t_w(\frac{d}{2} - t_f - y_2)(\frac{d-t_f+y_2}{2})^2 & 0 < y_2 < \frac{d}{2} - t_f \end{cases} \quad (6.5)$$

Table 6.1 shows the proportions of second moment of area that each segment of the cross-section provide. With the flanges providing close to 80% of the stiffness of a cross-section, it is likely that a hinge occurs when the reduced stiffness is less than 20% of the original I_{xx}.

Member	Dimensions	$I_{xx}(cm^4)$	Flange $I_{xx}(cm^4)$	% of I_{xx}	Web $I_{xx}(cm^4)$	% of I_{xx}
Column	533x210x101	5.814×10^4	2.331×10^4	40.085%	1.153×10^4	19.830%
Rafter	457x191x67	2.898×10^4	1.171×10^4	40.407%	5.560×10^3	19.186%

Table 6.1: Proportions of Second Moment of Area and Stiffness from Flanges and Web

The table below provides a method to calibrate the reduced second moment of area. The table above shows that 80% of the I_{xx} lies in the flanges, and so the reduced second moment of area should be less than 20% in a hinge. When these hinges appear, knowing the order in which they form for a range of values of the reduced second moment of area will permit criteria to be established as to the presence of a fail-capable section of plasticity. In the

table below, the three-letter names for members denote either right-or left-hand side by their first letter, and whether a column or rafter by their third: Left-Hand Column (LHC); Left-Hand Rafter (LHR); Right-Hand Column (RHC); and Right-Hand Rafter (RHR).

Stiffness Reduction, %		20	50	80	85	89	90	91	95
First Hinge	w_y	8.36	8.66	8.86	9.06	9.36	9.36	9.46	9.66
	Member	LHC	LHC	LHC	LHC	LHC	LHC	LHC	LHC
	Span	6344-6400	6329-6400	6331-6400	6341-6400	6316-6400	6369-6400	6337-6400	6361-6400
Second Hinge	w_y	9.16	9.46	9.66	9.96	10.96	10.96	11.06	11.16
	Member	LHR	LHR	LHR	LHR	LHR	RHR	RHR	RHR
	Span	3000-3029	3000-3014	3000-3006	3000-3016	3000-3003	1500-1596	1500-2417	1500-2383
Third Hinge	w_y	9.66	10.06	10.56	10.86	10.96	11.16	11.16	11.26
	Member	RHC	RHC	RHC	RHR	RHR	LHR	LHR	LHR
	Span	600-655	600-625	600-608	1500-2288	1500-2032	3000-3037	3000-3017	3000-3083
Fourth Hinge	w_y	10.56	10.66	10.76	11.06	11.16	11.16	11.36	11.36
	Member	RHR	RHR	RHR	LHR	LHR	LHR	LHR	LHR
	Span	1500-2271	1500-2047	1500-2189	13120-13583	13367-13583	13582-13583	13454-13583	13036-13583

Table 6.2: Sequence of hinge formation for varying severity of plastic hinges (w_y in kN/m, Span distances in mm from start of member

This shows an unexpected pattern of plasticity, with the appearance of plastic sections in the left-hand rafter and right-hand column before any plasticity emerges in the right-hand rafter. The distinction is so great that both left-hand rafter and right-hand column are very near to no elastic second moment of area as small portions of plasticity appear in the right-hand rafter. Also, a second portion of plasticity emerges in the left-hand rafter at the end of the apex haunch at failure. Despite these additional areas of plasticity, the failure relies upon hinging mechanisms at the base of the eaves haunch on the left-hand side and at the end of the apex haunch in the right-hand rafter, shown by the scale of reduced stiffness in the right-hand rafter in the each column in which it appears, typically being an order of magnitude larger in length than comparable portions of the left-hand rafter or right-hand column. The point at which this behaviour predominates over the other regions of plasticity is at 10% of the full cross-sectional stiffness. This suggests the 10% of a section's I_{xx} is the boundary at which reduced stiffness plastic hinging occurs and further provides a rule-of-thumb boundary for the furthest infringement of plasticity in an I-section member appearing at $\pm\frac{2}{3}\frac{d}{2}$.
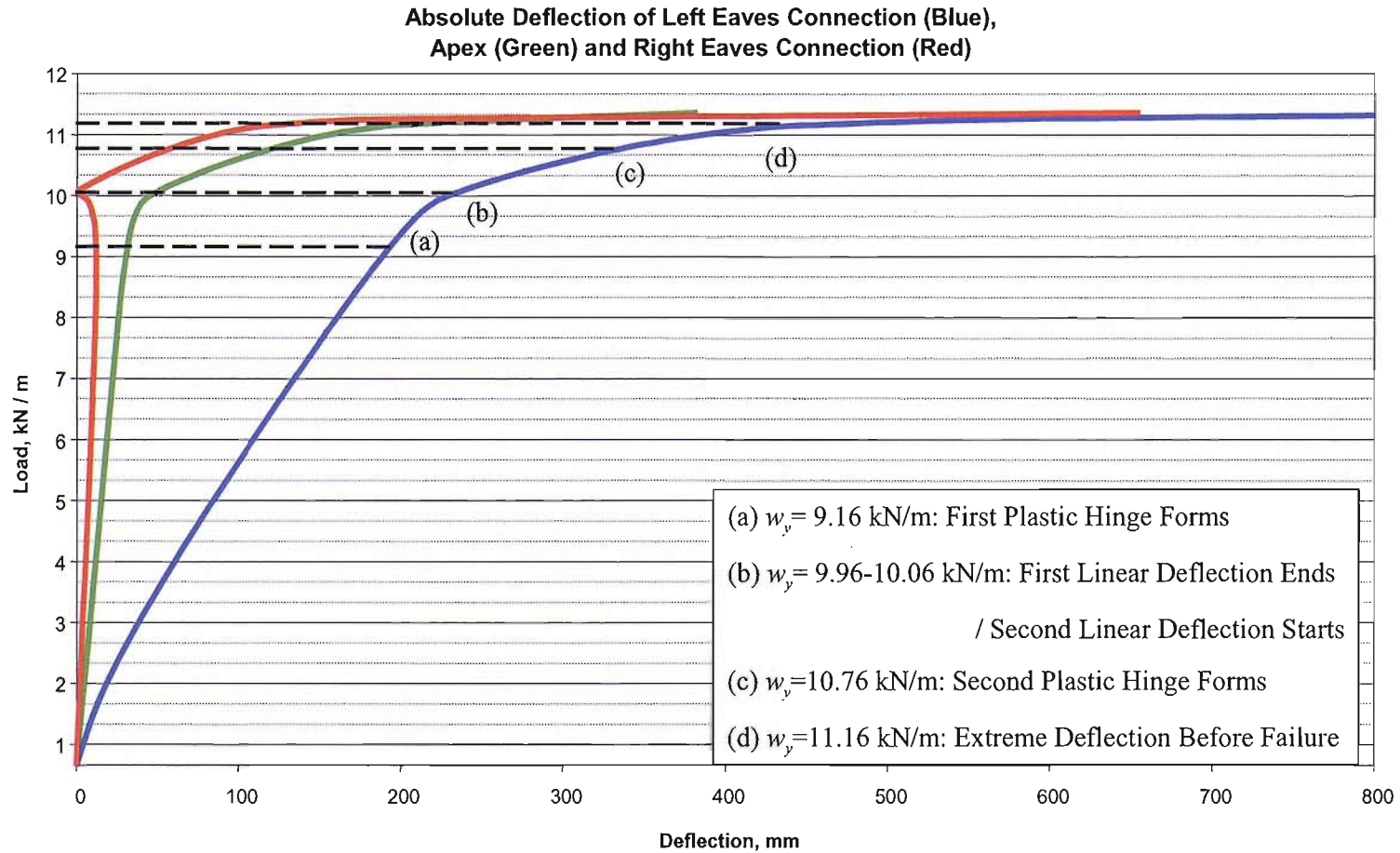
Figure 6.8: Absolute Deflection of Left Eaves Connection (Blue), Apex (Green) and Right Eaves Connection (Red) NB: Initial value 0.66 kN/m is self weight of frame rafters
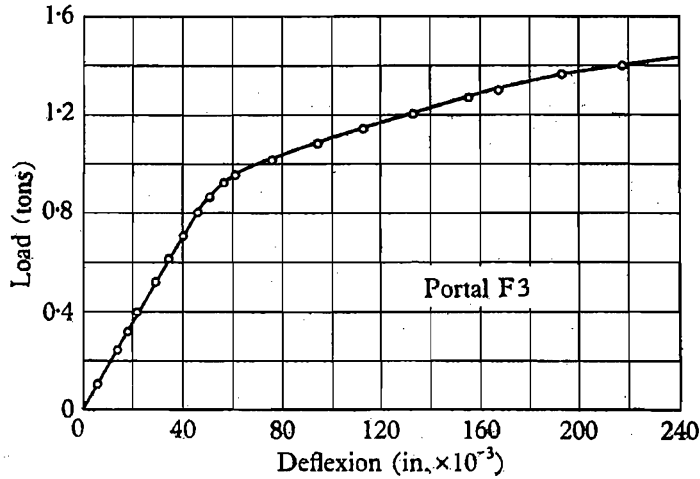
Figure 6.9: Load-deflection curve from Baker (1956) showing second linear section of deflection

Figure 6.8 shows the absolute distance of the right eaves (red), apex (green) and left eaves (blue) from their respective starting positions as the loading increases. The line marked (a) shows the appearance of plasticity in the frame. The load here, w_y, is 9.16 kN/m, but the near-linear deflection continues until the line marked (b), between w_y=9.96 and w_y= 10.06 kN/m. The line (b) shows the end of linear deflection and the start of a second linear stage of deflection, similar to that of Baker (1956), as shown below in Figure 6.9. The additional stiffness after w_y=10.06 is supported by the graphs of strain in the extreme fibres of the cross-section: at w_y=10.06 kN/m strain hardening appears in the left-hand column. The ability of the strain-hardened portions of the structure to resist the weakness of plasticity ends when w_y reaches 11.06 kN/m (c), where uncontrolled deflection begins before eventual failure of the simulation at w_y =11.36 kN/m.

Development of First Plastic Hinge (Figure 6.8(a))

The elastic limit of the frame was reached when w_y =9.16 kN/m (80.6% of collapse load), seen in the red highlighted portion of the Bending Moment

133

Diagram of Figure 6.10. Whilst this load signals the true limit to elastic behaviour, deflections remain linear until a load of 9.96kN/m was exceeded. Figure 6.8 shows that the eaves cease spreading apart and begin to sway sideways after w_y=9.66 kN/m.

(a)

M_P exceeded at (a) for 333.28mm below start of haunch
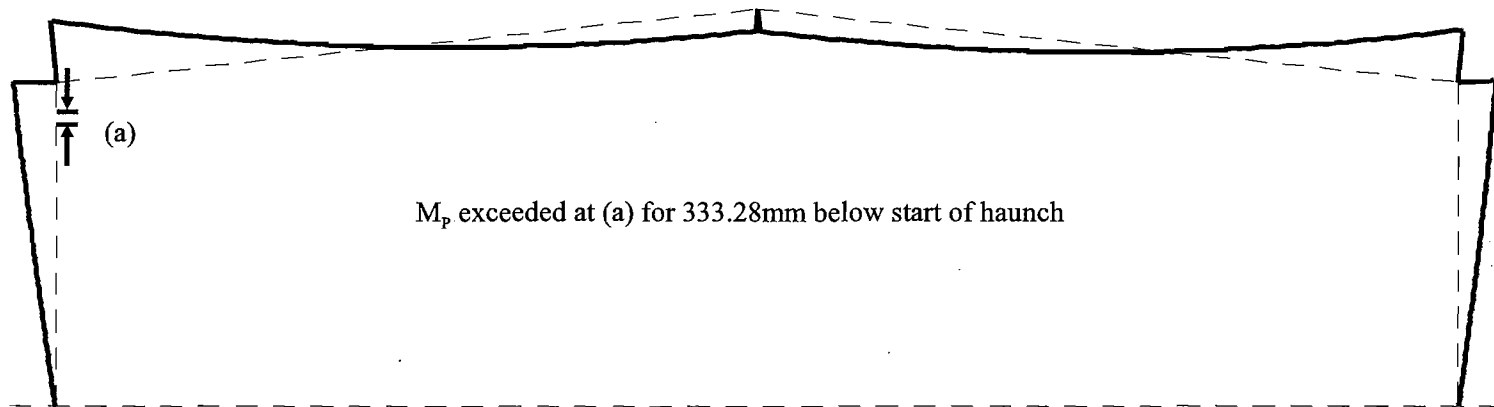
Figure 6.10: Bending Moment Diagram for w_y=9.16 kN/m (80.6% of failure load)

First Reduced Stiffness Hinge

The behaviour of the structure at w_y=9.36 kN/m is classified as having a plastic hinge in the left-hand column, beginning below the eaves haunch and extending down the column. Figure 6.11 shows the reduction of member stiffness at w_y=9.36 kN/m, with the minimal values of remaining elastic portion of the cross-section provided as an annotation: the left-hand column has a minimum of 9.40% at the hinge marked (a); the left-hand rafter has its least elastic portion marked by (b) which clearly indicates that significant (in this case more than 40%) plasticity does not correlate with plastic hinging. Interpolation between steps of loading shows that the 10% reduced stiffness criterion is exceeded – and the hinge appears in the left-hand column – when w_y=9.32 kN/m.
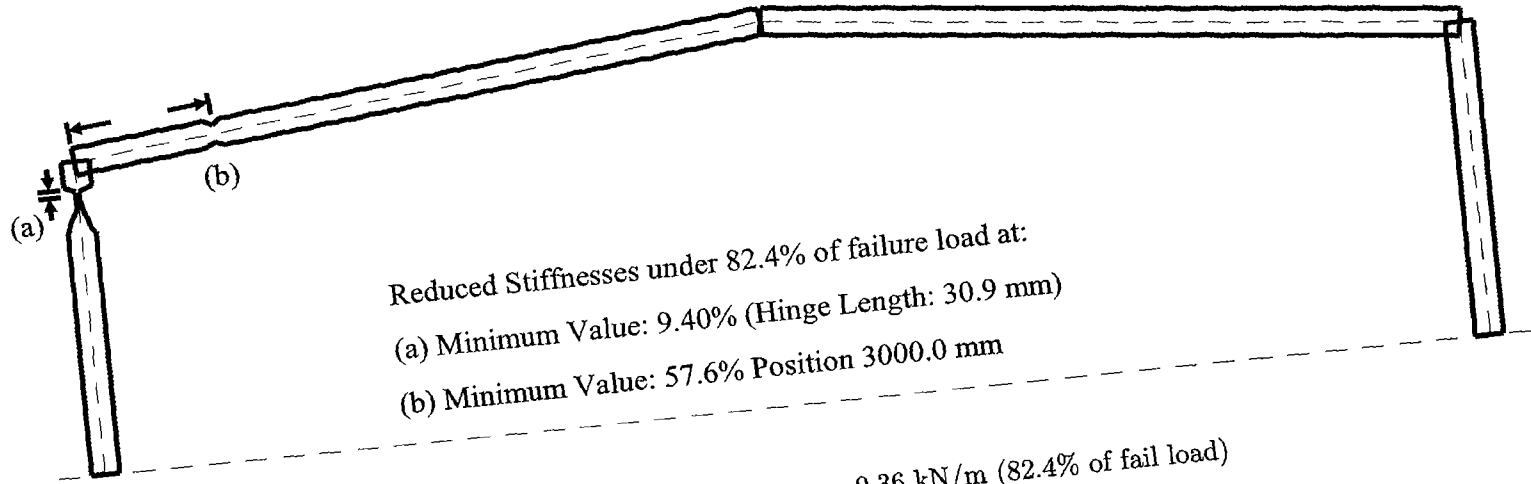
Figure 6.11: Reduced Stiffness at w_y=9.36 kN/m (82.4% of fail load)

Reduced Stiffnesses under 82.4% of failure load at:

(a) Minimum Value: 9.40% (Hinge Length: 30.9 mm)

(b) Minimum Value: 57.6% Position 3000.0 mm

Appearance of Strain Hardening (Figure 6.8(b))

Figure 6.12 shows the formation of the first hinge at 88.6% of the collapse load. The figure shows that the hinge has formed fully and strain hardening begun. Plastic strains are shown in yellow; strain-hardening in red, indicating that the hinging portion of the left column is resisting unhindered plastic deflection. This additional resistance drives the frame into a sway deflection pattern where prior deflection was spread (Figure 6.8).
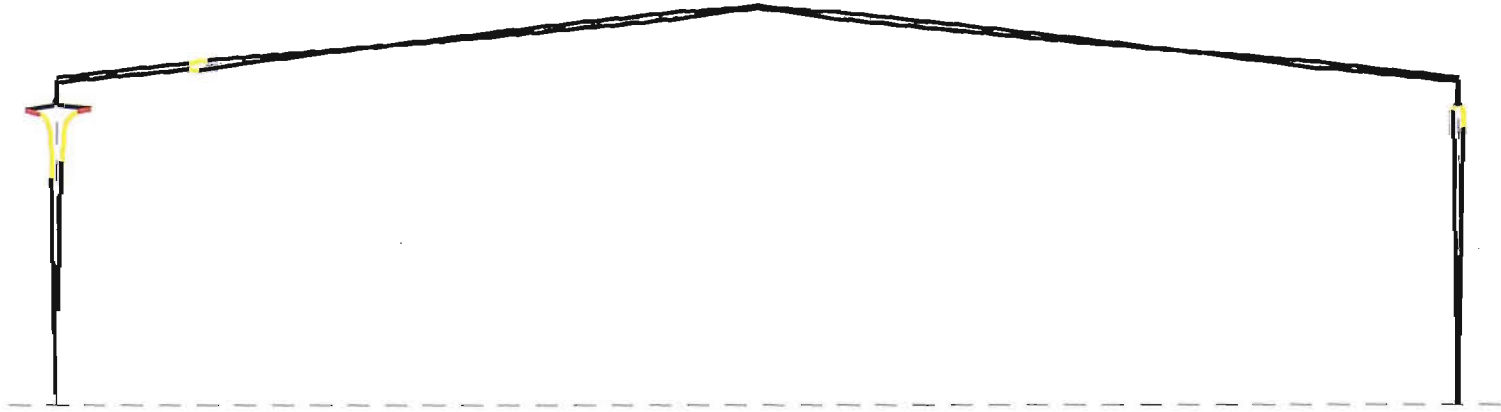
Figure 6.12: Cross-section's Extreme Fibre Strain at w_y=10.06 kN/m, (88.6% of fail load), with plastic strains shown in yellow; strain-hardening in red.

M_P exceeded at:

(a) for 1281.21mm below start of haunch

(b) for 531.98mm right of apex haunch
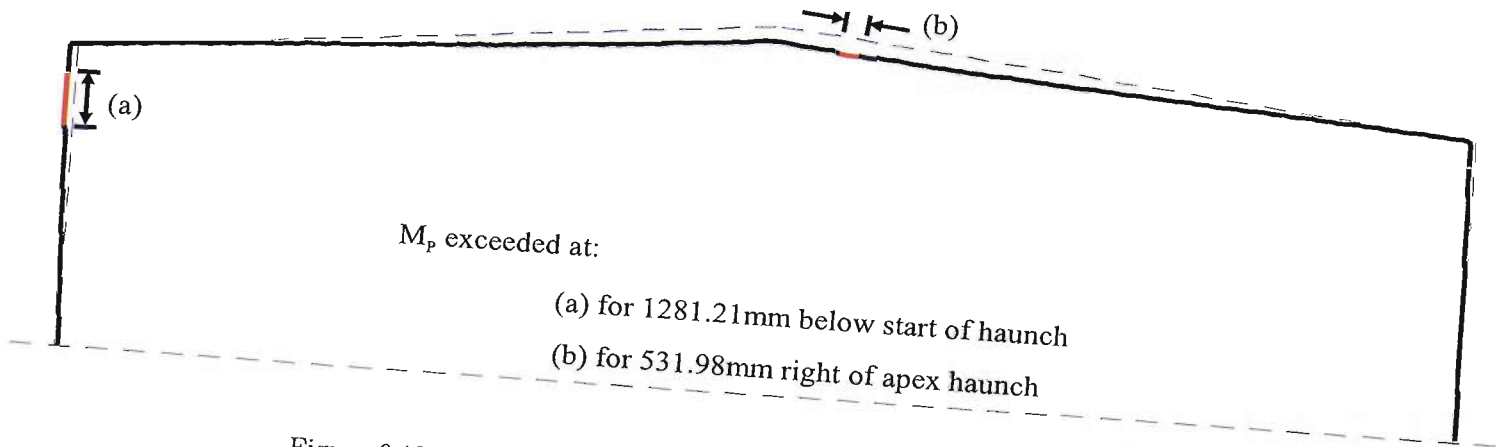
Figure 6.13: Deflection of Frame at w_y=10.76 kN/m (94.7% of failure load)

Development of Second Plastic Hinge (Figure 6.8(c))

The second Plastic Hinge began to form at a load of w_y=10.76 kN/m. At this load, M_E is exceeded in two sections: one, 1281mm long below the eaves haunch in the left column; the other 532mm long to the right of the apex haunch taper. This is shown in Figure 6.13. It should be noted that the predictions of hinging behaviour based upon M_E do not correlate to the large changes in deflection of Figure 6.8. They may provide a safe conservative criterion for increased risk of structural failure but do not describe actual structural behaviour.

The second Reduced Stiffness Hinge appears in the right-hand rafter when w_y=10.95 kN/m and is shown in the figure of w_y=10.96 kN/m (Figure 6.14). Highlights of the Reduced Stiffness Figure for w_y=10.96 kN/m include the two hinging portions of the structure, (a) and (b), highlighted in red, with three additional portions of reduced stiffness without appreciable hinges formed. The lowest values of remaining cross-sectional stiffness are labelled at positions (c), (d) and (e), which make clear that these portions, while flexing, are not hinging. Hinging caused by reduced cross-sectional stiffness better matches the expected progress of frame failure than conventional elastic-plastic hinge predictions, particularly at w_y=11.16 kN/m where the appearance of Reduced Stiffness Hinges (Figure 6.15) in the left rafter causes the final kink in Figure 6.8, marked with the line (d).

Reduced Stiffnesses under 96.5% of failure load :

(a) Min. Value: 2.28% at 5762mm (Hinge Length: 1023mm)

(b) Min. Value: 9.90% at 1500mm (Hinge Length: 95.7mm)

(c) Minimum Value: 10.8% Position 3000.0 mm

(d) Minimum Value: 15.3% Position 13583 mm

(e) Minimum Value: 16.1% Position 600.0 mm
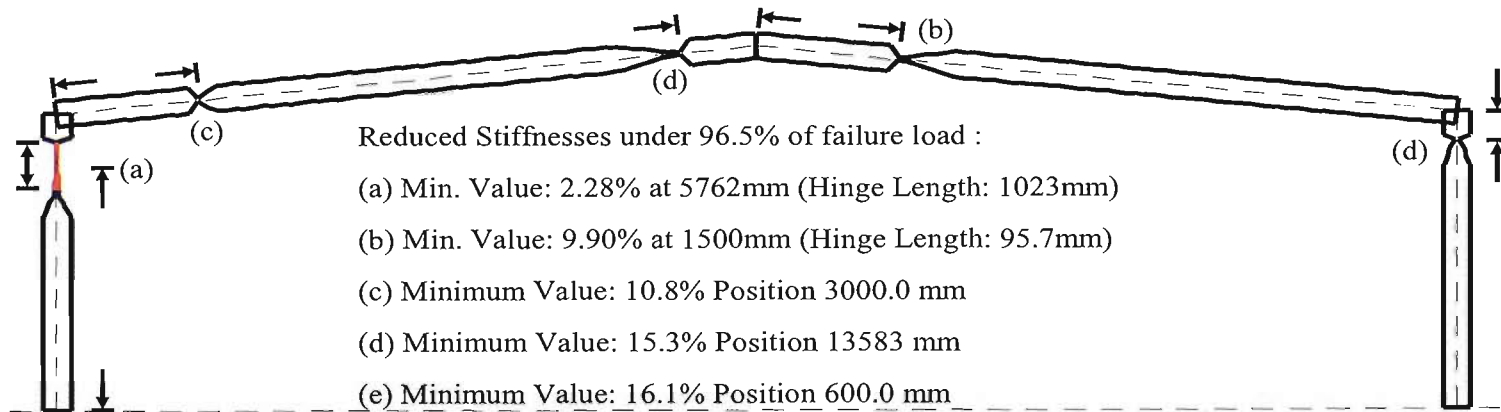
Figure 6.14: Reduced Stiffness at w_y=10.96 kN/m (96.5% of fail load)

Reduced Stiffnesses under 98.23% of failure load:

(a) Min. Value: 2.29% at 5597mm (Hinge Length: 1954mm)

(b) Min. Value: 2.83% at 3000mm (Hinge Length: 3171mm)

(c) Min. Value: 9.79% at 13583mm (Hinge Length: 1920mm)

(d) Min. Value: 8.06% at 3000mm (Hinge Length: 413mm)
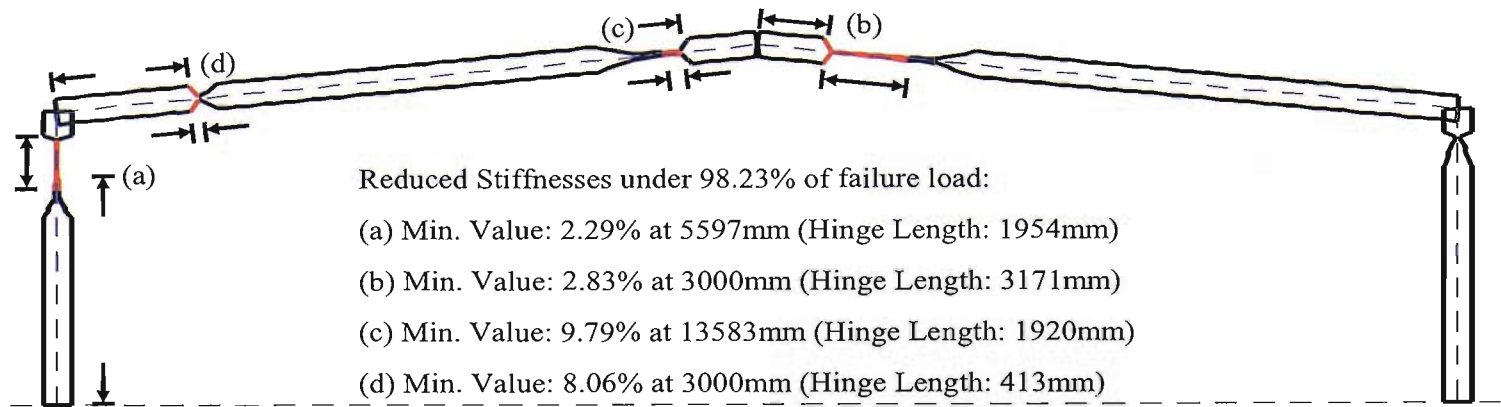
Figure 6.15: Reduced Stiffness at w_y=11.16 kN/m (98.23% of fail load)

The simulation fails at w_y=11.36 kN/m. The figure showing the reduced stiffnesses of the frame's members at this load identifies five portions of hinging behaviour. The least values of reduced cross-sectional stiffness are labelled (a) to (e) in Figure 6.16. The hinge containing (a) is known to be the first to appear, as before. This final state of the frame shows clearly that the next longest hinge is in the right-hand rafter, in agreement with existing known failure modes for Portal frames. As the Analytic Structures method does not follow elastic-plastic method and assume that plasticity establishes a freely-rotating hinge in the structure wherever it appears, these five portions still have remaining stiffness. However it is insufficient to deem the structure stable at this load – especially when Analytic Structures has failed to find a stable standing position for the structure (Figure 6.17).

Reduced Stiffnesses under 100% of failure load:

(a) Min. Value: 2.29% at 5048mm (Hinge Length: 1674mm)

(b) Min. Value: 3.82% at 3000mm (Hinge Length: 2763mm)

(c) Min. Value: 2.19% at 13522mm (Hinge Length: 971.6mm)

(d) Min. Value: 2.19% at 3211mm (Hinge Length: 383.6mm)

(e) Min. Value: 3.31% at 600mm (Hinge Length: 456.3mm)
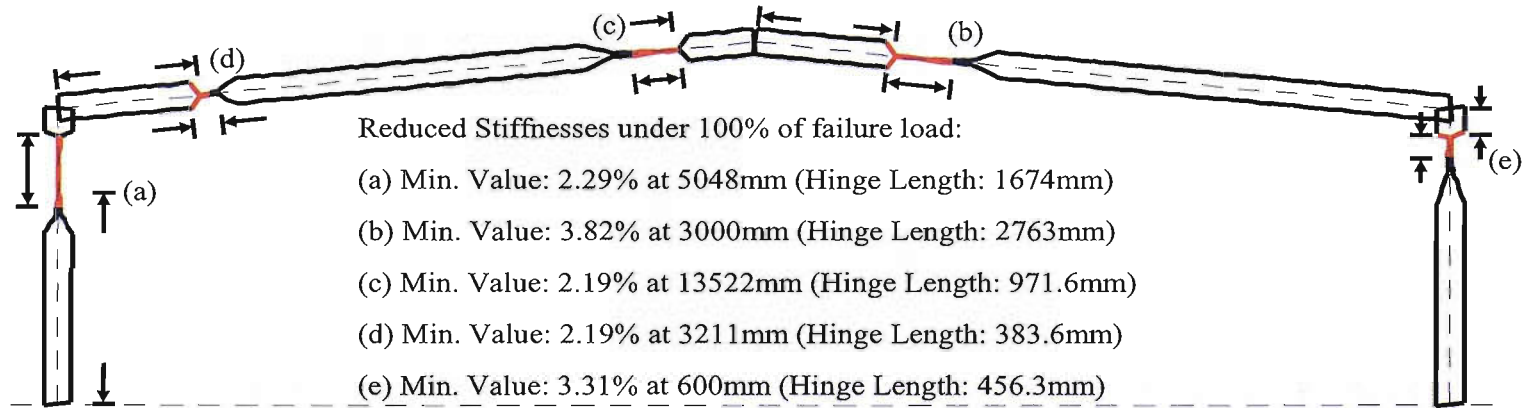
Figure 6.16: Reduced Stiffness at w_y=11.36 kN/m (100% of fail load)

6.3.2 Failure Load

The next table of results shows the Collapse Load for the Manual method, Fastrak and the Analytic Structures simulations. In contrast to the worked example of SCI P-252, Analytic Structures found its failure load from progressive increases of the load w_y. The structure remains stable despite the establishment of significant portions of plasticity. The simulation continues to stand under increased loadings up to the Collapse Load, despite the existence of more than two significant sections of member plasticity At the point at which Analytic structures cannot find a set of initial conditions for the Differential Equations of State of Chapter Three, the structure is deemed to not be able to meet the material and loading conditions and so has failed. In practical terms, the frame has failed. In mathematical terms, a singularity has been found.

Value	Manual Calculation	Fastrak 4.1	Analytic Structures
Collapse Load	11.71 kN / m	11.64 kN / m	11.36 kN / m

Table 6.3: Comparison of the Failure Loads Predicted by Manual Calculation, Fastrak and the Analytic Structures method

It is important to note that the simulation software failed at w_y=11.36 kN/m. This means something precise: that the process of solving the Differential Equations of State (from Chapter Three) could not be completed within the bounds of the material properties and structural layout of the portal frame. This failure to meet the constraints of the computer model supports the sensible claim that the frame will fail at this level of load. However, this is not always the case, as sometimes the initial guesses supplied to the Analytic Structures system can cause it to terminate early, as can too large a step incrementing the loading. Great care was taken to ensure early termination did not occur. Careful initial guesses of the boundary conditions were input, using interpolation based on the previous two increments of load-

ing. At the later stages, the increments of loading were shrunk to 10% of their initial values, ensuring that it was possible to find solutions to the boundary conditions right up to the failure load. Fine-tuning these parameters of the simulation requires careful application of basic structural design methods to ensure that good initial values and small increments yield reliable simulation results. Figure 6.17 shows an impossible state of deflection provided by a failed simulation set, where the portal frame could not resist the loading put on it, i.e. a "real" solution to the problem does not exist because the frame has failed.
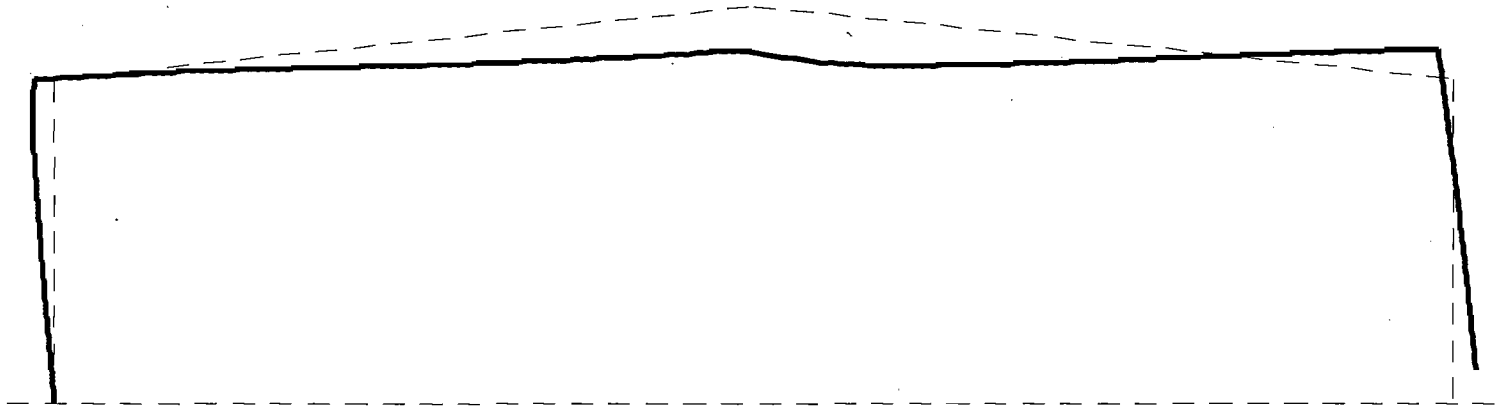
Figure 6.17: Final state of deflection, with Analytic Structures failing to meet the right foot of the structure to the pin joint
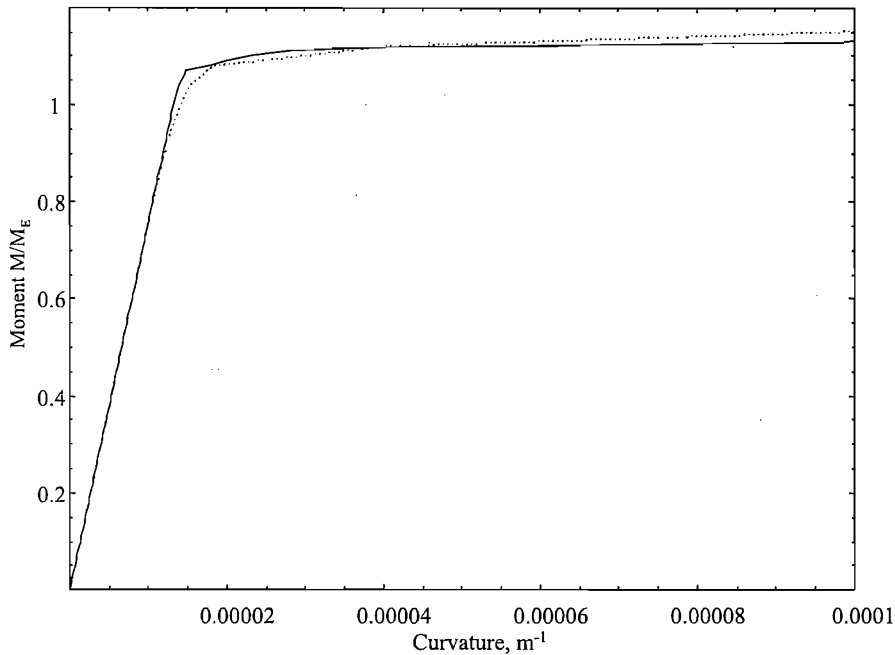
Figure 6.18: Moment against Curvature comparing non-internal strain Curvature Table (line (a)) and internal-strain Curvature Table (line (b))

6.3.3 Comparison between Analytic Structures, Fastrak and manual calculations

The path to failure of all three structural analysis methods involves hinging. All three correlate the position of their hinges: the first is in the column below the start of the eaves haunch and the second at the end of the apex haunch taper. This coincidence of hinge position is reassuring. However, both the results from the manual calculations and Fastrak make use of point-hinges, where Analytic Structures has hinging lengths. This will have an adverse effect upon the load-carrying capacity of the structure as larger portions of the structure have reduced stiffness associated with plastic or post-plastic behaviour and so deflect further (numbers) than the elastic-plastic method used in Fastrak; the manual method makes no use of elastic flexure.

The failure loads for each method are within reasonable bounds. Both the manual calculation and Fastrak Portal Frame aim for a required frame

148

Position of Deflection, mm	Analytic Structures Deflection	Fastrak Deflection
Eaves Join	114	18.92
Apex	333	186.2

Table 6.4: Absolute Deflection (mm) of Key Frame Points

strength of 11.3 kN/m, failing 1.03 and 1.036 times that value, respectively. This difference is likely to arise from the manual calculations using a rigid-plastic stress-strain model, where Fastrak deems hinges to form where the moment reaches 99% of MP. The shortfall of the predicted failure loads of Analytic Structures, while meeting the required frame strength, is caused by the automatic inclusion of $P - \delta$ and $P - \Delta$ effects in its model and with the increased deflection of the method. Figure 4.11 of Chapter Four (here as Figure 6.18) shows the behaviour of the Curvature Look-Up Table used in this portal frame simulation (dashed line). The gentler knee of line (b) (in comparison to the solid line – an identical curvature table but for internal strain data) shows comparatively earlier increase in curvature at the onset of plasticity. This causes greater deflection in the Analytic Structures portal frame simulations. The greatest contributor to the early failure of the Analytic Structures simulated Portal Frame is the lengths of each member behaving plastically when a hinge in formed. In contrast to a point hinge, a length within the frame which has a reduced-stiffness hinge deflects more than a purely elastic member of the same length and suffers from the cumulative effect of that increased deflection. It is of no surprise that the deflections in Analytic Structures are greater than those predicted by Fastrak, as highlighted in Table 6.4.

The data for Table 6.4 is taken at the emergence of the second hinge. In *Fastrak*, this coincides with the failure load of 11.64 kN/m, but for Analytic Structures this occurs at a load of 10.76 kN/m. Even under less load, the Analytic Structures frame has deflected further. The ongoing stability of

the Analytic Structures frame simulation at loads up to 11.36 kN/m is a testament to the capability of strain hardening to resist sway failure (Horne (1960)). These deflection figures highlight the importance of second-order frame and member effects ($P - \delta$ and $P - \Delta$, respectively) upon stability.

The second-order analyses within Fastrak are labelled 'Frame Stability - SCI-P292 Check'. Studying SCI Publication No292 (King, 2001) and following its worked example of a second-order analysis for the original frame with its 30.0m span, 7.0m eaves height and 6° pitch, the second-order load factor (λ_M) reduces λ_P such that the failure load is predicted to be 11.41 kN/m, a total 100.459% of the load at which Analytic Structures failed. Further to this, the computer model of the frame in the Analytic Structures analysis allows its members to shrink with the thrust strain (including shear strain is proposed as an extension to the model). This adds to the differences in structural behaviour shown between the three methods of analysis under discussion: neither the manual calculation nor Fastrak incorporate this, and as such it may be considered a higher-order effect than $P - \delta$ and $P - \Delta$ effects, which explains its present neglect.
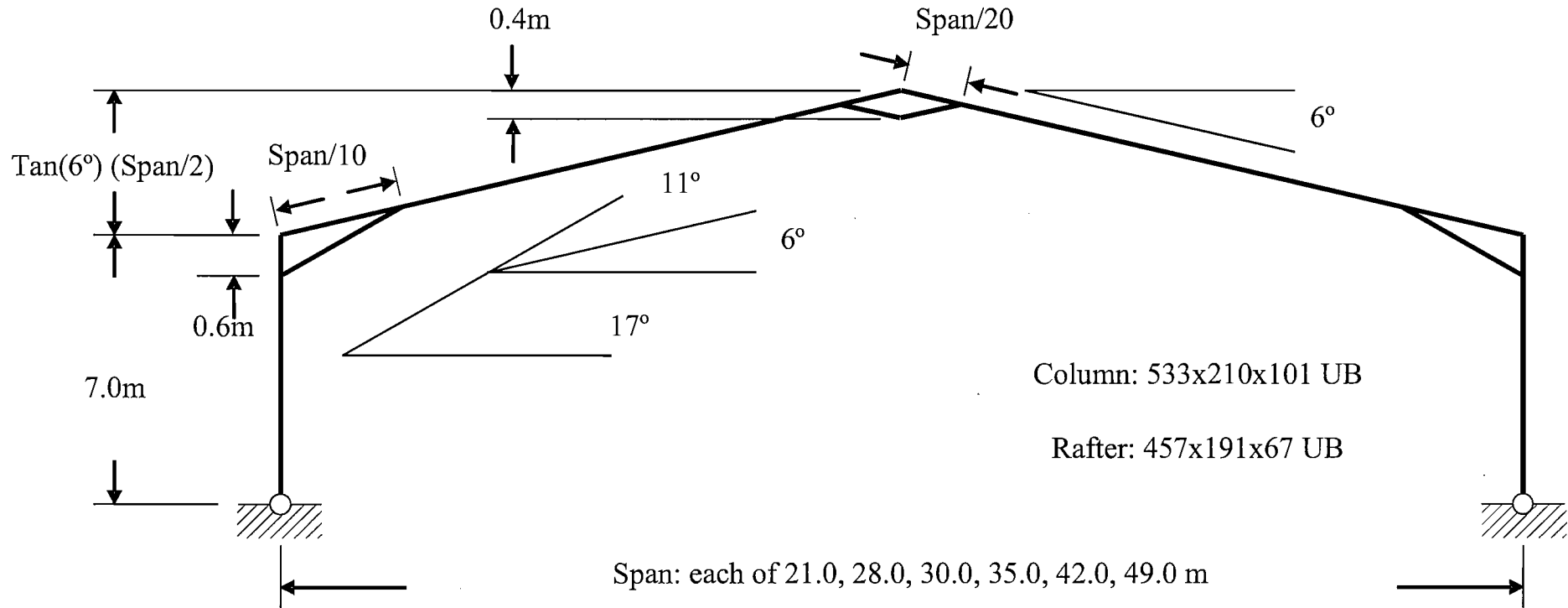
Figure 6.19: Sketched Dimensions of Span-to-Height Ratio Simulations

6.3.4 Span-to-Height Ratio

Additional simulations were run, changing only the length of the frame span so as to compare the stability of broad-based frames. The frame's geometry is sketched in Figure 6.19. The span ranged from 21.0 m to 49.0 m, reflecting span-to-height ratios of 3-to-1, 4-to-1, 5-to-1, 6-to-1 and 7-to-1 for the 7.0m height of the existing simulated Portal Frame. The dimensions of the haunch length retained their previous proportions: 10% of the span at the eaves and 5% at each side of the apex. The vertical depths of the haunch remained at 600mm and 400mm for the eaves and apex, respectively, due a lack of an explicit method in design documents for the depth of the haunch. It must be noted that the default settings in *Fastrak* take a haunch depth which depends on the length of the span. This was overridden for sake of comparison with simulations run in Analytic Structures.

Span	Span-Height Ratio	Analytic Structures	Elastic-Plastic	Elastic-Plastic plus $P - \delta$ & $P - \Delta$
21.0m	3-to-1	20.9	23.06	23.0
28.0m	4-to-1	12.3	13.36	13.2
35.0m	5-to-1	7.86	8.79	8.6
42.0m	6-to-1	5.86	6.27	6.0
49.0m	7-to-1	4.46	4.73	4.1

Table 6.5: Failure Loads (kN/m) using Analytic Structures, Elastic-Plastic (*Fastrak*) and $P - \delta$ modified Elastic-Plastic method for a Range of Values of Span-to Height Ratio

Table 6.5 and Figure 6.20 contrasts the predicted failure loads of Analytic Structures with those of *Fastrak Portal Frame* over a range of span-to-eaves-height ratios. Two sets of data are presented for comparison with Analytic Structures: one from the original Elastic-Plastic analysis method and a second, including the second-order analysis from SCI P-292. The percentage

difference is included at each stage, comparing the results from Analytic Structures with each of the other analyses. The data shows that the elastic-plastic model used in *Fastrak* provides distinctly higher load capacities than Analytic Structures. The shortfall of Analytic Structures' predicted Failure Loads in contrast to results obtained from Elastic-Plastic analysis is an average of 7.29%. There are two causes of these discrepancies in failure load: that the elastic-plastic method may be slightly overestimating the capacity of the structure because of lack of inclusion of internal strains in predictions of member behaviour, as well as failure to accommodate spread of plasticity with each member. This is supported by the Curvature Look-Up Table, shown above in Figure 6.18, showing additional curvature occurring at the elastic-plastic knee due to the presence of internal strains. This additional curvature will translate into additional deflection and consequently earlier onset of buckling.

The additional cause for the differences in failure loads is due to differences in the treatment of second order effects. The elastic-plastic (*Fastrak*) method uses a first-order model, neglecting second- and higher-order behaviour. It is however possible to extend the elastic-plastic analysis to incorporate second-order effects, using the methodology presented in SCI P-292. The second-order modified results are presented in Table 6.5, with the differences between the methods of analysis shown to reduce as the frames become more shallow. While an extreme case, the strength of the 7:1 ratio frame in Analytic Structures is higher than that for the SCI P-292 analysis, and this difference may be attributed to the absence, in the SCI P-292 analysis of additional post-elastic stiffness due to strain hardening.

153

**Failure Loads for 7.0m Eaves-Height Portals:
Elasto-Plastic Method (Red) vs SCI P-292 Second-Order Method (Blue)
vs Analytic Structures (Green)**
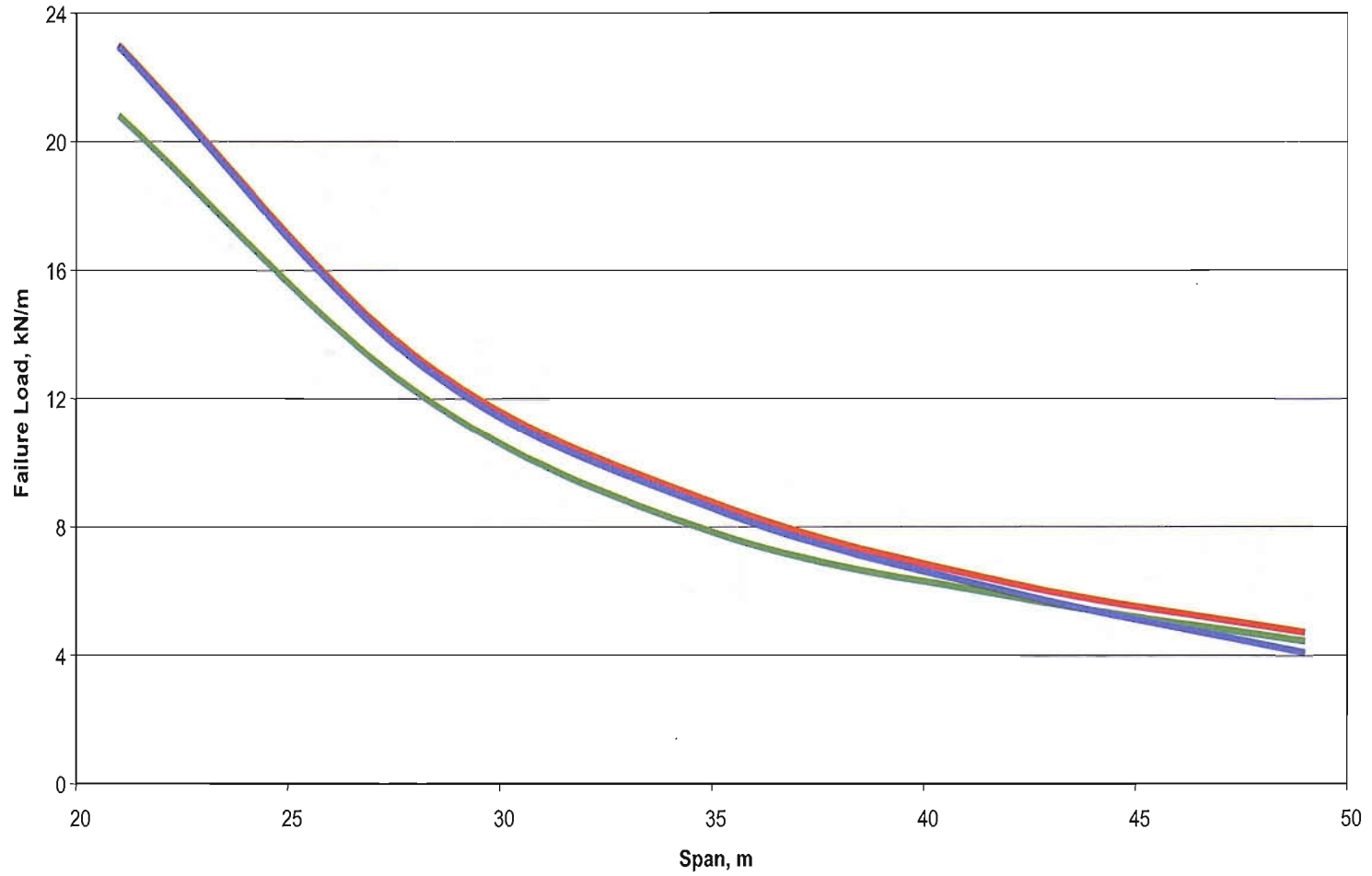
Figure 6.20: Graphical Comparison of Failure Loads at varying Span-to Height Ratios

The 7:1 span-to-eaves-height ratio matches the SCI P-292 predicted collapse load where the other results do not. The 7:1 ratio span is unusual in practice, having long rafters whose self-weight contributes such large moments and such significant second-order deflections that the frame is rarely economic. In the case of the simulated 7:1 ratio span, the self weight is 22% of the failure load and forms 26% of the moment in the column hinge at failure. Therefore the $P - \delta$ deflections are the explanation that the second-order SCI P-292 analysis matches that of Analytic Structures.

Table 6.6, below, shows the eaves deflection at failure and proportion at which 99% of M_P is achieved in each span. Analytic Structures consistently shows larger deflections which are the most likely root of the lower failure loads, despite the additional data in Analytic Structures' computer model. The 99% of M_P is the point at which Fastrak considers a hinge to have formed, and so can be used to highlight the similar way in which both methods have their frames fail across the range of spans. Both Analytic Structures and the SCI P-292 method show a shrinking of the proportion of fail that 99% of M_P appears in the frame, indicating that they follow similar paths to failure and that the larger values of fail load predicted by Fastrak are potentially dangerous overestimations due to their lack of accurate stress-strain, cross-sectional curvature or internal strain data.

The differences in Table 6.6 are startling. The established second-order analysis from SCI P-292 follows the expected progression whereby the stockier frames deflect less and the wider-based frames sway further as their longer members succumb to greater P-Δ effects. In contrast, the predicted eaves deflections calculated by Analytic Structures' simulations show no trend at all.

Without any trend, the most likely explanation for Analytic Structure's results is that the deflections shown here are not related to the strength of the frame or to M_P. The process by which each simulation was loaded to failure increased the UDL across the rafters by the same small increment irrespective

Eaves-Height to Span Ratio	Span, m	Analytic Structures: Eaves Deflection, mm	SCI P-292 Eaves Deflection, mm
3:1	21.0	327	25.7
4:1	28.0	203	65.7
5:1	35.0	213	109.1
6:1	42.0	205	155.9
7:1	49.0	342	205.5

Table 6.6: Absolute Eaves Deflection (mm) at Failure Load for Each Frame

of the span-to-height ratio of the frame simulation. The structures modelled by the simulation are deemed to fail when the equation-solvers cannot find a realistic position in which the frame may stand. This state corresponds to a mathematical singularity within the differential equations and will be accompanied by numerical instability to the deflection of the frame. The stability of this ultimate state of simulation may be disturbed even further by the unavoidable errors within the numerical equation solvers. When put together, these factors around failure can cause rapid variations in deflection as failure is approached and so bring a random property to how far each simulation has progressed before the computer system emits an error declaring its failure to complete the simulation. In such a case, the results of Table 6.6 may be produced. Such behaviour may be mitigated if the equation solvers are carefully managed to minimise the error and to carefully negotiate the mathematically-unstable behaviour close to portal frame failure. Further work is proposed to investigate the best methods for these processes.

6.4 Conclusions

Having previously shown the reliability of the Analytic Structures method when applied to columns, in Chapter Five, the task set out in this chapter has been to assess the accuracy of Analytic Structures predictions of frame load capacity in comparison with the state-of-the-art commercial portal frame design software (*Fastrak Portal Frame*). A sample single bay portal frame was selected and simulations run to ascertain its failure load.

From the data created by these simulations the process of failure was devised and qualified. The results were compared to contemporaneous methods of analysis (manual and computer-driven) and are comparable. The failure load predicted by Analytic Structures meets the required strength of the frame, but falls short of the predicted failure loads of rigid plastic manual calculations and elastic-plastic computer-based analysis. This lower load capacity is due to Analytic Structures producing larger deflections for given loads, which ultimately led to a lower load carrying capacity. The increase in deflection arises from the accurate quantification of the moment, thrust and curvature relationship in the Curvature Look-Up Table, which also includes the effects of internal strains on moment curvature response. In addition, additional deflections due to the spread of plasticity is automatically included. Analytic Structures models plasticity as a continuous behaviour within a portion of the member in contrast to the elastic-plastic method, which assumes that plasticity is confined to the node point. In addition, the Analytic Structures method provides an accurate account of $P - \delta$ destabilising effects. Regardless of these differences the final load capacities varied by on average only 7%. This difference was less where the elastic-plastic method incorporated the industry standard $P - \delta$ strength reduction.

Frames with a range of width to eaves height ratios were considered. It was found that a very close agreement between the Analytic Structures method and the elastic-plastic method were achieved when the aspect ra-

tion was 7:1, with predictions matching extremely closely when the $P - \delta$ modification was included in the elastic-plastic analysis method (SCI P-292).

The Analytic Structures method and program offer opportunities to examine and qualify structural behaviour in an efficient manner. Their application to the field of structural design is a necessary one, allowing frames to be analysed at a greater level of detail than previously permitted, at the desk of the engineer using contemporaneous personal computing power.

Chapter 7

Conclusions

7.1 Conclusions

The work presented here introduces a number of additions to the field of structural analysis, ranging from mathematical theory through to computer programming and results of structural analysis. It has the potential to be extended further, and has potential for a new class of structural analysis involving the direct solution of the member equations, rather than stiffness matrix solutions. The method is tied into the computer, using the ever-increasing power of personal computing to provide information about frame and member behaviour at any point within the structure. The work progresses to qualify its behaviour against empirical results and existing methods of analysis, in the particular cases of an Eulerian Strut and a single-span Portal Frame.

At the core of the work is a mathematical expression of member behaviour. Its most important contribution is to use differential equations at a particular cross-section position to quantify angle, loading and position. The equations additionally include the impact of axial shortening. The derivation of these equations is presented. Any examination of member behaviour using these differential equations avoids first- and second-order approximations. When the equations are solved within the computer program, the results are not stated in terms of x or y, but through a numerical interpolation function. The information within the interpolation includes every order of approximation and its accuracy is constrained to the accuracy of the equation-solving program.

Any computer method needs a knowledgeable expert to make best use of the uncritical automaton performing the calculation. While it is possible to program the Analytic Structures into a computer and realise excellent results, it is as possible to misuse the system and compromise its results by programming bad initial values, loading patterns and member properties. Care must be taken to estimate good boundary conditions when solving the

member's differential equations of state.

Care has also been taken to accurately predict the curvature in a cross-section under given loads. Contemporaneous methods of analysis ignore the additional curvature resulting from internal strains (residual stresses) and axial forces in beam members. In the present analysis the contribution to cross-sectional curvature from moment and axial thrust loading has been quantified, whilst taking into account the effects of internal strains. The curvature look-up tables calculated from the model of this relationship were developed using the nonlinear material properties and this was a significant technical challenge. In particular, iteration was essential to the calculation of the position of the neutral axis for given thrusts and moments. The resulting functions provide accurate curvature predictions and, in doing so, speed up the computation of structural behaviour by avoiding repeated calculations. Additionally they provide insight into the increased quantity of curvature (and corresponding deflection) brought about during the formation of plastic hinges. It was found that internal strains and axial thrusts have a significant influence on the moment-curvature relationship of steel I-sections bending about their strong axis. In particular, internal strains and axial thrusts result in significantly greater curvatures at the elastic-to-plastic transition point of the moment curvature curve.

In contrast to the elastic-plastic method programmed into an industrial design package for portal frames (*Fastrak Portal Frame*), the Analytic Structures method will appear inefficient. The core Elastic-Plastic analysis was developed in the 1960's on calculating machines which are less powerful than today's school calculators. The same software runs on today's personal computers in a fraction of a second, while a portal frame analysis in Analytic Structures typically takes an hour and requires the previously-prepared tables of Curvature data, each of which uses about a day's computation time each. Analytic Structures, as used to provide the results of Chapters Five and Six, is not yet optimised for speedy computation, but performance ben-

efits can be found within the system: reducing the required accuracy of the equation solvers and using larger increments of loading are available options.

This thesis describes the results of simulated struts derived from a series of computer models. The struts were a common I-section restrained to buckle along their major axis. The most-detailed computer model is correlated exceptionally well ($\rho = 0.99994780$) with the BS5950 Class A Strut Buckling Curve (Table 24(a)). This model contained the internal strains (residual stresses) arising from the hot-rolled steel manufacturing process. A comparison between two families of simulations, one with internal strain data and one without, revealed that internal strains can delay the onset of buckling. The comparisons of the Analytic Structures' Elastic Struts to the Euler Strut-Buckling formula shows exceptional correlation, with $\rho = 0.99990690$.

The model was extended to consider failure of single-span portal frames and the predicted failure loads provide a close match with those derived using existing analysis methods. The predictions from two such existing two such existing design analysis methods are compared, one a manual calculation and the other by a computer-based design package (*Fastrak Portal Frame* by CSC Ltd.). All three methods predict failure by creation of an identical series of plastic hinges, a statement that comes with the warning that point-hinges, as predicted in the manual calculation and *Fastrak* analyses, are not a part of the Analytic Structures method. Due to the continuous modelling of the cross-section in the differential equations of Analytic Structures, plasticity emerges in lengths of the frame. Consequently the equation-solving mechanism models large portions of the frame as softened by plasticity. The additional curvature brought about by these large zones of softening causes larger deflections than those predicted using the elastic-plastic method. This additional deflection is the major cause of Analytic Structures falling short of the predicted failure loads from the other methods. The presence of internal strains or residual stresses of hot-rolled member manufacturing, as mentioned above, advances the onset of non-elastic flexure while stiffening

the strain-hardening behaviour. This has the effect of permitting significant contiguous portions of a simulated portal frame to flex plastically but to have the strain-hardening of the flexing member resist structural failure as predicted by Horne (1960). The thesis simulated a portal frame with 30.0m span, 7.0m eaves height and 6° pitch angle has required strength of 11.3 kN/m. Analytic Structures predicts a failure load of 11.36 kN/m, lower than the 11.71 kN/m failure load of the manual calculation, or the 11.64 kN/m of the elastic-plastic analysis from *Fastrak*. This happens due to Analytic Structures tolerating larger portions of the frame behaving plastically and strain-hardening, leading to increased frame deflection and mildly earlier failure. Analytic Structures does, however, show that the frame meets the required strength of 11.3 kN/m.

Work was also completed comparing results from Analytic Structures and Elastic-Plastic analysis for a variety of ratios of span-to-eaves height. Analytic Structures showed the same shortfall in results through these simulations. However, including allowance for second-order frame and member deflections provided a agreement in failure modes in the wider span frames.

While the predicted failure loads were in close agreement, the predicted deflections recorded by the elastic-plastic (*Fastrak*) analyses were substantially less than those predicted by Analytic Structures. As stated, the greater deflections resulted from spread of plasticity and the inclusion of internal strains and axial thrusts in the moment curvature relationship. These additional deflections were responsible for the lower failure loads predicted using the Analytical structures method.

7.2 Further Work

As discussed above, some of the shortcomings of the Analytic Structures method as implemented here can be alleviated by additions to the mathematical model, curvature tables or the simulations themselves. The following

material introduces these adaptations, hoping to make clear their purpose and discuss their suitability.

Improvements to the Structural Mathematics

Future developments here may include out-of-plane loading and an extension to the internal stress function. The six Differential Equations of State become 12 when the third dimension is included:

$$\frac{\mathrm{d}f_x}{\mathrm{d}s} = w_x \qquad \frac{\mathrm{d}f_y}{\mathrm{d}s} = w_y \qquad \frac{\mathrm{d}f_z}{\mathrm{d}s} = w_z \qquad (7.1)$$

$$\frac{\mathrm{d}M_x}{\mathrm{d}s} = q_x(1-\epsilon) \quad \frac{\mathrm{d}M_y}{\mathrm{d}s} = q_y(1-\epsilon) \quad \frac{\mathrm{d}M_z}{\mathrm{d}s} = q_z(1-\epsilon)$$

$$\frac{\mathrm{d}\theta_x}{\mathrm{d}s} = \kappa_x \qquad \frac{\mathrm{d}\theta_y}{\mathrm{d}s} = \kappa_y \qquad \frac{\mathrm{d}\theta_z}{\mathrm{d}s} = \kappa_z$$

$$\frac{\mathrm{d}x}{\mathrm{d}s} = \sin(\theta_y) \qquad \frac{\mathrm{d}y}{\mathrm{d}s} = \sin(\theta_x) \qquad \frac{\mathrm{d}z}{\mathrm{d}s} = \cos(\theta_x)\cos(\theta_y).$$

The equations for position are stated in terms of θ_x and θ_y because a simplifying assumption about M_z, κ_z and θ_z makes a reasonable case that they may be ignored: that κ_z and θ_z are likely to destroy compliance with the assumption that plane sections remain planes, whenever they become large enough to cause deflection which stretches one end of a member and compresses the other. The need for initial values and estimates of final values remains the same: for each equation, at least one boundary condition is needed or found from Shooting. The inclusion of out-of-plane loading will necessitate extensions to the Curvature Functions, which are discussed below. One of the obvious uses for out-of-plane deflection is the modelling of an entire building made of linked Portal Frames.

The internal stress function approximates empirical tests of hot-rolled members, using the close-enough concept of a parabolic or linear stress distribution through the member. It could be extended to use a computer model built from the first principles of locked-in strains from cooling, which supply the assumption that locked-in strain follows the position in the cross-section which cooled most slowly. This is directly that portion of the cross-section

164
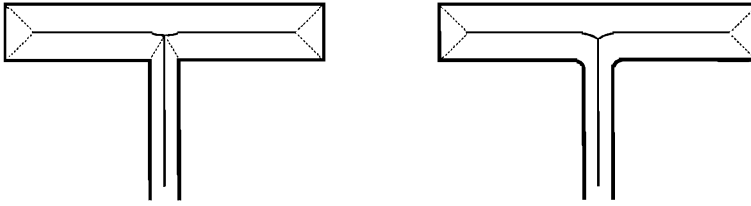
Figure 7.1: Lines of Slowest Cooling or Most Distance to Edge within an I-section (with/without Flange Fillets)

furthest from the surface of the member (Figure 7.1). Consequently, the path of maximum locked in stress can be graphed and the parameters by which the parabola of internal stresses follow can be determined from the sum of the stresses across an unloaded cross-section being zero:

$$\int \sigma_{int} \mathrm{d}x \mathrm{d}y = 0. \tag{7.2}$$

Numerical investigation is planned for the entire cross-section to ascertain the parameters of the parabolae which define the internal strains. Further extension to this work would also account for volume expansion in the hot-rolling process and its influence in causing the locked-in strains.

Improvements to the Curvature Look-Up Tables

It is recommended that the Curvature function be updated to supply a value of curvature from a pair of moments, one about the x-axis and one about the y-axis. This is required for the extensions proposed above for out-of-plane loading and deflection. With the two Moment loadings, the resulting curvature may be calculated either as two values of curvature, or as one value of curvature and the angle at which it acts, analogous to measuring in Cartesian or Polar coordinates.

Shear deflections are generally low in comparison with bending deflections for steel portal frames. The Shear modulus of most cross-sections is sufficient that this aspect of structural behaviour is neglected in analysis. Should the Analytic Structures method be adapted for use modelling the behaviour
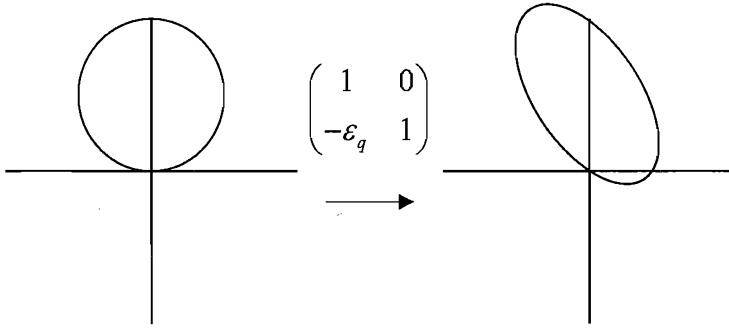
Figure 7.2: Circle Sheared to Ellipse

of structures constructed from other materials, it would be beneficial to incorporate the impact of the shear strain upon the member curvature. It is appropriate to do this to the models of Chapter Four, as the changes will be made in the creation of tables of Curvature data. It may not be necessary to calculate new tables of Curvature data, as the impact of shear strain may be included in the program directly.

In the general case of a member with constant curvature, this is equivalent to a circle of radius r placed so that it touches the origin at its lowest point. The equations are, either in $x-$ and $y-$coordinates or parameterised for s:

$$x^2 + (y - r)^2 = r^2 \qquad (7.3)$$

$$\begin{cases} x &= r\cos(s) \\ y &= r\left(\sin(s) + 1\right) \end{cases} \qquad (7.4)$$

The portion of the curve at the origin occurs when $s = \frac{-\pi}{2}$. If this space is sheared by the matrix (as per Figure 7.2):

$$T = \begin{pmatrix} 1 & 0 \\ -\epsilon_q & 1 \end{pmatrix}, \qquad (7.5)$$

the parametric form of the resulting ellipse is

$$\begin{cases} \overline{x} &= r\cos(s) \\ \overline{y} &= r\left(\sin(s) + 1\right) - \epsilon_q r \cos(s) \end{cases} \qquad (7.6)$$

166

The curvature κ uses the same equations as in Chapter Three:

$$\kappa \;=\; \frac{x'y'' - y'x''}{(x'^2 + y'^2)^{\frac{3}{2}}}$$

$$\;=\; \frac{1}{r}\left(\frac{1}{\epsilon_q^2 \sin^2(s) + 3\epsilon_q \sin(s)\cos(s) + 1}\right)^{\frac{3}{2}}. \qquad (7.7)$$

Even in the transformed coordinates (x', y'), the origin remains at $s = -\frac{\pi}{2}$, and so is:

$$\kappa\Big|_{s=-\frac{\pi}{2}} = \frac{1}{r}\Big(\frac{1}{1 + \epsilon_q^2}\Big)^{\frac{3}{2}}. \qquad (7.8)$$

Therefore the factor by which an existing known value of curvature is amplified by the shear strain is:

$$\kappa_{\text{shear}} = \kappa\Big(\frac{1}{1 + \epsilon_q^2}\Big)^{\frac{3}{2}}. \qquad (7.9)$$

Extensions to Strut Simulations

As mentioned above, a fuller set of strut-buckling curves is planned, with the inclusion of a series bounded by plastic behaviour, and a series using the internal strain data but ignoring the impact of axial thrusts. Also, the test of a built-in crushing strut, with its full-Sine deflection pattern, would provide good qualitative information about the influence of p-δ effects in struts across the range of simulations performed here. The simulation would need to ensure that the upper built-in end of the strut falls as the member contracts and deflects under the load; which could be one of the three unknowns at the upper end found by shooting. This simulation would be able to check the common assumption arising from the Euler Strut Formula of the sine-curve deflection pattern, and should it not be

Extensions to Portal Frames Simulations

The scope is extensive for further work on the Portal Frame models. Among potential other frames for study: multi-bay frames, hit-and-miss portal framed buildings, and tied frames. The move to haunched sections solid in their own

167
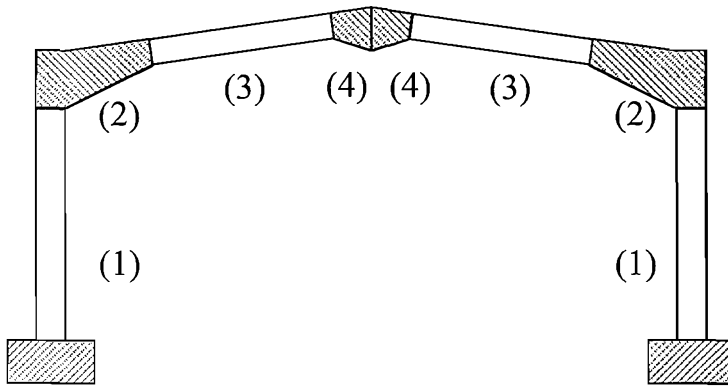
Figure 7.3: Segmented Portal Frame Model

right (not overlapped as at present) is a high priority, as is the move to consider loading and deformation out-of-plane.

Additionally, a more complete model of a portal frame span could be constructed by splitting the structure into 8 segments, mirrored around the apex (Figure 7.3), with the haunches at the eaves and apex simulated as if their own members. The non-haunched sections of the columns and rafters are modelled as before. Initial steps could use haunches which have an elastic Curvature Function, which could require the exact cross-section dimensions to calculate the area, I_{xx} and weight where they appear in the system. The joins of members in an Analytic Structures simulation do not have any flexibility, as the end-points of the previous members have their final conditions passed to the next member as its starting conditions. It would be possible to insert elastic shims to flex under the loading. These improvements are facilitated by the parametric nature of the Analytic Structures method: the member loading and properties can be programmed to depend on the parameter s for position in a given member.

Chapter 8

Resources

8.1 Curvature Look-Up Tables

The following tables contain the data for the Curvature Look-Up Tables (a), (b) and (c) as introduced in Chapter Four. The I-Section applicable to these curvature data is the 203x102x23 I-section from Table B-4 of SCI P202 (6th Ed., 2001). The two groups (one beginning on Page 171 and ending 178 and the other beginning on Page 179 and ending 185) recording the curvature for increases in axial thrust while holding moment constant and recording the curvature for increases in moment while holding the thrust constant, respectively. The curvature predicted by Equation 3.2 (see Page 43) is included for comparison.

Moment	Normalised Moment (M/M_E)	Axial Thrust	Normalised Axial Thrust (p/p_{cr})	Elastic Curvature	Curvature Look-Up Table (a)	Curvature Look-Up Table (b)	Curvature Look-Up Table (c)	Direct Shooting
0	0	0	0	0	6.09E-23	-8.34E-24	4.85E-23	4.85E-23
0	0	79483.8	0.1	0	6.09E-23	-1.09E-23	3.99E-23	3.99E-23
0	0	158967.6	0.2	0	6.09E-23	9.98E-24	3.83E-23	3.83E-23
0	0	238451.4	0.3	0	6.09E-23	1.21E-23	4.31E-23	4.31E-23
0	0	317935.2	0.4	0	6.09E-23	7.72E-24	1.43E-23	1.43E-23
0	0	397419	0.5	0	6.09E-23	6.50E-24	2.55E-23	2.55E-23
0	0	476902.8	0.6	0	6.09E-23	1.35E-23	-3.36E-24	-3.36E-24
0	0	556386.6	0.7	0	6.09E-23	8.12E-24	1.21E-23	1.21E-23
5.59E+06	0.1	0	0	1.32E-06	1.32E-06	1.32E-06	1.32E-06	1.32E-06
5.59E+06	0.1	79483.8	0.1	1.32E-06	1.32E-06	1.32E-06	1.32E-06	1.32E-06
5.59E+06	0.1	158967.6	0.2	1.32E-06	1.32E-06	1.32E-06	1.32E-06	1.32E-06
5.59E+06	0.1	238451.4	0.3	1.32E-06	1.32E-06	1.32E-06	1.32E-06	1.32E-06
5.59E+06	0.1	317935.2	0.4	1.32E-06	1.32E-06	1.32E-06	1.32E-06	1.32E-06
5.59E+06	0.1	397419	0.5	1.32E-06	1.32E-06	1.32E-06	1.32E-06	1.32E-06
5.59E+06	0.1	476902.8	0.6	1.32E-06	1.32E-06	1.32E-06	1.32E-06	1.32E-06
5.59E+06	0.1	556386.6	0.7	1.32E-06	1.32E-06	1.32E-06	1.32E-06	1.32E-06

Moment	Normalised Moment (M/M_E)	Axial Thrust	Normalised Axial Thrust (p/p_{cr})	Elastic Curvature	Curvature Look-Up Table (a)	Curvature Look-Up Table (b)	Curvature Look-Up Table (c)	Direct Shooting
1.12E+07	0.2	0	0	2.64E-06	2.64E-06	2.64E-06	2.64E-06	2.64E-06
1.12E+07	0.2	79483.8	0.1	2.64E-06	2.64E-06	2.64E-06	2.64E-06	2.64E-06
1.12E+07	0.2	158967.6	0.2	2.64E-06	2.64E-06	2.64E-06	2.64E-06	2.64E-06
1.12E+07	0.2	238451.4	0.3	2.64E-06	2.64E-06	2.64E-06	2.64E-06	2.64E-06
1.12E+07	0.2	317935.2	0.4	2.64E-06	2.64E-06	2.64E-06	2.64E-06	2.64E-06
1.12E+07	0.2	397419	0.5	2.64E-06	2.64E-06	2.64E-06	2.64E-06	2.64E-06
1.12E+07	0.2	476902.8	0.6	2.64E-06	2.64E-06	2.64E-06	2.64E-06	2.64E-06
1.12E+07	0.2	556386.6	0.7	2.64E-06	2.64E-06	2.64E-06	2.77E-06	2.77E-06
1.68E+07	0.3	0	0	3.96E-06	3.96E-06	3.96E-06	3.96E-06	3.96E-06
1.68E+07	0.3	79483.8	0.1	3.96E-06	3.96E-06	3.96E-06	3.96E-06	3.96E-06
1.68E+07	0.3	158967.6	0.2	3.96E-06	3.96E-06	3.96E-06	3.96E-06	3.96E-06
1.68E+07	0.3	238451.4	0.3	3.96E-06	3.96E-06	3.96E-06	3.96E-06	3.96E-06
1.68E+07	0.3	317935.2	0.4	3.96E-06	3.96E-06	3.96E-06	3.96E-06	3.96E-06
1.68E+07	0.3	397419	0.5	3.96E-06	3.96E-06	3.96E-06	3.96E-06	3.96E-06
1.68E+07	0.3	476902.8	0.6	3.96E-06	3.96E-06	3.96E-06	4.08E-06	4.08E-06
1.68E+07	0.3	556386.6	0.7	3.96E-06	3.96E-06	3.96E-06	4.92E-06	4.92E-06

Moment	Normalised Moment (M/M_E)	Axial Thrust	Normalised Axial Thrust (p/p_{cr})	Elastic Curvature	Curvature Look-Up Table (a)	Curvature Look-Up Table (b)	Curvature Look-Up Table (c)	Direct Shooting
2.23E+07	0.4	0	0	5.28E-06	5.28E-06	5.28E-06	5.28E-06	5.28E-06
2.23E+07	0.4	79483.8	0.1	5.28E-06	5.28E-06	5.28E-06	5.28E-06	5.28E-06
2.23E+07	0.4	158967.6	0.2	5.28E-06	5.28E-06	5.28E-06	5.28E-06	5.28E-06
2.23E+07	0.4	238451.4	0.3	5.28E-06	5.28E-06	5.28E-06	5.28E-06	5.28E-06
2.23E+07	0.4	317935.2	0.4	5.28E-06	5.28E-06	5.28E-06	5.28E-06	5.28E-06
2.23E+07	0.4	397419	0.5	5.28E-06	5.28E-06	5.28E-06	5.37E-06	5.37E-06
2.23E+07	0.4	476902.8	0.6	5.28E-06	5.28E-06	5.28E-06	6.09E-06	6.09E-06
2.23E+07	0.4	556386.6	0.7	5.28E-06	5.28E-06	1.65645E-05	1.70816E-05	1.70816E-05
2.79E+07	0.5	0	0	6.60E-06	6.60E-06	6.60E-06	6.60E-06	6.60E-06
2.79E+07	0.5	79483.8	0.1	6.60E-06	6.60E-06	6.60E-06	6.60E-06	6.60E-06
2.79E+07	0.5	158967.6	0.2	6.60E-06	6.60E-06	6.60E-06	6.60E-06	6.60E-06
2.79E+07	0.5	238451.4	0.3	6.60E-06	6.60E-06	6.60E-06	6.60E-06	6.60E-06
2.79E+07	0.5	317935.2	0.4	6.60E-06	6.60E-06	6.60E-06	6.69E-06	6.69E-06
2.79E+07	0.5	397419	0.5	6.60E-06	6.60E-06	6.60E-06	7.35E-06	7.35E-06
2.79E+07	0.5	476902.8	0.6	6.60E-06	6.60E-06	1.13419E-05	1.36155E-05	1.36155E-05
2.79E+07	0.5	556386.6	0.7	6.60E-06	6.60E-06	8.97467E-05	8.2346E-05	8.2346E-05

Moment	Normalised Moment (M/M_E)	Axial Thrust	Normalised Axial Thrust (p/p_{cr})	Elastic Curvature	Curvature Look-Up Table (a)	Curvature Look-Up Table (b)	Curvature Look-Up Table (c)	Direct Shooting
3.35E+07	0.6	0	0	7.92E-06	7.92E-06	7.92E-06	7.92E-06	7.92E-06
3.35E+07	0.6	79483.8	0.1	7.92E-06	7.92E-06	7.92E-06	7.92E-06	7.92E-06
3.35E+07	0.6	158967.6	0.2	7.92E-06	7.92E-06	7.92E-06	7.92E-06	7.92E-06
3.35E+07	0.6	238451.4	0.3	7.92E-06	7.92E-06	7.92E-06	7.99E-06	7.99E-06
3.35E+07	0.6	317935.2	0.4	7.92E-06	7.92E-06	7.92E-06	8.58E-06	8.58E-06
3.35E+07	0.6	397419	0.5	7.92E-06	7.92E-06	1.12052E-05	1.24605E-05	1.24605E-05
3.35E+07	0.6	476902.8	0.6	7.92E-06	7.92E-06	7.48989E-05	6.76851E-05	6.76851E-05
3.35E+07	0.6	556386.6	0.7	7.92E-06	7.92E-06	0.000134408	0.000126892	0.000126892
3.91E+07	0.7	0	0	9.24E-06	9.24E-06	9.24E-06	9.24E-06	9.24E-06
3.91E+07	0.7	79483.8	0.1	9.24E-06	9.24E-06	9.24E-06	9.24E-06	9.24E-06
3.91E+07	0.7	158967.6	0.2	9.24E-06	9.24E-06	9.24E-06	9.31E-06	9.31E-06
3.91E+07	0.7	238451.4	0.3	9.24E-06	9.24E-06	9.24E-06	9.86E-06	9.86E-06
3.91E+07	0.7	317935.2	0.4	9.24E-06	9.24E-06	1.18302E-05	1.30616E-05	1.30616E-05
3.91E+07	0.7	397419	0.5	9.24E-06	9.24E-06	5.9921E-05	5.23558E-05	5.23558E-05
3.91E+07	0.7	476902.8	0.6	9.24E-06	9.24E-06	0.000120019	0.000112537	0.000112537
3.91E+07	0.7	556386.6	0.7	9.24E-06	9.24E-06	0.0001785	0.000170923	0.000170923

Moment	Normalised Moment (M/M_E)	Axial Thrust	Normalised Axial Thrust (p/p_{cr})	Elastic Curvature	Curvature Look-Up Table (a)	Curvature Look-Up Table (b)	Curvature Look-Up Table (c)	Direct Shooting
4.47E+07	0.8	0	0	1.05627E-05	1.05561E-05	1.05627E-05	1.05898E-05	1.05898E-05
4.47E+07	0.8	79483.8	0.1	1.05627E-05	1.05561E-05	1.05627E-05	1.06077E-05	1.06077E-05
4.47E+07	0.8	158967.6	0.2	1.05627E-05	1.05561E-05	1.05627E-05	1.11063E-05	1.11063E-05
4.47E+07	0.8	238451.4	0.3	1.05627E-05	1.05561E-05	1.27194E-05	1.36248E-05	1.36248E-05
4.47E+07	0.8	317935.2	0.4	1.05627E-05	1.05561E-05	3.31289E-05	3.34073E-05	3.34073E-05
4.47E+07	0.8	397419	0.5	1.05627E-05	1.05561E-05	0.000105707	9.84064E-05	9.84064E-05
4.47E+07	0.8	476902.8	0.6	1.05627E-05	1.05561E-05	0.000164231	0.000156778	0.000156778
4.47E+07	0.8	556386.6	0.7	1.05627E-05	1.05561E-05	0.000222544	0.000215002	0.000215002
5.03E+07	0.9	0	0	1.1883E-05	1.18756E-05	1.1883E-05	1.20734E-05	1.20734E-05
5.03E+07	0.9	79483.8	0.1	1.1883E-05	1.18756E-05	1.1883E-05	1.24376E-05	1.24376E-05
5.03E+07	0.9	158967.6	0.2	1.1883E-05	1.18756E-05	1.37318E-05	1.4638E-05	1.4638E-05
5.03E+07	0.9	238451.4	0.3	1.1883E-05	1.18756E-05	2.47447E-05	2.73854E-05	2.73854E-05
5.03E+07	0.9	317935.2	0.4	1.1883E-05	1.18756E-05	9.19585E-05	8.50671E-05	8.50671E-05
5.03E+07	0.9	397419	0.5	1.1883E-05	1.18756E-05	0.000150631	0.000143223	0.000143223
5.03E+07	0.9	476902.8	0.6	1.1883E-05	1.18756E-05	0.000209003	0.000201454	0.000201454
5.03E+07	0.9	556386.6	0.7	1.1883E-05	1.18756E-05	0.000267265	0.000259648	0.000259648

Moment	Normalised Moment (M/M_E)	Axial Thrust	Normalised Axial Thrust (p/p_{cr})	Elastic Curvature	Curvature Look-Up Table (a)	Curvature Look-Up Table (b)	Curvature Look-Up Table (c)	Direct Shooting
5.59E+07	1	0	0	1.32034E-05	1.33364E-05	1.32034E-05	1.413E-05	1.413E-05
5.59E+07	1	79483.8	0.1	1.32034E-05	1.33364E-05	1.48117E-05	1.58366E-05	1.58366E-05
5.59E+07	1	158967.6	0.2	1.32034E-05	1.33364E-05	2.26839E-05	2.48239E-05	2.48239E-05
5.59E+07	1	238451.4	0.3	1.32034E-05	1.33364E-05	8.26015E-05	7.59706E-05	7.59706E-05
5.59E+07	1	317935.2	0.4	1.32034E-05	1.33364E-05	0.000139092	0.000131851	0.000131851
5.59E+07	1	397419	0.5	1.32034E-05	1.33364E-05	0.000196778	0.000189234	0.000189234
5.59E+07	1	476902.8	0.6	1.32034E-05	1.33364E-05	0.000254714	0.000247073	0.000247073
5.59E+07	1	556386.6	0.7	1.32034E-05	1.33364E-05	0.000312734	0.000305046	0.000305046
6.15E+07	1.1	0	0	1.45237E-05	2.29563E-05	2.30575E-05	2.91319E-05	2.91319E-05
6.15E+07	1.1	79483.8	0.1	1.45237E-05	2.29563E-05	3.81539E-05	5.32328E-05	5.32328E-05
6.15E+07	1.1	158967.6	0.2	1.45237E-05	2.29563E-05	0.000108693	9.9639E-05	9.9639E-05
6.15E+07	1.1	238451.4	0.3	1.45237E-05	2.29563E-05	0.000153457	0.000145257	0.000145257
6.15E+07	1.1	317935.2	0.4	1.45237E-05	2.29563E-05	0.00019799	0.000190807	0.000190807
6.15E+07	1.1	397419	0.5	1.45237E-05	2.29563E-05	0.000244928	0.00023788	0.00023788
6.15E+07	1.1	476902.8	0.6	1.45237E-05	2.29563E-05	0.000301529	0.000293921	0.000293921
6.15E+07	1.1	556386.6	0.7	1.45237E-05	2.29563E-05	0.000359002	0.000351312	0.000351312

Moment	Normalised Moment (M/M_E)	Axial Thrust	Normalised Axial Thrust (p/p_{cr})	Elastic Curvature	Curvature Look-Up Table (a)	Curvature Look-Up Table (b)	Curvature Look-Up Table (c)	Direct Shooting
6.70E+07	1.2	0	0	1.58441E-05	0.00015785	0.000172344	0.000158531	0.000158531
6.70E+07	1.2	79483.8	0.1	1.58441E-05	0.00015785	0.000181944	0.000167888	0.000167888
6.70E+07	1.2	158967.6	0.2	1.58441E-05	0.00015785	0.000206269	0.000193094	0.000193094
6.70E+07	1.2	238451.4	0.3	1.58441E-05	0.00015785	0.00023961	0.000227606	0.000227606
6.70E+07	1.2	317935.2	0.4	1.58441E-05	0.00015785	0.000275655	0.000266124	0.000266124
6.70E+07	1.2	397419	0.5	1.58441E-05	0.00015785	0.000310509	0.000303205	0.000303205
6.70E+07	1.2	476902.8	0.6	1.58441E-05	0.00015785	0.000350485	0.000343125	0.000343125
6.70E+07	1.2	556386.6	0.7	1.58441E-05	0.00015785	0.000406319	0.000398629	0.000398629

Axial Thrust	Normalised Axial Thrust (p/p_{cr})	Moment	Normalised Moment (M/M_E)	Elastic Curvature	Curvature Look-Up Table (a)	Curvature Look-Up Table (b)	Curvature Look-Up Table (c)	Direct Shooting
0	0	0	0	0	6.09E-23	-8.34E-24	4.85E-23	4.85E-23
0	0	5.59E+06	0.1	1.32E-06	1.32E-06	1.32E-06	1.32E-06	1.32E-06
0	0	1.12E+07	0.2	2.64E-06	2.64E-06	2.64E-06	2.64E-06	2.64E-06
0	0	1.68E+07	0.3	3.96E-06	3.96E-06	3.96E-06	3.96E-06	3.96E-06
0	0	2.23E+07	0.4	5.28E-06	5.28E-06	5.28E-06	5.28E-06	5.28E-06
0	0	2.79E+07	0.5	6.60E-06	6.60E-06	6.60E-06	6.60E-06	6.60E-06
0	0	3.35E+07	0.6	7.92E-06	7.92E-06	7.92E-06	7.92E-06	7.92E-06
0	0	3.91E+07	0.7	9.24E-06	9.24E-06	9.24E-06	9.24E-06	9.24E-06
0	0	4.47E+07	0.8	1.05627E-05	1.05561E-05	1.05627E-05	1.05898E-05	1.05898E-05
0	0	5.03E+07	0.9	1.1883E-05	1.18756E-05	1.1883E-05	1.20734E-05	1.20734E-05
0	0	5.59E+07	1	1.32034E-05	1.33364E-05	1.32034E-05	1.413E-05	1.413E-05
0	0	6.15E+07	1.1	1.45237E-05	2.29563E-05	2.30575E-05	2.91319E-05	2.91319E-05
0	0	6.70E+07	1.2	1.58441E-05	0.00015785	0.000172344	0.000158531	0.000158531

Axial Thrust	Normalised Axial Thrust (p/p_{cr})	Moment	Normalised Moment (M/M_E)	Elastic Curvature	Curvature Look-Up Table (a)	Curvature Look-Up Table (b)	Curvature Look-Up Table (c)	Direct Shooting
79483.8	0.1	0	0	0	6.09E-23	-1.09E-23	3.99E-23	3.99E-23
79483.8	0.1	5.59E+06	0.1	1.32E-06	1.32E-06	1.32E-06	1.32E-06	1.32E-06
79483.8	0.1	1.12E+07	0.2	2.64E-06	2.64E-06	2.64E-06	2.64E-06	2.64E-06
79483.8	0.1	1.68E+07	0.3	3.96E-06	3.96E-06	3.96E-06	3.96E-06	3.96E-06
79483.8	0.1	2.23E+07	0.4	5.28E-06	5.28E-06	5.28E-06	5.28E-06	5.28E-06
79483.8	0.1	2.79E+07	0.5	6.60E-06	6.60E-06	6.60E-06	6.60E-06	6.60E-06
79483.8	0.1	3.35E+07	0.6	7.92E-06	7.92E-06	7.92E-06	7.92E-06	7.92E-06
79483.8	0.1	3.91E+07	0.7	9.24E-06	9.24E-06	9.24E-06	9.24E-06	9.24E-06
79483.8	0.1	4.47E+07	0.8	1.05627E-05	1.05561E-05	1.05627E-05	1.06077E-05	1.06077E-05
79483.8	0.1	5.03E+07	0.9	1.1883E-05	1.18756E-05	1.1883E-05	1.24376E-05	1.24376E-05
79483.8	0.1	5.59E+07	1	1.32034E-05	1.33364E-05	1.48117E-05	1.58366E-05	1.58366E-05
79483.8	0.1	6.15E+07	1.1	1.45237E-05	2.29563E-05	3.81539E-05	5.32328E-05	5.32328E-05
79483.8	0.1	6.70E+07	1.2	1.58441E-05	0.00015785	0.000181944	0.000167888	0.000167888

Axial Thrust	Normalised Axial Thrust (p/p_{cr})	Moment	Normalised Moment (M/M_E)	Elastic Curvature	Curvature Look-Up Table (a)	Curvature Look-Up Table (b)	Curvature Look-Up Table (c)	Direct Shooting
158967.6	0.2	0	0	0	6.09E-23	9.98E-24	3.83E-23	3.83E-23
158967.6	0.2	5.59E+06	0.1	1.32E-06	1.32E-06	1.32E-06	1.32E-06	1.32E-06
158967.6	0.2	1.12E+07	0.2	2.64E-06	2.64E-06	2.64E-06	2.64E-06	2.64E-06
158967.6	0.2	1.68E+07	0.3	3.96E-06	3.96E-06	3.96E-06	3.96E-06	3.96E-06
158967.6	0.2	2.23E+07	0.4	5.28E-06	5.28E-06	5.28E-06	5.28E-06	5.28E-06
158967.6	0.2	2.79E+07	0.5	6.60E-06	6.60E-06	6.60E-06	6.60E-06	6.60E-06
158967.6	0.2	3.35E+07	0.6	7.92E-06	7.92E-06	7.92E-06	7.92E-06	7.92E-06
158967.6	0.2	3.91E+07	0.7	9.24E-06	9.24E-06	9.24E-06	9.31E-06	9.31E-06
158967.6	0.2	4.47E+07	0.8	1.05627E-05	1.05561E-05	1.05627E-05	1.11063E-05	1.11063E-05
158967.6	0.2	5.03E+07	0.9	1.1883E-05	1.18756E-05	1.37318E-05	1.4638E-05	1.4638E-05
158967.6	0.2	5.59E+07	1	1.32034E-05	1.33364E-05	2.26839E-05	2.48239E-05	2.48239E-05
158967.6	0.2	6.15E+07	1.1	1.45237E-05	2.29563E-05	0.000108693	9.9639E-05	9.9639E-05
158967.6	0.2	6.70E+07	1.2	1.58441E-05	0.00015785	0.000206269	0.000193094	0.000193094

Axial Thrust	Normalised Axial Thrust (p/p_{cr})	Moment	Normalised Moment (M/M_E)	Elastic Curvature	Curvature Look-Up Table (a)	Curvature Look-Up Table (b)	Curvature Look-Up Table (c)	Direct Shooting
238451.4	0.3	0	0	0	6.09E-23	1.21E-23	4.31E-23	4.31E-23
238451.4	0.3	5.59E+06	0.1	1.32E-06	1.32E-06	1.32E-06	1.32E-06	1.32E-06
238451.4	0.3	1.12E+07	0.2	2.64E-06	2.64E-06	2.64E-06	2.64E-06	2.64E-06
238451.4	0.3	1.68E+07	0.3	3.96E-06	3.96E-06	3.96E-06	3.96E-06	3.96E-06
238451.4	0.3	2.23E+07	0.4	5.28E-06	5.28E-06	5.28E-06	5.28E-06	5.28E-06
238451.4	0.3	2.79E+07	0.5	6.60E-06	6.60E-06	6.60E-06	6.60E-06	6.60E-06
238451.4	0.3	3.35E+07	0.6	7.92E-06	7.92E-06	7.92E-06	7.99E-06	7.99E-06
238451.4	0.3	3.91E+07	0.7	9.24E-06	9.24E-06	9.24E-06	9.86E-06	9.86E-06
238451.4	0.3	4.47E+07	0.8	1.05627E-05	1.05561E-05	1.27194E-05	1.36248E-05	1.36248E-05
238451.4	0.3	5.03E+07	0.9	1.1883E-05	1.18756E-05	2.47447E-05	2.73854E-05	2.73854E-05
238451.4	0.3	5.59E+07	1	1.32034E-05	1.33364E-05	8.26015E-05	7.59706E-05	7.59706E-05
238451.4	0.3	6.15E+07	1.1	1.45237E-05	2.29563E-05	0.000153457	0.000145257	0.000145257
238451.4	0.3	6.70E+07	1.2	1.58441E-05	0.00015785	0.00023961	0.000227606	0.000227606

Axial Thrust	Normalised Axial Thrust (p/p_{cr})	Moment	Normalised Moment (M/M_E)	Elastic Curvature	Curvature Look-Up Table (a)	Curvature Look-Up Table (b)	Curvature Look-Up Table (c)	Direct Shooting
317935.2	0.4	0	0	0	6.09E-23	7.72E-24	1.43E-23	1.43E-23
317935.2	0.4	5.59E+06	0.1	1.32E-06	1.32E-06	1.32E-06	1.32E-06	1.32E-06
317935.2	0.4	1.12E+07	0.2	2.64E-06	2.64E-06	2.64E-06	2.64E-06	2.64E-06
317935.2	0.4	1.68E+07	0.3	3.96E-06	3.96E-06	3.96E-06	3.96E-06	3.96E-06
317935.2	0.4	2.23E+07	0.4	5.28E-06	5.28E-06	5.28E-06	5.28E-06	5.28E-06
317935.2	0.4	2.79E+07	0.5	6.60E-06	6.60E-06	6.60E-06	6.69E-06	6.69E-06
317935.2	0.4	3.35E+07	0.6	7.92E-06	7.92E-06	7.92E-06	8.58E-06	8.58E-06
317935.2	0.4	3.91E+07	0.7	9.24E-06	9.24E-06	1.18302E-05	1.30616E-05	1.30616E-05
317935.2	0.4	4.47E+07	0.8	1.05627E-05	1.05561E-05	3.31289E-05	3.34073E-05	3.34073E-05
317935.2	0.4	5.03E+07	0.9	1.1883E-05	1.18756E-05	9.19585E-05	8.50671E-05	8.50671E-05
317935.2	0.4	5.59E+07	1	1.32034E-05	1.33364E-05	0.000139092	0.000131851	0.000131851
317935.2	0.4	6.15E+07	1.1	1.45237E-05	2.29563E-05	0.00019799	0.000190807	0.000190807
317935.2	0.4	6.70E+07	1.2	1.58441E-05	0.00015785	0.000275655	0.000266124	0.000266124

Axial Thrust	Normalised Axial Thrust (p/p_{cr})	Moment	Normalised Moment (M/M_E)	Elastic Curvature	Curvature Look-Up Table (a)	Curvature Look-Up Table (b)	Curvature Look-Up Table (c)	Direct Shooting
397419	0.5	0	0	0	6.09E-23	6.50E-24	2.55E-23	2.55E-23
397419	0.5	5.59E+06	0.1	1.32E-06	1.32E-06	1.32E-06	1.32E-06	1.32E-06
397419	0.5	1.12E+07	0.2	2.64E-06	2.64E-06	2.64E-06	2.64E-06	2.64E-06
397419	0.5	1.68E+07	0.3	3.96E-06	3.96E-06	3.96E-06	3.96E-06	3.96E-06
397419	0.5	2.23E+07	0.4	5.28E-06	5.28E-06	5.28E-06	5.37E-06	5.37E-06
397419	0.5	2.79E+07	0.5	6.60E-06	6.60E-06	6.60E-06	7.35E-06	7.35E-06
397419	0.5	3.35E+07	0.6	7.92E-06	7.92E-06	1.12052E-05	1.24605E-05	1.24605E-05
397419	0.5	3.91E+07	0.7	9.24E-06	9.24E-06	5.9921E-05	5.23558E-05	5.23558E-05
397419	0.5	4.47E+07	0.8	1.05627E-05	1.05561E-05	0.000105707	9.84064E-05	9.84064E-05
397419	0.5	5.03E+07	0.9	1.1883E-05	1.18756E-05	0.000150631	0.000143223	0.000143223
397419	0.5	5.59E+07	1	1.32034E-05	1.33364E-05	0.000196778	0.000189234	0.000189234
397419	0.5	6.15E+07	1.1	1.45237E-05	2.29563E-05	0.000244928	0.00023788	0.00023788
397419	0.5	6.70E+07	1.2	1.58441E-05	0.00015785	0.000310509	0.000303205	0.000303205

Axial Thrust	Normalised Axial Thrust (p/p_{cr})	Moment	Normalised Moment (M/M_E)	Elastic Curvature	Curvature Look-Up Table (a)	Curvature Look-Up Table (b)	Curvature Look-Up Table (c)	Direct Shooting
476902.8	0.6	0	0	0	6.09E-23	1.35E-23	-3.36E-24	-3.36E-24
476902.8	0.6	5.59E+06	0.1	1.32E-06	1.32E-06	1.32E-06	1.32E-06	1.32E-06
476902.8	0.6	1.12E+07	0.2	2.64E-06	2.64E-06	2.64E-06	2.64E-06	2.64E-06
476902.8	0.6	1.68E+07	0.3	3.96E-06	3.96E-06	3.96E-06	4.08E-06	4.08E-06
476902.8	0.6	2.23E+07	0.4	5.28E-06	5.28E-06	5.28E-06	6.09E-06	6.09E-06
476902.8	0.6	2.79E+07	0.5	6.60E-06	6.60E-06	1.13419E-05	1.36155E-05	1.36155E-05
476902.8	0.6	3.35E+07	0.6	7.92E-06	7.92E-06	7.48989E-05	6.76851E-05	6.76851E-05
476902.8	0.6	3.91E+07	0.7	9.24E-06	9.24E-06	0.000120019	0.000112537	0.000112537
476902.8	0.6	4.47E+07	0.8	1.05627E-05	1.05561E-05	0.000164231	0.000156778	0.000156778
476902.8	0.6	5.03E+07	0.9	1.1883E-05	1.18756E-05	0.000209003	0.000201454	0.000201454
476902.8	0.6	5.59E+07	1	1.32034E-05	1.33364E-05	0.000254714	0.000247073	0.000247073
476902.8	0.6	6.15E+07	1.1	1.45237E-05	2.29563E-05	0.000301529	0.000293921	0.000293921
476902.8	0.6	6.70E+07	1.2	1.58441E-05	0.00015785	0.000350485	0.000343125	0.000343125

Axial Thrust	Normalised Axial Thrust (p/p_{cr})	Moment	Normalised Moment (M/M_E)	Elastic Curvature	Curvature Look-Up Table (a)	Curvature Look-Up Table (b)	Curvature Look-Up Table (c)	Direct Shooting
556386.6	0.7	0	0	0	6.09E-23	8.12E-24	1.21E-23	1.21E-23
556386.6	0.7	5.59E+06	0.1	1.32E-06	1.32E-06	1.32E-06	1.32E-06	1.32E-06
556386.6	0.7	1.12E+07	0.2	2.64E-06	2.64E-06	2.64E-06	2.77E-06	2.77E-06
556386.6	0.7	1.68E+07	0.3	3.96E-06	3.96E-06	3.96E-06	4.92E-06	4.92E-06
556386.6	0.7	2.23E+07	0.4	5.28E-06	5.28E-06	1.65645E-05	1.70816E-05	1.70816E-05
556386.6	0.7	2.79E+07	0.5	6.60E-06	6.60E-06	8.97467E-05	8.2346E-05	8.2346E-05
556386.6	0.7	3.35E+07	0.6	7.92E-06	7.92E-06	0.000134408	0.000126892	0.000126892
556386.6	0.7	3.91E+07	0.7	9.24E-06	9.24E-06	0.0001785	0.000170923	0.000170923
556386.6	0.7	4.47E+07	0.8	1.05627E-05	1.05561E-05	0.000222544	0.000215002	0.000215002
556386.6	0.7	5.03E+07	0.9	1.1883E-05	1.18756E-05	0.000267265	0.000259648	0.000259648
556386.6	0.7	5.59E+07	1	1.32034E-05	1.33364E-05	0.000312734	0.000305046	0.000305046
556386.6	0.7	6.15E+07	1.1	1.45237E-05	2.29563E-05	0.000359002	0.000351312	0.000351312
556386.6	0.7	6.70E+07	1.2	1.58441E-05	0.00015785	0.000406319	0.000398629	0.000398629

8.2 Notation

b	width of a plate element
b_e	effective width of a plate element
f	generic force
f_c	compressive stress due to axial load
l	effective length of deflected section along its original axis
l_x	distance from a point of inflexion in a buckled beam
p_c	average critical stress
p_E	Euler buckling stress
q_y	shear force in the y-direction
r	radius of gyration, calculated from $r = \sqrt{\frac{I_{xx}}{a}}$
r_c	radius of curvature
s	variable following path of member along its length
s_1	plateau width for the 1972 adapted Perry curve, by Dwight. $s_1 = \frac{\pi}{5}\sqrt{\frac{E}{p_y}}$
t	thickness of plate in a beam
t_z	thrust along z-axis
w_y	load in y-direction
w_z	load in z-direction
y_M	partial safety factor in EN1993 for ultimate limit state
y_{M1}	relates the partial safety factor resistance of a member to buckling
A	cross-sectional area of the beam
A_{eff}	effective cross-sectional area of member
E	Young's Elastic Modulus for Steel
E_s	strain-hardening elastic modulus, taken to be $\frac{E}{25}$ by Dwight (1972)
F	mathematical function
I	second moment of area of the beam
M	moment

P_{cr}	mean load at failure of the strut
P_E	Euler buckling load,
P_y	design strength or yield stress
S	Plastic Modulus
W	generic load
W_c	collapse load
α	imperfection factor
β, γ	constants used in differential equation solution
δ	initial lack-of-straightness, $\delta = \text{Max}(3mm, \frac{l}{1000})$
δs	length of a small segment of beam
δy	small length in y-direction
δz	small length in z-direction
$\delta \theta$	small change in angle of beam arising from curvature of a small segment
$\sigma_\epsilon []$	interpolation function supplying a value of stress for a given value of strain
η	a non-dimensional factor measuring initial crookedness
κ	curvature
κ_s	inherent lack-of-straightness in a beam
λ	slenderness of column, $\lambda = \frac{l}{r}$
λ_{load}	load factor
θ	angle of curvature of the beam
$\epsilon_\sigma []$	interpolation function supplying a value of strain for a given value of stress
ξ	constant used in differential equation solution, $\xi^2 = \frac{p_{cr}}{EI}$
Δs	the length a small segment of beam changes under thrust

187

Bibliography

ENV-1992 'Eurocode 3 Normalisation document', 1992.

BSI449 'For the use of structural use of steel in building', 1932.

BSI5950:1990 'Structural use of steelwork in building', 1990.

BSI5950:2000 'Structural use of steelwork in building', 2000.

S.L. Andrade and L.J. Morris. Assessment of parameters affecting the behaviour of haunched rafters. *Pacific Structural Steel Conference, Auckland NZ*, 2:365, 1986.

S.T. Ariatnam. *Quarterly Journal of Mechanics and Applied Mathematics*, 14:137, 1961.

W.E. Ayrton and J. Perry. On struts. *The Engineer*, 62, 1886.

J.F. Baker. *The Steel Skeleton Vol. 2*. Cambridge, 1956.

Eduardo Bayo and Alfonso Loureiro. An efficient and direct method for buckling analysis of steel frame structures. *Journal of Constructional Steel Research*, 57:1321–1336, 2001.

M.P. Byfield and D.A. Nethercot. An analysis of the true bending strength of steel beams. *Procedures of the Institute of Civil Engineers: Structuress & Buildings*, 128:188–197, 1998.

M.P. Byfield and R. Ofner. e-mail contact. 2004.

M.P. Byfield, J.M. Davies, and M. Dhanalakshmi. Calculation of the strain hardening behaviour of steel structures based on mill tests. *Journal of Constructional Steel Research*, 61:133–150, 2005.

S.L. Chan. 2001.

J.M. Davies. Frame instability and strain hardening in plastic theory. *Proceedings of the American Society of Civil Engineers*, 92(ST3), 1966.

J.M. Davies. Collapse and shakedown loads of plane frames. *Journal of the Structural Division, Proceedings of the American Society of Civil Engineers*, 93(ST3), 1967.

J.M. Davies. False mechanisms in elastic-plastic analysis. *The Structural Engineer*, 66(16):268, 1988.

J.M. Davies. In-plane stability in portal frames. *Structural Engineer*, 68(8): 141–147, 1990.

J.M. Davies. Second-order elastic-plastic anaylsis of plane frames. *Journal of Constructional Steel Research*, 58:1315–1330, 2002.

J.M. Davies. Strain hardening, local buckling and lateral torsional buckling in plastic hinges. *Journal of Constructional Steel Research*, 62:27–34, 2006.

J.M. Davies, P. Engel, T.T.C. Liu, and L.J. Morris. Realistic modelling of steel portal frame behaviour. *The Structural Engineer*, 68(1):1–6, 1990.

J.B. Dwight. *Use of Perry formula to represent the new European strut-curves*. Cambridge, 1972a.

J.B. Dwight. Use of perry formula to represent the new european strut-curves. In *I.A.B.S.E. International Colloquim on Column Strength*, 1972b.

J.B. Dwight. Lecture 3: Design of axially-loaded columns including interactive buckling. In *The Background to the New British Standard for Structural Steelwork*, 1978.

L. Euler. *Mechanica.* 1736.

J.A. Ewing. *Strength of Materials.* Cambridge, 1899.

Godfrey G.B. The allowable stresses in axially-loaded steel struts. *The Structural Engineer*, 40(3), 1962.

J.X. Gu and S.L. Chan. Second-order analysis and design of steel structures allowing for member and frame imperfections. *International Journal for Numerical Methods in Engineering*, 62:601–615, 2005.

M. Herzog. Die größe der eigenspannungen in walz-und schweißprofilen nach messungen (the size of internal stresses in rolled and welded profiles after measurements. *Der Stahlbau*, 1977.

H.R. Horne. Instability and the plastic theory of structures. *Transactions of the Engineering Institute of Canada*, 4(2):31–43, 1960.

M.R. Horne. A moment distribution method for the analysis and design of structures by the plastic theory. *Proc. Inst. Civil Eng. Part III*, 3:51, 1954.

M.R. Horne. *Progress in Solid Mechanics*, 2:277, 1961.

M.R. Horne. Elastic-plastic fail loads of plane frames. *Proceedings of the Royal Society, Series A*, 274:343, 1963.

M.R. Horne. An approximate method for calculating the elastic critical load to multi-storey plane frames. *The Structural Engineer*, 53(6), 1975.

M.R. Horne and M.W. Chin. *Plastic Design of Portal Frames in Steel to BS968*, 1966.

M.R. Horne and I.C. Medland. Collapse loads of steel frameworks allowing for the effect of strain hardening. *Proceedings of the Royal Society, Scheme A*, 3:381, 1966.

W. Horne, editor. *Proc. Conf. Behavioural Slender Structures.* 1977.

A.R. Kemp, M.P. Byfield, and D.A. Nethercot. Effect of strain hardening on flexural properties of steel beams. *Structural Engineer*, 80(8):29–35, 2002.

C. King. In-plane stability of portal frames. *New Steel Construction*, 9(4): 17–19, 2001a.

C. King. *In-plane stability of Portal Frames to BS5950:2000*, 2001b.

M.G. Lay and T.V. Galambos. Inelastic steel beams under uniform moment. *Proceedings of the American Society of Civil Engineers*, 91(ST6):67–93.

M.G. Lay and P.D. Smith. Role of strain hardening in plastic design. *Journal of Structural division of the American Society of Civil Engineers*, page 25, 1965.

A.E.H. Love. *Treatise on the Mathematical Theory of Elasticity*. Cambridge, 1892.

H. Maier-Liebnitz. Test results, their interpretation and application. In *Preliminary Publication, 2nd Congress of the International Association for Bridge and Structure Engineering*, Berlin, 1936.

I.C. Medland. *Strain Hardening and the Collapse Loads of Steel Frameworks*. PhD thesis, University of Manchester, 1963.

T.H.G. Megson. *Strength of Materials for Civil Engineers, 2nd ed.* Edward Arnold, 1987.

W. Merchant. The failure load of rigid joints as influenced by stability. *Structural Engineer*, 32:185, 1954.

W. Merchant, editor. *Proc. 9th Int. Congress of App. Mech.* Brussels, 1956.

W. Merchant, C.A. Rashid, A. Bolton, and A. Salem. The behaviour of unclad frames. In *Proceedings of the Fiftieth Annual Conference of the Institute of Structural Engineers*, 1958.

S.S.J. Moy. *Plastic Methods for Steel and Concrete Structures, 2nd ed.* MacMillan, 1996. ISBN 0-333-64177-9.

B.G. Neal. *The plastic methods of structural analysis.* Chapman and Hall, 1956.

W.J.M Rankine. *Useful Rules and Tables.* London, 1866.

A. Robertson. The strength of struts. *Institute of Civil Engineers Selected Engineering Paper*, (28), 1925.

J.M. Rolfe. An alternative mathematical framework for structural theory. *The Structural Engineer*, 2005.

P.R. Salter, Malik A.S., and C. King. *Design of Single-Span Steel Portal Frames to BS5950-1:2000*, 2004.

H. Schmidt, editor. *Beuth-Kommentar DIN-18800 Teil 7: Stahlbauten, Ausfurungen und herstellequalifikation (Steel Structures, design and manufacture qualification.* 2004.

J. Szalai and F. Papp. A new residual stress distribution for hot-rolled I-shaped sections. *Journal of Constructional Steel Research*, 61:845–861, 2005.

J.C. Taylor. EN1993 Eurocode 3: Design of Steel Structures. *Civil Engineering*, (144):29–32, 2001.